OAK RIDGE NATIONAL LABORATORY LIBRARIES
3 4456 0555826 9

CENTRAL RESEARCH LIBRARY

ORNL/TM-5563
(ENDF-236)

Cy 92

Application of FORSS Sensitivity and Uncertainty Methodology to Fast Reactor Benchmark Analysis

C. R. Weisbin
J. H. Marable
J. L. Lucius
E. M. Oblow
F. R. Mynatt
R. W. Peelle
F. G. Perey

OAK RIDGE NATIONAL LABORATORY
CENTRAL RESEARCH LIBRARY
DOCUMENT COLLECTION
LIBRARY LOAN COPY
DO NOT TRANSFER TO ANOTHER PERSON
If you wish someone else to see this document, send in name with document and the library will arrange a loan.
UCN-7969
(3 3-67)

OAK RIDGE NATIONAL LABORATORY
OPERATED BY UNION CARBIDE CORPORATION FOR THE ENERGY RESEARCH AND DEVELOPMENT ADMINISTRATION

Printed in the United States of America. Available from
National Technical Information Service
U.S. Department of Commerce
5285 Port Royal Road, Springfield, Virginia 22161
Price: Printed Copy $6.00 ; Microfiche $2.25

This report was prepared as an account of work sponsored by the United States Government. Neither the United States nor the Energy Research and Development Administration/United States Nuclear Regulatory Commission, nor any of their employees, nor any of their contractors, subcontractors, or their employees, makes any warranty, express or implied, or assumes any legal liability or responsibility for the accuracy, completeness or usefulness of any information, apparatus, product or process disclosed, or represents that its use would not infringe privately owned rights.

ORNL/TM-5563
Distribution Category UC-79d
(ENDF-236)

Contract No. W-7405-eng-26

Neutron Physics Division

APPLICATION OF FORSS SENSITIVITY AND UNCERTAINTY METHODOLOGY TO FAST REACTOR BENCHMARK ANALYSIS

C. R. Weisbin, J. H. Marable, J. L. Lucius,* E. M. Oblow,
F. R. Mynatt, R. W. Peelle, and F. G. Perey

Date Published: December 1976

*Computer Science Division.

NOTICE This document contains information of a preliminary nature and was prepared primarily for internal use at the Oak Ridge National Laboratory. It is subject to revision or correction and therefore does not represent a final report.

OAK RIDGE NATIONAL LABORATORY
Oak Ridge, Tennessee 37830
operated by
UNION CARBIDE CORPORATION
for the
ENERGY RESEARCH AND DEVELOPMENT ADMINISTRATION

OAK RIDGE NATIONAL LABORATORY LIBRARIES
3 4456 0555826 9

Manuscript typed by Virginia Glidewell

Table of Contents

		Page No.
	ABSTRACT	v
I.	INTRODUCTION	1
II.	FORMULATION FOR SENSITIVITY PROFILES	3
	A. General Development	3
	B. k-Sensitivity	8
III.	SENSITIVITY REPRESENTATION IN MULTIGROUP DISCRETE ORDINATES THEORY	9
	A. k-Profiles	15
	1. Absorption Reactions	15
	2. Scattering Reactions	16
	3. Fission Reactions	17
	4. ν-Sensitivity	17
	B. Central Reaction Rate Ratio Profiles	18
	1. Absorption Reactions	19
	2. Scattering Reactions	20
	3. Fission Reactions	20
	4. ν-Sensitivity	20
	C. Total Profiles	21
IV.	k-RESET	21
V.	SPECIFIC EXAMPLES OF SENSITIVITY ANALYSIS	22
	A. Assembly Description	22
	B. Tabulation of Integral Sensitivities	23
	C. Calculational Procedure	23
	1. Generation of Multigroup Cross Sections	28
	2. Flux and Response Calculations	35
	3. Adjoints, Generalized Source, and Generalized Adjoints	40
	4. Energy Dependent Sensitivity Profiles	48
	D. Verification of Sensitivity Profiles	48
VI.	MULTIGROUP COVARIANCE MATRICES	71
	A. Formulation	73
	B. Results for Processed Uncertainty Files	75
VII.	UNCERTAINTIES DUE EXCLUSIVELY TO NUCLEAR DATA UNCERTAINTIES	84

Page No.

VIII. UNCERTAINTIES WITH INTEGRAL EXPERIMENTS TAKEN INTO ACCOUNT ---------- 88

A. General Development ---------- 89
B. Two Brief Examples ---------- 92

IX. INVERSE PROBLEM ---------- 102

X. CONCLUSIONS ---------- 105

App. A. DERIVATION OF THE EXPRESSION FOR k-SENSITIVITY -------- 113

App. B. NUCLIDE DENSITIES IN THE ONE-DIMENSIONAL MODEL FOR ZPR-6/7 AND ZPR-6/6A ---------- 115

Abstract

FORSS is a code system used to study relationships between nuclear reaction cross sections, integral experiments, reactor performance parameter predictions, and associated uncertainties. This paper presents the theory and code description as well as the first results of applying FORSS to fast reactor benchmarks. Specifically, for various assemblies and reactor performance parameters, the nuclear data sensitivities were computed by nuclide, reaction type, and energy. Comprehensive libraries of energy-dependent coefficients have been developed in a computer retrievable format and released for distribution by RSIC and NNCSC. Uncertainties induced by nuclear data were quantified using preliminary, energy-dependent relative covariance matrices evaluated with ENDF/B-IV expectation values and processed for $^{238}U(n,f)$, $^{238}U(n,\gamma)$, $^{239}Pu(n,f)$, and $^{239}Pu(\bar{\nu})$. Nuclear data accuracy requirements to meet specified performance criteria at minimum experimental cost were determined.

Based on our estimated correlations and standard deviations, a conclusion to be drawn is that design accuracy goals of 0.5% in k and 2% in the central $^{28}c/^{49}f$ ratio in conventional mixed oxide LMFBR cores (neutronic behavior similar to ZPR-6/7) are unlikely to be attained in the next 5 to 10 years if the nuclear data is based only on microscopic measurements and the level of effort on the most crucial cross sections is not increased dramatically. Results of integral experiments may be incorporated through FORSS to improve uncertainty estimates of reactor performance for devices being designed. Using the measurements in ZPR-6/7 for k and for central $^{28}c/^{49}f$ with assigned uncorrelated standard deviations of 1 and 2 percent, standard deviations of the same parameters for similar systems are computed to be 0.82% and 1.8% (compared to 3.5% and 8.6% with only differential covariance information) when the integral data is included in a cross-section adjustment which changes the basic multigroup file less than one standard deviation.

I. Introduction

FORSS[1] is an analytical tool used to study the relationships between nuclear reaction cross sections and their uncertainties, integral experiments and their uncertainties, and reactor performance parameter predictions and their uncertainties. Given a problem (or set of problems) with specified geometry, composition, source, and response, ORNL uses FORSS to determine:

1) What data are important; i.e., for a given performance parameter, what is the nuclear data sensitivity as a function of nuclide, reaction type, and energy?

2) How much does a given performance parameter change as a result of alternative data sets or specific differences in various elements of the data field?

3) How similar are two problems; e.g., a design problem and an integral experiment, with respect to cross-section data? One may synthesize several integral experiments to construct a simulation to the design problem.

4) How uncertain are performance parameters; i.e., for given cross-section and uncertainty files and selected integral experiments with their uncertainties and sensitivity profiles, what are the uncertainties in an ensemble of performance parameters?

5) What new measurements should be performed; i.e., given (1) present cross-section and uncertainty files, (2) selected integral experiments with their uncertainties and sensitivity profiles, (3) an approximate cost functional for potential uncertainty improvement in the cross-section uncertainties, and (4) an ensemble of performance parameters with specified tolerances, what is a "best" set of experimental accuracies required for reducing cross-section uncertainties?

6) What the relative importance of the basic physical processes involved in any analytical or experimental problem are so that qualitative and quantitative conclusions reached in one area can be extrapolated into many others (e.g., the extrapolation of results in critical experiments to commercial reactor design).

These objectives have been an implicit part of the Cross Section Evaluation Working Group mission since its inception, and the work reported here will help permit such goals to be achieved. Due to the diversity of interests and problems within the CSEWG domain, the FORSS development is based upon transport theory (there is a diffusion theory option) so that the same tool is applicable to both shielding and reactor core problems in multidimensional geometry.

This paper presents the first results of applying FORSS to the analysis of fast reactor benchmarks. Specifically, for a variety of assemblies and performance parameters, the nuclear data sensitivity is tabulated as a function of nuclide, reaction type, and energy. Nuclear data induced uncertainties are quantified and results of integral experiments are incorporated in a consistent fashion resulting in improved uncertainty estimates of reactor performance for devices being designed. A first attempt is made in the quantitative specification of new cross section measurements required to satisfy specific design goals.

Although there has been considerable work in this field,[2-11] many of the results to date have been of limited utility because of the paucity of covariance information for nuclear data, the lack of comprehensive libraries of sensitivity coefficients derived consistently from a well recognized nuclear data base (e.g., ENDF/B) and the lack of documented uncertainties (including correlations as well as statistical and systematic errors) in the integral experiments.

II. Formulation for Sensitivity Profiles

The theoretical development using transport theory has been derived from a differential point of view[12] and leads to analogous results to those obtained in earlier studies by Stacey[13] (using a variational approach), Usachev[14] and Gandini[15] using generalized perturbation theory. The derivation is repeated here to establish notation, to indicate how the general operator notation is implemented within multigroup transport theory approximations, and for completeness.

A. General Development

Consider for generality the complex case of a reactor integral design parameter, R, of the homogeneous bilinear ratio form

$$R \equiv \frac{\int \phi^*(\underline{\xi})\ H_1[\Sigma(\underline{\xi})]\ \phi(\underline{\xi})\ d\underline{\xi}}{\int \phi^*(\underline{\xi})\ H_2[\Sigma(\underline{\xi})]\ \phi(\underline{\xi})\ d\underline{\xi}} \tag{1}$$

where H_1 and H_2 are suitable operators which depend on the various cross sections, $\phi(\underline{\xi})$ and $\phi^*(\underline{\xi})$ are the forward and adjoint fluxes respectively, and $\underline{\xi}$ and $d\underline{\xi}$ are the position vector and differential volume element in phase space. We first outline procedures for calculating the sensitivity profile $[dR/R/(d\Sigma(\underline{\rho})/\Sigma(\underline{\rho})]$ which is the rate of change in the response per rate of change in some specific cross section, $\Sigma(\underline{\rho})$, at point $\underline{\rho}$ per unit volume in phase space. The notation $H[\Sigma(\underline{\xi})]\ \phi(\underline{\xi})$ denotes the application of the operator H on the flux ϕ, the result being a function of point $\underline{\xi}$ in phase space.

Oblow[12] has demonstrated that the required derivatives can be obtained directly using differential calculus with the concept of functional derivatives. The following steps summarize the procedure for the homogeneous bilinear response ratio of interest. Differentiating Eq. (1)

$$\left(\frac{dR}{R}\right) \Big/ \left(\frac{d\Sigma(\underline{\rho})}{\Sigma(\underline{\rho})}\right) = I_1 + I_2 + I_3 + I_4 \tag{2}$$

where

$$I_1 = \Sigma(\underline{\rho}) \frac{\int \phi^*(\underline{\xi}) \frac{dH_1[\Sigma(\underline{\xi})]}{d\Sigma(\underline{\rho})} \phi(\underline{\xi}) \, d\underline{\xi}}{\int \phi^*(\underline{\xi}) \, H_1[\Sigma(\underline{\xi})] \, \phi(\underline{\xi}) \, d\underline{\xi}} \tag{3}$$

$$I_2 = -\Sigma(\underline{\rho}) \frac{\int \phi^*(\underline{\xi}) \frac{dH_2[\Sigma(\underline{\xi})]}{d\Sigma(\underline{\rho})} \phi(\underline{\xi}) \, d\underline{\xi}}{\int \phi^*(\underline{\xi}) \, H_2[\Sigma(\underline{\xi})] \, \phi(\underline{\xi}) \, d\underline{\xi}} \tag{4}$$

$$I_3 = \frac{\Sigma(\underline{\rho})}{R} \int \frac{\partial R}{\partial \phi(\underline{\xi})} \frac{d\phi(\underline{\xi})}{d\Sigma(\underline{\rho})} \, d\underline{\xi} \tag{5}$$

$$I_4 = \frac{\Sigma(\underline{\rho})}{R} \int \frac{\partial R}{\partial \phi^*(\underline{\xi})} \frac{d\phi^*(\underline{\xi})}{d\Sigma(\underline{\rho})} \, d\underline{\xi} \tag{6}$$

Each of the derivatives above are functional derivatives characterizing the rate of change of some variable with respect to another per unit volume in phase space. The sum of I_1 and I_2 is called the direct effect, i.e., the induced change in response due to a change in a cross-section type appearing in the response definition. The cross section, $\Sigma(\underline{\rho})$ can clearly affect the fluxes at many points in phase space since fluxes at all energies are correlated through downscattering terms. For a linear, rather than a bi-linear, response function, Eqs. (3) and (4) apply with $\phi^*(\underline{\xi})$ set to unity. All integral reaction rates are assumed to be relative to some power level so that they, too, can be considered the framework of response rate ratios (reaction rate/fission).

We develop an expression for $[d\phi(\underline{\xi})/d\Sigma(\underline{\rho})]$ by differentiating the Boltzmann equation.

$$L[\Sigma(\underline{\xi})] \, \phi(\underline{\xi}) \equiv \left\{A[\Sigma(\underline{\xi})] - \lambda \, B[\Sigma(\underline{\xi})]\right\} \phi(\underline{\xi}) = 0 \tag{7}$$

$$\lambda \equiv 1/k \tag{8}$$

All terms except the fission operator, $B[\Sigma(\underline{\xi})]$, are included in the $A[\Sigma(\underline{\xi})]$ operator.

Differentiating Eq. (7) assuming λ is a constant,

$$L[\Sigma(\underline{\xi})] \frac{d\phi(\underline{\xi})}{d\Sigma(\underline{\rho})} = - \frac{dL[\Sigma(\underline{\xi})]}{d\Sigma(\underline{\rho})} \phi(\underline{\xi}) \tag{9}$$

or symbolically

$$L[\Sigma(\underline{\xi})] \psi(\underline{\xi},\underline{\rho}) = Q(\underline{\xi},\underline{\rho}) = - \frac{dL[\Sigma(\underline{\xi})]}{d\Sigma(\underline{\rho})} \phi(\underline{\xi}) \tag{10}$$

Oblow has pointed out that since $\psi(\underline{\xi},\underline{\rho})$ is to be folded with $[\partial R/\partial\phi(\underline{\xi})]$, then the integral

$$I_3(\underline{\xi}) = \int \frac{\partial R}{\partial\phi(\underline{\xi})} \psi(\underline{\xi},\underline{\rho}) \, d\underline{\xi} \tag{11}$$

might best be solved using the source $Q(\underline{\xi},\underline{\rho})$ and the function adjoint to $\psi(\underline{\xi},\underline{\rho})$. This adjoint function, Γ^*, is the solution to:

$$L^*[\Sigma(\underline{\xi})] \Gamma^*(\underline{\xi}) = S^* = \frac{\partial R}{\partial\phi(\underline{\xi})} \tag{12}$$

This equation is shown using the definition of the adjoint operator

$$\int \Gamma^*(\underline{\xi}) \, L[\Sigma(\underline{\xi})] \, \psi(\underline{\xi},\underline{\rho}) \, d\underline{\xi} = \int \psi(\underline{\xi},\underline{\rho}) \, L^*[\Sigma(\underline{\xi})] \, \Gamma^*(\underline{\xi}) \, d\underline{\xi} \tag{13}$$

and cross multiplying Eqs.(10) and (12) by Γ^* and ψ respectively, integrating and subtracting leads to

$$\int \Gamma^*(\underline{\xi}) \, Q(\underline{\xi},\underline{\rho}) \, d\underline{\xi} = \int \psi(\underline{\xi},\underline{\rho}) \frac{\partial R}{\partial\phi(\underline{\xi})} \, d\underline{\xi} \quad . \tag{14}$$

Note that it is required by the definition of R that $[\partial R/\partial\phi(\underline{\xi})]$ be orthogonal to $\phi(\underline{\xi})$. From Eq. (12):

$$\int \phi(\underline{\xi})\ L^*[\Sigma(\underline{\xi})]\ \Gamma^*(\underline{\xi})\ d\underline{\xi} = \int \phi(\underline{\xi})\ \frac{\partial R}{\partial\phi(\underline{\xi})}\ d\underline{\xi} \tag{15}$$

$$\int \Gamma^*(\underline{\xi})\ L[\Sigma(\underline{\xi})]\ \phi(\underline{\xi})\ d\underline{\xi} = \int \phi(\underline{\xi})\ \frac{\partial R}{\partial\phi(\underline{\xi})}\ d\underline{\xi} \tag{16}$$

$$0 = \int \phi(\underline{\xi})\ \frac{\partial R}{\partial\phi(\underline{\xi})}\ d\underline{\xi} \tag{17}$$

Equation (17) will be true for linear and bi-linear response <u>ratios</u> of the form of Eq. (1).

The solution to Eq. (12) is not unique to within an arbitrary addative of the solution to the homogeneous equation ϕ^*. This solution can be added to the solution of Eq. (12) and the result is also a solution of Eq. (12). To pick a unique solution, we impose the physical constraint (this or any other choice does not affect the overall calculation of the functional derivative),

$$\int \Gamma^*(\underline{\xi})\ B[\Sigma(\underline{\xi})]\ \phi(\underline{\xi})\ d\underline{\xi} = 0 \tag{18}$$

To satisfy Eq. (18), we apply an orthogonalization procedure to "sweep out" any contamination introduced by numerical procedures as follows:[a]

$$\Gamma^*(\underline{\xi}) = \Gamma_a^*(\underline{\xi}) - \left(\frac{\int \Gamma_a^*(\underline{\xi})\ B[\Sigma(\underline{\xi})]\ \phi(\underline{\xi})\ d\underline{\xi}}{\int \phi^*(\underline{\xi})\ B[\Sigma(\underline{\xi})]\ \phi(\underline{\xi})\ d\underline{\xi}}\right) \phi^*(\underline{\xi}) \tag{19}$$

where Γ_a^* represents any calculated solution to the generalized adjoint.

---

[a]Equation (19) is actually implemented by operating on $\chi\Gamma^*$ integrated over angle and energy space.

In an analogous fashion [to the derivation of Eq. (12)], it is easy to show

$$I_4(\underline{\rho}) = \int \frac{\partial R}{\partial \phi^*(\underline{\xi})} \frac{d\phi^*(\underline{\xi})}{d\Sigma(\underline{\rho})} d\underline{\xi} = \int \Gamma(\underline{\xi})\ q^*(\underline{\xi},\underline{\rho})\ d\underline{\xi} \tag{20}$$

where $\Gamma(\underline{\xi})$ is obtained by solving

$$L[\Sigma(\underline{\xi})]\ \Gamma(\underline{\xi}) = \frac{\partial R}{\partial \phi^*(\underline{\xi})} \tag{21}$$

and

$$q^*(\underline{\xi},\underline{\rho}) = - \left[\frac{dL^*[\Sigma(\underline{\xi})]}{d\Sigma(\underline{\rho})}\right] \phi^*(\underline{\xi}) \tag{22}$$

Hence, the indirect effect is comprised of two terms. The first

$$\frac{\Sigma(\underline{\rho})}{R} \int \frac{\partial R}{\partial \phi(\underline{\xi})} \frac{d\phi(\underline{\xi})}{d\Sigma(\underline{\rho})} d\underline{\xi} = - \frac{\Sigma(\underline{\rho})}{R} \int \Gamma^*(\underline{\xi}) \frac{dL[\Sigma(\underline{\xi})]}{d\Sigma(\underline{\rho})} \phi(\underline{\xi})\ d\underline{\xi} \tag{23}$$

and the second term

$$\frac{\Sigma(\underline{\rho})}{R} \int \frac{\partial R}{\partial \phi^*(\underline{\xi})} \frac{d\phi^*(\underline{\xi})}{d\Sigma(\underline{\rho})} d\underline{\xi} = - \frac{\Sigma(\underline{\rho})}{R} \int \Gamma(\underline{\xi}) \frac{dL^*[\Sigma(\underline{\xi})]}{d\Sigma(\underline{\rho})} \phi^*(\underline{\xi})\ d\underline{\xi} \tag{24}$$

For a linear ratio, this last equation should be zero on both sides since $(\partial R/\partial \phi^*) = 0$.

The final form of the sensitivity profile is:

$$\left(\frac{dR}{R}\right) \Big/ \left(\frac{d\Sigma(\underline{\rho})}{\Sigma(\underline{\rho})}\right) \tag{25}$$

$$= \left[\frac{\Sigma(\underline{\rho}) \int \phi^*(\underline{\xi}) \frac{dH_1[\Sigma(\underline{\xi})]}{d\Sigma(\underline{\rho})} \phi(\underline{\xi})\, d\underline{\xi}}{\int \phi^*(\underline{\xi})\, H_1[\Sigma(\underline{\xi})]\, \phi(\underline{\xi})\, d\underline{\xi}} - \frac{\Sigma(\underline{\rho}) \int \phi^*(\underline{\xi}) \frac{dH_2[\Sigma(\underline{\xi})]}{d\Sigma(\underline{\rho})} \phi(\underline{\xi})\, d\underline{\xi}}{\int \phi^*(\underline{\xi})\, H_2[\Sigma(\underline{\xi})]\, \phi(\underline{\xi})\, d\underline{\xi}}\right]$$

$$- \frac{\Sigma(\underline{\rho})}{R} \left[\int \Gamma^*(\underline{\xi}) \frac{dL[\Sigma(\underline{\xi})]}{d\Sigma(\underline{\rho})} \phi(\underline{\xi})\, d\underline{\xi} + \int \Gamma(\underline{\xi}) \frac{dL^*[\Sigma(\underline{\xi})]}{d\Sigma(\underline{\rho})} \phi^*(\underline{\xi})\, d\underline{\xi}\right]$$

For a linear ratio, Eq. (25) holds with ϕ^* set to unity in the first two terms and with omission of the fourth term. It should be noted here that the leakage operator $(\Omega \cdot \nabla)$ is unaffected by changes in cross section so that sensitivity through leakage is manifested indirectly through the fluxes and adjoint fluxes. Finally, it should be noted that the Boltzmann operator, $L[\Sigma(\underline{\xi})]$, includes an integral operator component (e.g., scattering).

Once ϕ, ϕ^*, Γ, and Γ^* have been determined, sensitivity functions for any and all elements of the cross section data field for a given problem can be calculated from Eq. (25). Graphical display of this function, called the sensitivity profile, provides a direct measure of the differential rate of change in R as a function of change in Σ and thus the sensitivity of R to Σ.

B. k-Sensitivity

Sensitivity profiles can be obtained from Eq. (25) for k by considering it to be a reaction rate ratio of production divided by loss (each multiplied by some arbitrary function g). From Eq. (7) we see that k can be viewed as

$$k = \frac{\int g(\underline{\xi})\ B[\Sigma(\underline{\xi})]\ \phi(\underline{\xi})\ d\underline{\xi}}{\int g(\underline{\xi})\ A[\Sigma(\underline{\xi})]\ \phi(\underline{\xi})\ d\underline{\xi}} \tag{26}$$

However, in this special case where the response of interest is the eigenvalue, it is simpler to derive the expression for the cross section sensitivity of k directly (viewed as the eigenvalue number) rather than deduce it from the more general Eq. (25). This is done in Appendix A with the result:

$$\frac{dk/k}{d\Sigma(\underline{\rho})/\Sigma(\underline{\rho})} = -\frac{\Sigma(\underline{\rho})}{k}\ \frac{\left\langle \phi^*(\underline{\xi})\ \left(\frac{dA[\Sigma(\underline{\xi})]}{d\Sigma(\underline{\rho})} - \frac{1}{k}\frac{dB[\Sigma(\underline{\xi})]}{d\Sigma(\underline{\rho})}\right)\ \phi(\underline{\xi})\right\rangle}{\left\langle \phi^*(\underline{\xi})\ \frac{1}{k^2}\ B[\Sigma(\underline{\xi})]\ \phi(\underline{\xi})\right\rangle} \tag{27}$$

The brackets imply integration over the $\underline{\xi}$ phase space. The numerator of Eq. (27) [including the $-\Sigma(\underline{\rho})/R$ term] is the same as one would obtain by ignoring the direct effect terms and evaluating only the third term of Eq. (25) setting Γ^* equal to ϕ^*. In point of fact, Γ^* is not the same as ϕ^*, but the difference between the third term contributions exactly cancels the direct effect.

III. Sensitivity Representation in Multigroup Discrete Ordinates Theory

The multigroup approximation to Eqs. (25) and (27) with spatial finite difference [16,17] is given below for the special case of spherically-symmetric, spherical geometry. These results with only slight modifications can be made to apply to the other one-dimensional configurations, namely slab and infinite-cylinder geometries.

Phase space for spherical geometry can be expressed in three variables: the radius, the energy of the particle E, and the cosine of the angle of the particle direction (μ) relative to the radius vector.

$$\text{differential phase space cell} = 8\pi^2 r^2 \, dr \, dE \, d\mu \tag{28}$$

$$\text{finite-difference cell} = V_I \, \Delta E_G \, \Delta\mu_D \, 2\pi$$

where

$$V_I = \frac{4}{3}\pi(r_{i+1}^3 - r_i^3),$$

$$\Delta E_G = E_{g+1} - E_g,$$

$$\Delta\mu_D = \mu_{d+1} - \mu_d.$$

In this spherical geometry Eq. (7), the Boltzmann equation, has the specific form:

$$\mu \frac{\partial\phi}{\partial r}(\underline{r},E,\mu) + \frac{1-\mu^2}{r}\frac{\partial\phi}{\partial\mu} + \Sigma_T(\underline{r},E)\,\phi \tag{29}$$

$$= 2\pi\int_0^\infty \int_{-1}^{+1} dE' \, d\mu' \, \phi(\underline{r},E',\mu') \, \Sigma(\underline{r},E'\to E,\mu'\to\mu)$$

$$+ \frac{1}{k}\int_0^\infty \int_{-1}^{+1} \frac{\nu\,\Sigma_f(\underline{r},E'\to E)}{2}\,\phi(\underline{r},E',\mu') \, d\mu' \, dE'$$

$\phi(\underline{r},E,\mu)$ is the flux per unit solid angle per unit energy. The adjoint Boltzmann equation takes the form:

$$- \mu \frac{\partial \phi^*}{\partial r} (\underline{r},E,\mu) - \frac{1 - \mu^2}{r} \frac{\partial \phi^*}{\partial \mu} + \Sigma_T(r,E)\ \phi^* \tag{30}$$

$$= 2\pi \int_0^\infty \int_{-1}^{+1} dE'\ d\mu'\ \phi^*(\underline{r},E',\mu')\ \Sigma(\underline{r},E\to E',\mu\to\mu')$$

$$+ \frac{1}{k} \int_0^\infty \int_{-1}^{+1} \frac{\nu\ \Sigma_f(\underline{r},E\to E')}{2}\ \phi^*(r,E',\mu')\ d\mu'\ dE'$$

$\phi^*(\underline{r},E,\mu)$ is the "value" of a neutron at position $\underline{r}$, energy E, and cosine μ. $2\pi\ \Sigma(\underline{r},E'\to E,\mu'\to\mu)$ is the cross section for a neutron with initial energy E' and direction cosine μ' to undergo a scattering collision at $\underline{r}$, resulting in a final energy lying in dE about E and a new direction which lies in $d\mu$ about μ. The discrete ordinates difference equation is obtained by applying the integral operator

$$\int_{r\varepsilon V_I} \int_{E\varepsilon\Delta E_G} \int_{\mu\varepsilon\Delta\mu_D} 8\pi^2\ r^2\ dr\ dE\ d\mu$$

to Eqs. (29) and (30) using the following definitions (note that small letters correspond to interval boundary values and capital letters indicate interval values)

$$\phi_G(\underline{r},\mu) \equiv \int_{E\varepsilon\Delta E_G} \phi(\underline{r},E,\mu)\ dE \tag{31}$$

$$\phi_{i,G}(\mu) = \phi_G(r_i,\mu) \tag{32}$$

$$\phi_{i,G,D} = \phi_{I,G}(\overline{\mu}_D) \tag{33}$$

$$\underline{A}_i = 4\pi r_i^2 \tag{34}$$

$$\text{curvature coefficient } \underline{B}_{I,d} \equiv 4\pi r_i\ \Delta r_i(1 - \mu_d) \tag{35}$$

$$2\pi\ \Sigma(\underline{r},E'\rightarrow E,\mu'\rightarrow\mu) = \int \Sigma(\underline{r},E'\rightarrow E,\underline{\Omega}'\rightarrow\underline{\Omega})\ d\alpha \tag{36}$$

α is the azimuthal angle.

χ_g = the fission spectrum.

The results[17] of applying the integral operator to Eq. (29) (using the notation established above) is

$$\bar{\mu}_D(\underline{A}_{i+1}\ \phi_{i+1,G,D} - \underline{A}_i\ \phi_{i,G,D}) + \frac{1}{\Delta\mu_D}(\underline{B}_{I,d+1}\ \phi_{I,G,d+1} - \underline{B}_{I,d}\ \phi_{I,G,d}) + V_I\ \Sigma^T_{G,I}\ \phi_{I,G,D} \tag{37}$$

$$= V_I \sum_{\ell=0}^{LMAX} \frac{2\ell+1}{4\pi} P_\ell(\bar{\mu}_D) \sum_{G'=1}^{NOG} \Sigma^{\ell,I}_{G'\rightarrow G}\ \phi^\ell_{I,G'} + \frac{V_I\ \chi_G}{4\pi\ k_{eff}} \sum_{G'=1}^{NOG} \nu\ \Sigma^I_{fG'}\ \phi^0_{I,G'}$$

Equation (37) contains the discrete-flux variables having both centered and end point subscripts which must be related in some consistent fashion. The diamond difference technique is the most widely used method for this purpose.

$$\phi_{i,G,D} = 2\ \phi_{I,G,D} - \phi_{i+1,G,D} \text{ for all } \mu \tag{38}$$

and

$$\phi_{I,G,d+1} = 2\ \phi_{I,G,D} - \phi_{I,G,d} \tag{39}$$

Combining Eqs. (37), (38), and (39) results in the following discrete ordinates approximation for the transport equation:

$$- \bar{\mu}_D(A_{i+1} + A_i)\ \phi_{i,G,D} + 2\ \bar{\mu}_D\ A_{i+1}\ \phi_{I,G,D} \tag{40}$$

$$- \frac{1}{\Delta\mu_D}\ (B_{I,d+1} + B_{I,d})\ \phi_{I,G,d} + \frac{2\ B_{I,d+1}}{\Delta\mu_D}\ \phi_{I,G,D}$$

$$+ V_I\ \Sigma^T_{G,I}\ \phi_{I,G,D} - V_I \sum_{\ell=o}^{LMAX} \frac{2\ell+1}{4\pi}\ P_\ell(\bar{\mu}_D) \sum_{G'=1}^{NOG} \Sigma^{\ell,I}_{G'\to G}\ \phi^{\ell}_{I,G'}$$

$$- \frac{V_I\ \chi_G}{4\pi\ k_{eff}} \sum_{G'=1}^{NOG} \nu\ \Sigma^I_{fG'}\ \phi^0_{I,G'} = 0$$

The equation adjoint to Eq. (40) is:

$$+ \bar{\mu}_D(A_{i+1} + A_i)\ \phi^*_{i,G,D} - 2\bar{\mu}_D\ A_{i+1}\ \phi^*_{I,G,D} \tag{41}$$

$$+ \frac{1}{\Delta\mu_D}\ (B_{I,d+1} + B_{I,d})\ \phi^*_{I,G,d} - \frac{2\ B_{I,d+1}}{\Delta\mu_D}\ \phi^*_{I,G,D}$$

$$+ V_I\ \Sigma^T_{G,I}\ \phi^*_{I,G,D} - V_I \sum_{\ell=o}^{LMAX} (2\ell+1)\ P_\ell(\bar{\mu}_D) \sum_{G'=1}^{NOG} \Sigma^{\ell,I}_{G\to G'}\ \phi^{*\ell}_{I,G'}$$

$$- \frac{V_I\ \nu\ \Sigma^I_{fG}}{k_{eff}} \sum_{G'=1}^{NOG} \chi_{G'}\ \phi^{*0}_{I,G'} = 0$$

Although derived for spherical geometry, that is, for $\underline{A}_i = 4\pi r_i^2$ and $V_I = \frac{4}{3}\pi(r_{i+1}^3 - r_i^3)$, Eqs. (40) and (41) are general discrete ordinates difference equations for one-dimensional geometries. The equations for the other geometries are obtained by merely setting $\underline{A}_i = 1.0$ and $V_i = \Delta r_i$ for slab and $\underline{A}_i = 2\pi r_i$ and $V_i = \pi(r_{i+1}^2 - r_i^2)$ for cylinder, and including associated Legendre polynomial expansions for cylindrical geometry.

One observes by inspection of Eqs. (40) and (41) that the streaming terms have no explicit cross-section dependence and so can be disregarded in evaluation of Eqs. (25) and (27). More explicit definitions of the applicable operators can now be made

$$A[\Sigma(\underline{\xi})]\ \phi(\underline{\xi}) \Rightarrow V_I\ \Sigma^T_{G,I}\ \phi_{I,G,D} - V_I \sum_{\ell=0}^{LMAX} \frac{2\ell+1}{4\pi} P_\ell(\bar{\mu}_D) \sum_{G'=1}^{NOG} \Sigma^{\ell,I}_{G'\to G}\ \phi^{\ell}_{I,G'} \tag{42}$$

$$\lambda B[\Sigma(\underline{\xi})]\ \phi(\underline{\xi}) \Rightarrow + \frac{V_I\ \chi_g}{4\pi\ k_{eff}} \sum_{G'=1}^{NOG} \nu\ \Sigma^I_{fG'}\ \phi^0_{I,G'} \tag{43}$$

$$A^*[\Sigma(\underline{\xi})]\ \phi^*(\underline{\xi}) \Rightarrow V_I\ \Sigma^T_{G,I}\ \phi^*_{I,G,D} - V_I \sum_{\ell=0}^{LMAX} (2\ell+1)\ P_\ell(\bar{\mu}_D) \sum_{G'=1}^{NOG} \Sigma^{\ell,I}_{G\to G'}\ \phi^{*\ell}_{I,G'} \tag{44}$$

$$\lambda B^*[\Sigma(\underline{\xi})]\ \phi^*(\underline{\xi}) \Rightarrow \frac{V_I\ \nu\ \Sigma^I_{fG}}{k_{eff}} \sum_{G'=1}^{NOG} \chi_{G'}\ \phi^{*0}_{I,G'} \tag{45}$$

We make the following definitions:

- Z spatial zone (Z=1,NZONE); cross sections constant across zone,
- D quadrature angle (D=1,NOA); associated weight WT_D,
- X particular material and cross-section type (X=1,NTYP),
- d_{XZ} atomic number density for cross section X in zone Z,
- I spatial interval (I=1,INT), $I \varepsilon$ IZONE(Z),
- IZONE(Z) the set of integers representing the intervals belonging to zone Z,
- ℓ Legendre moment (ℓ=0,LMAX).

in order to evaluate the expression for the sensitivity profiles.

A. k-Profiles*

1. Absorption reactions [e.g., (n,p), (n,α), (n,γ), etc.]. Consider the denominator of Eq. (27) using the definitions above and applying Eq. (43)

$$\mathcal{J}_1 \equiv \frac{1}{k^2}\left\langle \phi^*(\underline{\xi})\ B[\Sigma(\underline{\xi})]\ \phi(\underline{\xi})\right\rangle = \tag{46}$$

$$\frac{1}{k^2}\sum_{X=1}^{NF}\ \sum_{Z=1}^{NZONE} d_{XZ} \sum_{I\varepsilon IZONE(Z)} V_I \sum_{G=1}^{NOG} \phi^{*0}_{I,G}\ \chi^{XZ}_G$$

$$\times \sum_{G'=1}^{NOG} \nu^Z_{X,G'}\ \sigma^Z_{X,G'}\ \phi^0_{I,G'}$$

In Eq. (46), the sum is over X corresponding to the sum of all fission reactions F.

$$\frac{dk/k}{d\Sigma^{XZ}_G/\Sigma^{XZ}_G} = -\frac{\frac{1}{k}\, d_{XZ}\ \sigma^Z_{X,G} \sum_{I\varepsilon IZONE(Z)} V_I \sum_{D=1}^{NOA} \phi_{I,G,D}\ \phi^*_{I,G,D}\ WT_D}{\mathcal{J}_1} \tag{47}$$

This then is the relative sensitivity of k with respect to the cross section of (absorption) type X in group G and zone Z.

---

*All of the following represent straightforward extensions to the formalism derived and implemented in the SWANLAKE[18] code for fixed source problems; superscript zero on flux quantities implies an integration of the angular flux and angle (i.e., $\phi^{*0}_{I,G} = \sum_{D=1}^{NOA} \phi^*_{I,G,D}\ WT_D$).

2. Scattering reactions [e.g., (n,n), (n,n'), (n,2n), etc.]. We are interested in the sensitivity with respect to the ℓ'th moment of a group-to-group scattering for material X in zone Z from group G' to group G. In addition to a contribution similar to that of Eq. (47) (from the zero'th component of the elastic scattering cross section) there is an additional contribution arising from differentiating the scattering integral term [second term of Eq. (42)]. The process of differentiation imposes delta functions on initial and final group, material, zone of interest, and Legendre scattering order leading to the additional term

$$\frac{\partial}{\partial \Sigma^{Z,\ell}_{X,G'\to G}} \left[- \sum_{X} \sum_{Z=1}^{NZONE} d_{XZ} \sum_{I\varepsilon IZONE(Z)} V_I \sum_{\ell=o}^{LMAX} (2\ell+1) \sum_{G=1}^{NOG} \sum_{G'=1}^{NOG} \times \phi^{*\ell}_{I,G}\, \sigma^{Z,\ell}_{X,G'\to G}\, \phi^{\ell}_{I,G'} \right] = \tag{48}$$

$$- d_{XZ} \sum_{I\varepsilon IZONE(Z)} V_I\, (2\ell+1)\, \phi^{*\ell}_{I,G}\, \sigma^{Z,\ell}_{X,G'\to G}\, \phi^{\ell}_{I,G'} \tag{49}$$

The sensitivity of k to the ℓ'th moment of a particular group-to-group transfer for a specific material and zone is:

$$\frac{dk/k}{\left(\dfrac{d\Sigma^{Z,\ell}_{X,G'\to G}}{\Sigma^{Z,\ell}_{X,G'\to G}}\right)} = - \frac{1}{k} \frac{\left[d_{XZ}\, \sigma^{Z,\ell}_{X,G'\to G}\, \delta_{\ell,o} \sum_{I\varepsilon IZONE(Z)} V_I \sum_{D=1}^{NOA} \phi_{I,G',D}\, \phi^{*}_{I,G',D}\, WT_D - d_{XZ} \sum_{I\varepsilon IZONE(Z)} V_I\, (2\ell+1)\, \phi^{*\ell}_{I,G}\, \sigma^{Z,\ell}_{X,G'\to G}\, \phi^{\ell}_{I,G'} \right]}{\mathcal{S}_1} \tag{50}$$

In the case where the functional dependence of all transfers is the same (e.g., the dependence on the elastic scattering cross section being through the magnitude of the cross section rather than through the

probability of transfers to various energy groups), the rate of change with respect to the scattering cross section is obtained by summing Eq. (50) over all outgoing groups G and order types ℓ. The result for scattering cross section $\Sigma_{G'}^{XZ}$ of type X in zone Z for group G' is

$$\frac{dk/k}{d\Sigma_{G'}^{XZ}/\Sigma_{G'}^{XZ}} = -\frac{1}{k}\left[d_{XZ}\,\sigma_{X,G'}^{Z}\sum_{I\varepsilon IZONE(Z)} V_I \sum_{D=1}^{NOA} \phi_{I,G',D}\,\phi_{I,G',D}^{*}\,WT_D - d_{XZ}\sum_{I\varepsilon IZONE(Z)} V_I \sum_{G=1}^{NOG}\sum_{\ell=o}^{LMAX} (2\ell+1)\,\phi_{I,G}^{*\ell}\,\sigma_{X,G'\to G}^{Z,\ell}\,\phi_{I,G'}^{\ell}\right] \Big/ \mathcal{J}_1 \tag{51}$$

3. Fission reactions. This case is similar to that for Eq. (47) with X being the fission cross section. The main difference is the contribution from the fission integral term [Eq. (43)]

$$\frac{dk/k}{d\Sigma_{G}^{FZ}/\Sigma_{G}^{FZ}} = -\frac{1}{k}\left\{d_{XZ}\,\sigma_{F,G}^{Z}\sum_{I\varepsilon IZONE(Z)} V_I \sum_{D=1}^{NOA} \phi_{I,G,D}\,\phi_{I,G,D}^{*}\,WT_D - \frac{1}{k}\,d_{XZ}\sum_{I\varepsilon IZONE(Z)} V_I \left[\nu_{F,G}^{Z}\,\sigma_{F,G}^{Z}\,\phi_{I,G}^{0}\sum_{G'=1}^{NOG} \phi_{I,G'}^{*0}\,\chi_{G'}^{F,Z}\right]\right\} \Big/ \mathcal{J}_1 \tag{52}$$

4. ν-Sensitivity. This case is identical to Eq. (52) except that ν is not part of the total cross section so that the removal term [first term of Eq. (52)] is not present

$$\frac{dk/k}{d\nu_{F,G}^{Z}/\nu_{F,G}^{Z}} = \frac{\frac{1}{k^2}\,d_{XZ}\sum_{I\varepsilon IZONE(Z)} V_I \left[\nu_{F,G}^{Z}\,\sigma_{F,G}^{Z}\,\phi_{I,G}^{0}\sum_{G'=1}^{NOG} \phi_{I,G'}^{*0}\,\chi_{G'}^{F,Z}\right]}{\mathcal{J}_1} \tag{53}$$

Here F refers to the particular fissile material and to the fission reaction. The ν-sensitivies for k correspond to the fraction of fissions taking place with a given fission reaction type F; clearly the ν-sensitivities sum to unity.

B. Central Reaction Rate Ratio Profiles

These calculations are similar to those described in the previous sections with the notable exceptions that contributions from the direct effect components [Eqs. (3) and (4)] must be included (when applicable) and that the generalized functions (Γ^*,Γ) must be used in the evaluation of the indirect effects [third and fourth term of Eq. (25)]. It should be noted that all reaction rate ratios analyzed in accordance with CSEWG critical measurements refer specifically to the central interval alone. Such a central reaction rate ratio has the following form:

$$R = \frac{d_{1C} \sum_{G=1}^{NOG} \sigma^{C}_{1,G} \phi^{0}_{C,G}}{d_{2C} \sum_{G=1}^{NOG} \sigma^{C}_{2,G} \phi^{0}_{C,G}} \tag{54}$$

The superscript and subscript C refers to the central interval (which is the same as the central zone for purposes of this analysis). The numerical subscripts refer to cross sections of type 1 and 2, respectively. The subscripts G and C refer to the integrated angular flux over energy group G and volume C; the scalar fluxes are obtained by integrating angular flux tapes (i.e., $\phi^{0}_{C,G} = \sum_{D=1}^{NOA} \phi_{C,G,D}\, WT_D$). For a response of the form of Eq. (54), $(\partial R/\partial\phi^*) = 0$ so that the contribution I_4 [see Eq. (6)] vanishes. The ℓ'th moment of the source for the generalized adjoint equation [Eq. (12)] is:

$$S^{*\ell}_{C,G} = \frac{\partial R}{\partial \phi^{\ell}_{C,G}} = R \left[\frac{\sigma^{C}_{1,G}}{\sum_{G=1}^{NOG} \sigma^{C}_{1,G} \phi^{0}_{C,G}} - \frac{\sigma^{C}_{2,G}}{\sum_{G=1}^{NOG} \sigma^{C}_{2,G} \phi^{0}_{C,G}} \right] \delta_{\ell o} \tag{55}$$

Note there would be a sum over intervals (zones) if the reaction rate were distributed in space.

Sensitivity profiles for cross sections appearing explicitly in the definition [Eq. (54)] can include direct effect terms (I_1 and I_2) as well as indirect effects (I_3). These direct contributions are

$$\left(\frac{dR/R}{d\Sigma_G^{XC}/\Sigma_G^{XC}}\right)_{direct} \tag{56}$$

$$= \frac{\sigma_{1,G}^{C}\ \phi_{C,G}^{0}\ \delta_{X,1}}{\sum_{G'=1}^{NOG} \sigma_{1,G'}^{C}\ \phi_{C,G'}^{0}} - \frac{\sigma_{2,G}^{C}\ \phi_{C,G}^{0}\ \delta_{X,2}}{\sum_{G'=1}^{NOG} \sigma_{2,G'}^{C}\ \phi_{C,G'}^{0}}$$

where the delta function, $\delta_{X,n}$, ensures that the cross section with index X occurs directly in the numerator (n=1) or in the denominator (n=2) to produce a non-zero contribution.

Reaction rate ratios studied to date include only the fission and capture reactions. For the central reaction rate ratios of the form in Eq. (54) we present below the explicit expressions for cross-section sensitivity profiles.

1. <u>Absorption reactions [e.g., (n,p), (n,α), (n,γ), etc.]</u>

$$\frac{dR/R}{d\Sigma_G^{XZ}/\Sigma_G^{XZ}} = \left[\frac{\sigma_{1,G}^{Z}\ \phi_{C,G}^{0}\ \delta_{X,1}}{\sum_{G'=1}^{NOG} \sigma_{1,G'}^{C}\ \phi_{C,G'}^{0}} - \frac{\sigma_{2,G}^{Z}\ \phi_{C,G}^{0}\ \delta_{X,2}}{\sum_{G'=1}^{NOG} \sigma_{2,G'}^{C}\ \phi_{C,G'}^{0}}\right] \delta_{ZC} \tag{57}$$

$$- \frac{1}{R}\, d_{XZ}\, \sigma_{X,G}^{Z} \sum_{I \varepsilon IZONE(Z)} V_I \sum_{D=1}^{NOA} \phi_{I,G,D}\ \Gamma_{I,G,D}^{*}\ WT_D$$

2. Scattering reactions [e.g., (n,n), (n,n'), (n,2n), etc.]. Assuming no direct effect component (response ratios of capture and fission cross sections), the sensitivity profile is:

$$\frac{dR/R}{d\Sigma^{XZ}_{G'}/\Sigma^{XZ}_{G'}} = -\frac{1}{R}\left[d_{XZ}\,\sigma^{Z}_{X,G'}\sum_{I\varepsilon IZONE(Z)} V_I \sum_{D=1}^{NOA}\phi_{I,G',D}\,\Gamma^{*}_{I,G',D}\,WT_D \right. \tag{58}$$

$$\left. - d_{XZ}\sum_{I\varepsilon IZONE(Z)} V_I \sum_{G=1}^{NOG}\sum_{\ell=o}^{LMAX}(2\ell+1)\,\Gamma^{*\ell}_{I,G}\,\sigma^{Z,\ell}_{X,G'\to G}\,\phi^{\ell}_{I,G'}\right]$$

As in Eq. (51), this assumes that scattering reactions are affected through the scattering cross section, with the probability distribution for scattering to the various final groups unaffected.

3. Fission reactions.

$$\frac{dR/R}{d\Sigma^{FZ}_{G}/\Sigma^{FZ}_{G}} = \left(\frac{\sigma^{C}_{1,G}\,\phi^{0}_{C,G}\,\delta_{F,1}}{\sum_{G'=1}^{NOG}\sigma^{C}_{1,G'}\,\phi^{0}_{C,G'}} - \frac{\sigma^{C}_{2,G}\,\phi^{0}_{C,G}\,\delta_{F,2}}{\sum_{G'=1}^{NOG}\sigma^{C}_{2,G'}\,\phi^{0}_{C,G'}}\right)\delta_{FC} \tag{59}$$

$$-\frac{1}{R}\left\{d_{XZ}\,\sigma^{Z}_{F,G}\sum_{I\varepsilon IZONE(Z)} V_I\sum_{D=1}^{NOA}\phi_{I,G,D}\,\Gamma^{*}_{I,G,D}\,WT_D - \right.$$

$$\left.\frac{1}{k}\,d_{XZ}\sum_{I\varepsilon IZONE(Z)} V_I\left[\nu^{Z}_{F,G}\,\sigma^{Z}_{F,G}\,\phi^{0}_{I,G}\sum_{G'=1}^{NOG}\Gamma^{*o}_{I,G'}\,\chi^{F,Z}_{G'}\right]\right\}$$

4. ν-Sensitivity.

$$\frac{dR/R}{d\nu^{Z}_{F,G}/\nu^{Z}_{F,G}} = \frac{1}{kR}\,d_{XZ}\sum_{I\varepsilon IZONE(Z)} V_I\,\nu^{Z}_{F,G}\,\sigma^{Z}_{F,G}\,\phi^{0}_{I,G}\sum_{G'=1}^{NOG}\Gamma^{*o}_{I,G'}\,\chi^{F,Z}_{G'} \tag{60}$$

C. Total Profiles

The concept of "total profile" for a given nuclide is here defined as the sum of the sensitivity coefficients for all reactions in a particular energy group with the nuclide of interest in every zone in which it appears. The energy integrated total profile is the equivalent of the rate of change in a result with respect to the atom density of that nuclide.

IV. k-Reset

The previous sections described calculation of sensitivity coefficients without regard to system constraints. For the design of new facilities, where criticality will be achieved in predetermined fashion (e.g., through control rod movement, change of enrichment etc.) sensitivity profiles must be calculated recognizing that the physical system will indeed be forced to become critical. Under these conditions, local derivatives for arbitrary response function must include compensating terms which ensure criticality. For example, one may envision a cross-section alteration (reset) in a fixed cross section Σ_C which would act to constrain k in evaluation of derivatives of other response functions with respect to other cross sections Σ_X.

$$\frac{dk/k}{d\Sigma_X^G/\Sigma_X^G} = - a^G \frac{dk/k}{d\Sigma_C/\Sigma_C} \tag{61}$$

However, compensation as regards Eq. (61) introduces the additional term $[(dk/k)/(d\Sigma_C^G/\Sigma_C^G)]$ so that the final expression for the sensitivity profile is:

$$\left(\frac{dR/R}{d\Sigma_X^G/\Sigma_X^G}\right)_{\substack{\text{including}\\ \text{reset}}} = \left(\frac{dR/R}{d\Sigma_X^G/\Sigma_X^G}\right)_{\substack{\text{without}\\ \text{reset}}} \tag{62}$$

$$- \frac{[(dR/R)/(d\Sigma_C/\Sigma_C)]}{[(dk/k)/(d\Sigma_C/\Sigma_C)]} \quad \frac{dk/k}{d\Sigma_X^G/\Sigma_X^G}$$

Equation (62) is most appropriate in design situations with determined procedures to achieve criticality. For as-built situations (e.g., integral measurements already performed, e.g., ZPR-6/7), with fixed dimensions, concentrations, etc., the use of one single degree of freedom ($d\Sigma_C/\Sigma_C$) is no longer appropriate. Constrained derivatives may be formulated using procedures which allow the compensation to be made by employing a variation of all system parameters which are not known precisely. A complete analysis would consider all possible combinations, weighted according to appropriate probability distributions. This work is still under active development. As of today, in our analysis of integral experiments, no k-reset mechanism has been implemented.

V. Specific Examples of Sensitivity Analysis

One-dimensional analyses are presented below for ZPR-6/6A, ZPR-6/7, and GODIVA. The first two assemblies are characteristic of LMFBR spectral environments while the latter has been used extensively to verify high energy cross section data for the uranium isotopes. (We also have completed similar analyses for ZPR-3/56B and ZPR-3/11; these are presented in a compansion document.[19]) Broad-group sensitivity coefficients for ZPR-6/7 and ZPR-6/6A have been generated independently at ANL; confidence in both the ORNL and ANL results has grown out of the successful comparison.

A. Assembly Description

All assemblies are described in detail in ENDF-202, the CSEWG Benchmark Specifications Book.[20]

ZPR-6/6A is a large (4000 liter), uranium oxide fueled fast critical assembly blanketed axially and radially with depleted uranium. The one-dimensional spherical homogeneous model used for the analysis (separate heterogeneity and two-dimensional corrections supplied) has a core radius of 95.7 cm and a blanket thickness of 33.8 cm. ZPR-6/7 is a large (3100 liter), plutonium oxide fueled, fast critical assembly composed of stainless steel drawers of fuel and diluent. It has a unit cell identical

to ZPR-6/6A except that Pu/U/Mo (28 w/o Pu, 69.5 w/o U, and 2.5 w/o Mo) is the fuel rather than enriched uranium. The plutonium is 11.5 w/o ^{240}Pu. The one-dimensional spherical homogeneous model used for the analysis has a core radius and blanket thickness of 88.2 and 33.8 cm, respectively. GODIVA, a bare sphere of enriched uranium metal, has a core radius of 8.74 cm and atomic densities of .045/.002498/.000392 atoms/barn-cm for $^{235}U/^{238}U/^{234}U$, respectively. The nuclide concentrations of the ZPR-6/6A and ZPR-6/7 assemblies are given in Appendix B.

B. Tabulation of Integral Sensitivities

Tables I, II, and III list the sensitivities of performance parameters for ZPR-6/6A, ZPR-6/7, and GODIVA to various important reaction types. The sensitivities tabulated correspond to a uniform one percent change in cross section over all energy. (Energy dependent sensitivity curves are given in later sections.) Also listed are our calculated results for these specific performance parameters and the ratio of calculation/experiment to indicate the type of agreement currently obtained.[21]

C. Calculational Procedure

The FORSS sensitivity code system, described here, is a modular system of programs developed to solve the equations presented in the previous section and thereby address directly questions of data-related design uncertainties and performance confidence limits. System description is best made with respect to the (simplified) diagram shown in Fig. 1. Pseudo composition-independent cross section data are prepared using MINX[22] for neutrons, AMPX[23] modules SMUG and LAPHNGAS for gamma-ray production and interaction, and PUFF[24] for covariance matrices. Composition-dependent coupled cross sections are prepared using SPHINX[25] and ANISN.[26] Calculations of both regular and generalized forward and adjoint fluxes can be made* using either ANISN, DOT,[27] or VENTURE.[28] The purpose of the JULIET module is to calculate generalized sources required for the

*To date, only ANISN has been used extensively.

Table I

Relative Sensitivity of ZPR-6/6A Performance Parameters to Various Cross Section Reaction Types[a]

k Calculated[b] 0.9999 Calculation/Experiment 0.9999		$^{28}c/^{25}f$ (Central) Calculated[b] 0.1388 Calculation/Experiment 1.007		$^{28}f/^{25}f$ (Central) Calculated[b] 0.02212 Calculation/Experiment 0.917	
Reaction	Relative Sensitivity[c]	Reaction	Relative Sensitivity[c]	Reaction	Relative Sensitivity[c]
$^{235}U(\bar{\nu})$:	+0.881	$^{235}U(n,f)$:	-1.033	$^{238}U(n,f)$:	+0.964
$^{235}U(n,f)$:	+0.537	$^{238}U(n,\gamma)$:	+0.966	$^{235}U(n,f)$:	-0.629
$^{238}U(n,\gamma)$:	-0.265	O(n,n):	+0.041	$^{238}U(n,\gamma)$:	+0.294
$^{238}U(\bar{\nu})$:	+0.119	$^{238}U(n,n')$:	+0.035	$^{238}U(n,n')$:	-0.279
$^{235}U(n,\gamma)$:	-0.100	Fe(n,n'):	+0.014	Fe(n,n'):	-0.226
$^{238}U(n,f)$:	+0.075	$^{235}U(n,\gamma)$:	-0.008	O(n,n):	-0.141
O(n,n):	+0.034	Na(n,n'):	+0.008	$^{235}U(n,\gamma)$:	+0.114
Fe(n,n):	+0.029	Fe(n,n):	+0.004	Na(n,n'):	-0.082
Na(n,n):	+0.027	$^{238}U(n,f)$:	+0.002	Na(n,n):	-0.069
Fe(n,γ):	-0.019	$^{235}U(\bar{\nu})$:	-0.002	Fe(n,n):	-0.056
$^{238}U(n,n')$:	-0.017	Fe(n,γ):	-0.001	Fe(n,γ):	+0.021
Fe(n,n'):	-0.014			$^{235}U(\bar{\nu})$:	+0.012
Na(n,n'):	-0.004			$^{238}U(\bar{\nu})$:	-0.008
Na(n,γ):	-0.003			Na(n,γ):	+0.003

[a]Calculated and C/E values listed for heterogeneous system (calculations include appropriate corrections);[20] responses reported are microscopic (atom densities divided out); sensitivity profiles based on homogeneous model. Multigroup cross sections do not include recent methods improvement in performing unresolved quadrature.

[b]Transport theory, 126 groups.

[c]This is percent change in response per percent change in cross section uniformly over all energy.

Table II

Relative Sensitivity of ZPR-6/7 Performance Parameters to Various Cross Section Reaction Types[a]

k Calculated[b] 0.9885 Calculation/Experiment 0.9885		$^{28}c/^{49}f$ (Central) Calculated[b] 0.1502 Calculation/Experiment 1.073		$^{28}f/^{49}f$ (Central) Calculated[b] 0.02246 Calculation/Experiment 0.961	
Reaction	Relative Sensitivity[c]	Reaction	Relative Sensitivity[c]	Reaction	Relative Sensitivity[c]
$^{239}Pu(\bar{\nu})$:	+0.818	$^{239}Pu(n,f)$:	-1.073	$^{238}U(n,f)$:	+0.960
$^{239}Pu(n,f)$:	+0.591	$^{238}U(n,\gamma)$:	+0.896	$^{239}Pu(n,f)$:	-0.761
$^{238}U(n,\gamma)$:	-0.239	O(n,n):	+0.109	$^{238}U(n,\gamma)$:	+0.271
$^{238}U(\bar{\nu})$:	+0.126	$^{235}U(n,n')$:	+0.068	$^{238}U(n,n')$:	-0.248
$^{238}U(n,f)$:	+0.079	Na(n,n):	+0.028	Fe(n,n'):	-0.199
$^{239}Pu(n,\gamma)$:	-0.067	Fe(n,n'):	+0.025	O(n,n):	-0.089
$^{238}U(n,n')$:	-0.042	Fe(n,n):	+0.024	$^{239}Pu(n,\gamma)$:	+0.079
Fe(n,n'):	-0.024	$^{239}Pu(n,\gamma)$:	-0.020	Na(n,n'):	-0.075
$^{240}Pu(\bar{\nu})$:	+0.023	Na(n,n'):	+0.016	Na(n,n):	-0.048
Fe(n,γ):	-0.020	Fe(n,γ):	-0.007	Fe(n,n):	-0.044
Fe(n,n):	+0.019	$^{238}U(n,f)$:	+0.005	Fe(n,γ):	+0.024
$^{241}Pu(\bar{\nu})$:	+0.018	$^{238}U(\bar{\nu})$:	+0.0034	$^{241}Pu(n,f)$:	+0.005
$^{240}Pu(n,f)$:	+0.016	$^{239}Pu(\bar{\nu})$:	-0.0033	Na(n,γ):	+0.003
$^{241}Pu(n,f)$:	+0.013	$^{240}Pu(n,\gamma)$:	-0.003	$^{240}Pu(n,f)$:	+0.003
Na(n,n'):	-0.010	$^{241}Pu(n,f)$:	-0.002		
O(n,n):	-0.009				
$^{240}Pu(n,\gamma)$:	-0.009				
Na(n,n):	+0.009				
$^{235}U(n,f)$:	+0.009				
$^{239}Pu(n,n')$:	-0.004				
Na(n,γ):	-0.003				
$^{235}U(n,\gamma)$:	-0.001				

[a]Calculated and C/E values listed for heterogeneous system (calculations include appropriate corrections);[20] responses reported are microscopic (atom densities divided out); sensitivity profiles based on homogeneous model. Multigroup cross sections do not include recent methods improvement in performing unresolved quadrature.

[b]Transport theory, 126 groups.

[c]This is percent change in response per percent change in cross section uniformly over all energy.

Table III

Relative Sensitivity of GODIVA Performance Parameters to Various Cross Section Reaction Types[a]

k Calculated[b]	Calculation/Experiment
1.0033	1.0033

Reaction	Relative Sensitivity[c]
$^{235}U(\bar{\nu})$:	+0.982
$^{235}U(n,f)$:	+0.659
$^{235}U(n,\gamma)$:	-0.037
$^{238}U(\bar{\nu})$:	+0.0098
$^{238}U(n,f)$:	+0.007
$^{234}U(\bar{\nu})$:	+0.0083
$^{234}U(n,f)$:	+0.006
$^{238}U(n,\gamma)$:	-0.001

[a]Calculated and C/E values listed for heterogeneous system (calculations include appropriate corrections);[20] sensitivity profiles based on homogeneous model. Multigroup cross sections do not include recent methods improvement in performing unresolved quadrature.

[b]Transport theory, 126 groups

[c]This is percent change in response to percent change in cross section uniformly over all energy.

ORNL DWG 75-15524

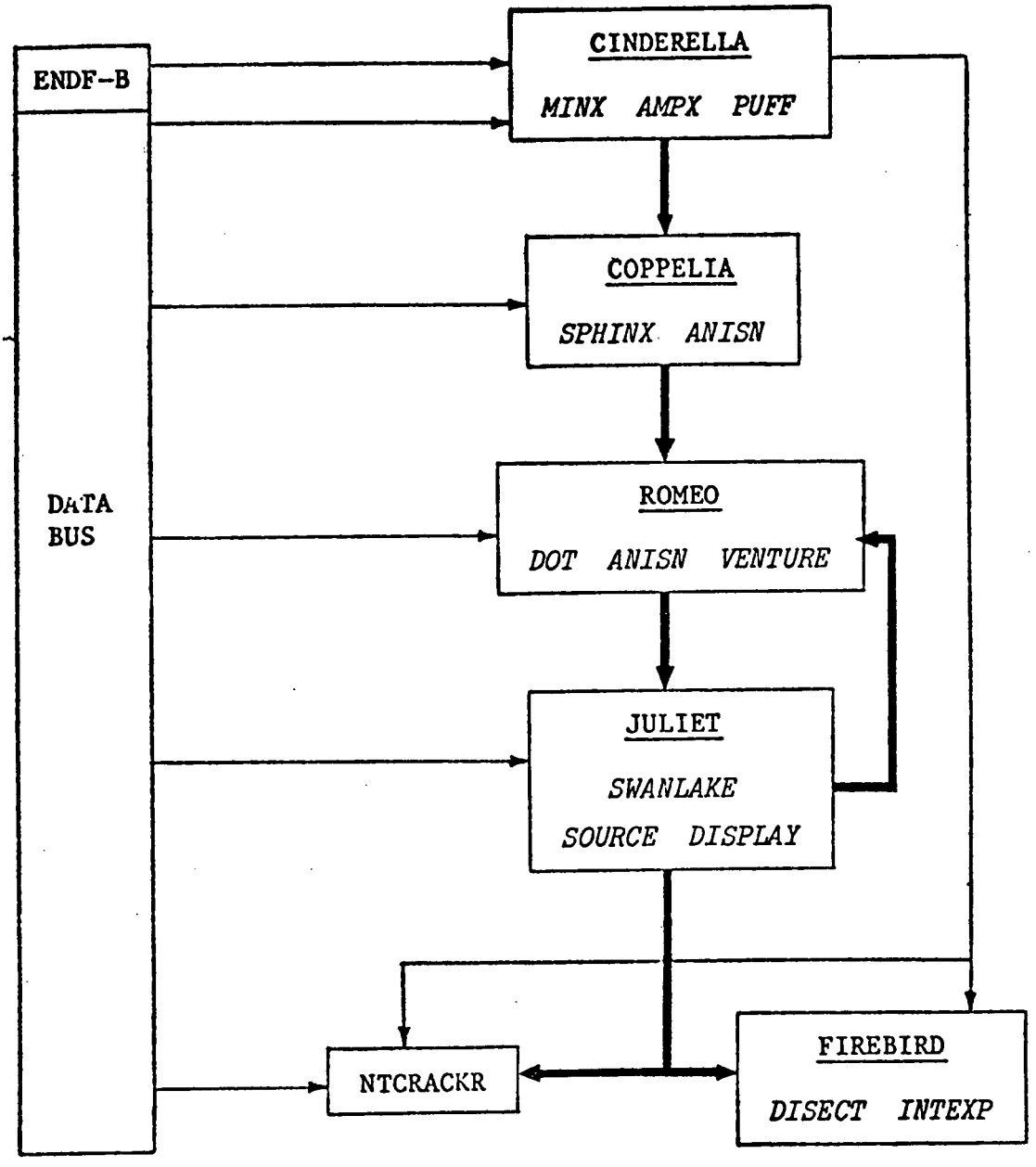

Fig. 1. The FORSS System.

calculation of the generalized adjoint functions, responses of interest, and sensitivity profiles. These three functions are currently being combined into a single code designated SOURCE. Currently, sensitivity profiles for one-dimensional problems are calculated using SWANLAKE[18] and profiles for two-dimensional cases with a code called VIP.[29] The FIREBIRD[24] module determines the uncertainties in the reactor parameters of interest based on the evaluated error files for all nuclides present in the calculational model. The DISECT[1] program permits the analysis of the variance into specific components including effects of uncertainties in different energy ranges as well as the various correlations between materials and reactions. The INTEXP program[30] is used to determine the impact on the multigroup covariance matrices and design uncertainties when the information from related integral measurements is included. Finally, the NTCRACKR module[31] determines the accuracy requirements for the entire data field necessary to meet a series of performance parameter constraints at minimum overall "cost" if relative cost functions are provided.

1. Generation of multigroup cross sections. The cross section library employed in these calculations was the 126-group MINX library[21] developed at ORNL under the joint sponsorship of the ERDA Divisions DRDD and DMFE. This neutron library is part of a more general project which led to the development of 126/36 pseudo-composition independent fine group as well as composition dependent fine and broad group LMFBR neutron-gamma coupled libraries. The detailed specifications have already been documented.[32] The group structure consists of 125 fast groups and one thermal group; the precise energy boundary selection was guided by sensitivity considerations and compatibility with previously existing sets. This list of energy bounds is presented in Table IV. The list of materials contained in the library is given in Table V; the weighting function employed is described in Table VI. Other relevant processing parameters include the Legendre order (P_3) and the error tolerances (reconstruction 0.005, linearization 0.01, thinning 0.005, and integration 0.001). Group constants, derived from ENDF/B-IV, were generated in the AMPX interface[23] and CCCC interface formats[33] using a version of MINX modified by ORNL to allow this dual output capability. The AMPX

Table IV

126 Neutron Energy Group Structure Compared to Other Proposed and Used Group Structures

Upper Energy (eV)	Lethargy	126 Group Structure	CSEWG Standard[a]	100n[b]	51n[c]
.17333E+08	-.55000E+00	1	7		
.12214E+08	-.20000E+00	2	21	3	2
.10000E+08	0.	3	29	5	3
.81873E+07	.20000E+00	4	37	7	4
.67032E+07	.40000E+00	5	45	9	5
.60653E+07	.50000E+00	6	51	10	
.54881E+07	.60000E+00	7	54	11	6
.44933E+07	.80000E+00	8	60	13	7
.36788E+07	.10000E+01	9	64	15	8
.31664E+07	.11500E+01	10	68		
.30119E+07	.12000E+01	11	70	17	9
.28650E+07	.12500E+01	12	71		
.27253E+07	.13000E+01	13	72	18	
.25924E+07	.13500E+01	14	73		
.24660E+07	.14000E+01	15	74	19	10
.23852E+07	.14333E+01	16	76		
.23653E+07	.14417E+01	17	77		
.23069E+07	.14667E+01	18	79		
.22313E+07	.15000E+01	19	81	20	
.21225E+07	.15500E+01	20	82		
.20190E+07	.16000E+01	21	83	21	11
.19205E+07	.16500E+01	22	85		
.18268E+07	.17000E+01	23	87	22	
.17377E+07	.17500E+01	24	88		
.16530E+07	.18000E+01	25	89	23	12
.15724E+07	.18500E+01	26	91		
.14957E+07	.19000E+01	27	93	24	
.14227E+07	.19500E+01	28	94		
.13534E+07	.20000E+01	29	95	25	13
.12873E+07	.20500E+01	30	96		
.12246E+07	.21000E+01	31	97	26	
.11648E+07	.21500E+01	32	99		
.11080E+07	.22000E+01	33	100	27	14
.10026E+07	.23000E+01	34	102	28	
.96164E+06	.23417E+01	35	104		
.90718E+06	.24000E+01	36	106	29	15
.86294E+06	.24500E+01	37	107		
.82085E+06	.25000E+01	38	108	30	
.78082E+06	.25500E+01	39	109		
.74274E+06	.26000E+01	40	110	31	16

[a]239 Group CSEWG Standard.

[b]100 Group GAM Structure.

[c]51 Group Previous ORNL Library.

Table IV (Cont'd.)

Upper Energy (eV)	Lethargy	126 Group Structure	CSEWG Standard[a]	100n[b]	51n[c]
.70651E+06	.26500E+01	41	111		
.67206E+06	.27000E+01	42	112	32	
.63928E+06	.27500E+01	43	113		
.60810E+06	.28000E+01	44	114	33	17
.57844E+06	.28500E+01	45	115		
.55023E+06	.29000E+01	46	116	34	
.52340E+06	.29500E+01	47	118		
.49787E+06	.30000E+01	48	120	35	18
.45049E+06	.31000E+01	49	122	36	
.40762E+06	.32000E+01	50	124	37	19
.36883E+06	.33000E+01	51	126	38	
.33373E+06	.34000E+01	52	128	39	20
.30197E+06	.35000E+01	53	131	40	
.29850E+06	.35116E+01	54			
.29720E+06	.35159E+01	55			
.29452E+06	.35250E+01	56	132		
.28725E+06	.35500E+01	57	133		
.27324E+06	.36000E+01	58	135	41	21
.24724E+06	.37000E+01	59	137	42	
.22371E+06	.38000E+01	60	139	43	22
.21280E+06	.38500E+01	61	140		
.20242E+06	.39000E+01	62	141	44	
.19255E+06	.39500E+01	63	142		
.18316E+06	.40000E+01	64	143	45	23
.17422E+06	.40500E+01	65	144		
.16573E+06	.41000E+01	66	146	46	
.15764E+06	.41500E+01	67	148		
.14996E+06	.42000E+01	68	149	47	24
.14264E+06	.42500E+01	69	150		
.13569E+06	.43000E+01	70	151	48	
.12907E+06	.43500E+01	71	152		
.12277E+06	.44000E+01	72	153	49	25
.11679E+06	.44500E+01	73	154		
.11109E+06	.45000E+01	74	155	50	
.98037E+05	.46250E+01	75	156		
.86517E+05	.47500E+01	76	157	51	26
.82500E+05	.47975E+01	77			
.79500E+05	.48346E+01	78			
.72000E+05	.49337E+01	79			
.67379E+05	.50000E+01	80	159	52	
.56562E+05	.51750E+01	81	162		
.52475E+05	.52500E+01	82	163	53	27
.46309E+05	.53750E+01	83	164		
.40868E+05	.55000E+01	84	165	54	28
.34307E+05	.56750E+01	85	168		
.31828E+05	.57500E+01	86	169	55	29
.28500E+05	.58604E+01	87			

Table IV (Cont'd.)

Upper Energy (eV)	Lethargy	126 Group Structure	CSEWG Standard[a]	100n[b]	51n[c]
.27000E+05	.59145E+01	88			
.26058E+05	.59500E+01	89	171		
.24788E+05	.60000E+01	90	172	56	30
.23579E+05	.60500E+01	91	174		
.21875E+05	.61250E+01	92	175		
.19305E+05	.62500E+01	93	177	57	31
.15034E+05	.65000E+01	94	179	58	32
.11709E+05	.67500E+01	95	181	59	
.91188E+04	.70000E+01	96	183	60	
.71017E+04	.72500E+01	97	185	61	33
.55308E+04	.75000E+01	98	187	62	
.43074E+04	.77500E+01	99	190	63	34
.37074E+04	.79000E+01	100	192		
.33546E+04	.80000E+01	101	193	64	35
.30354E+04	.81000E+01	102	194		
.27465E+04	.82000E+01	103	196		
.26126E+04	.82500E+01	104	197	65	36
.24852E+04	.83000E+01	105	198		
.22487E+04	.84000E+01	106	199		
.20347E+04	.85000E+01	107	200	66	37
.15846E+04	.87500E+01	108	203	67	38
.12341E+04	.90000E+01	109	206	68	39
.96112E+03	.92500E+01	110	207	69	40
.74852E+03	.95000E+01	111	208	70	
.45400E+03	.10000E+02	112	210	72	41
.27536E+03	.10500E+02	113	212	74	
.21445E+03	.10750E+02	114	213	75	42
.16701E+03	.11000E+02	115	214	76	
.10130E+03	.11500E+02	116	216	78	43
.61442E+02	.12000E+02	117	218	80	
.47851E+02	.12250E+02	118	219	81	44
.37267E+02	.12500E+02	119	220	82	
.22603E+02	.13000E+02	120	222	84	45
.10677E+02	.13750E+02	121	225	87	46
.50435E+01	.14500E+02	122	228	90	47
.23824E+01	.15250E+02	123	231	93	48
.11254E+01	.16000E+02	124	234	96	49
.41399E+00	.17000E+02	125		100	50
.10000E-00		126			51

Table V

Materials Processed into Multigroup Form for the LMFBR Neutron-Gamma Pseudo Composition Independent Library

(Pertinent data to be generated at 300, 900, and 2100°K)

Material	MAT[a]	Values of σ_o	Material	MAT[a]	Values of σ_o
*H-1	1269		Cu	1295	10^3 to 0.1
*H-2	1120		Zr	1284	10^3 to 0.1
H-3	1169		Nb-93	1189	10^3 to 0.1
He-4	1270		*Mo	1287	10^5 to 1
*Li-6	1271	10^3 to 1 by decades	Ag-107	1138	10^5 to 1
*Li-7	1272	10^3 to 1	Ag-109	1139	10^5 to 1
*Be-9	1289	10^3 to 1	Cd	1281	10^5 to 1
*B-10	1273	10^3 to 1	Sn	7029[b]	10^5 to 1
*B-11	1160	10^3 to 1	Eu-151	1290	10^5 to 1
*C-12	1274	10^3 to 0.1	Eu-152	1291	10^5 to 1
*N-14	1275		Eu-153	1292	10^5 to 1
*O-16	1276	10^3 to 0.1	Eu-154	1293	10^5 to 1
F	1277	10^3 to 0.1	Ta-181	1285	10^5 to 1
*Na-23	1156	10^3 to 0.1	W-182	1128	10^4 to 1
*Mg	1280	10^3 to 0.1	W-183	1129	10^4 to 1
*Al-27	1193	10^3 to 0.1	W-184	1130	10^4 to 1
*Si	1194	10^3 to 0.1	W-186	1131	10^4 to 1
P	7019[b]	10^3 to 0.1	*Pb	1288	10^4 to 1
S	7020[b]	10^3 to 0.1	Th-232	1296	10^4 to 1
*K	1150	10^3 to 0.1	U-233	1260	10^5 to 1
*Ca	1195	10^3 to 0.1	U-234	1043	10^5 to 1
Ti	1286	10^3 to 0.1	*U-235	1261	10^4 to 1
V	1196	10^3 to 0.1	U-236	1163	10^5 to 1
*Cr	1191	10^3 to 0.1	*U-238	1262	10^4 to 0.1
*Mn-55	1197	10^5 to 1	Pu-238	1050	10^5 to 1
*Fe	1192	10^3 to 0.1	*Pu-239	1264	10^5 to 1
Co-59	1199	10^3 to 0.1	*Pu-240	1265	10^5 to 1
*Ni	1190	10^3 to 0.1	*Pu-241	1266	10^5 to 1
Cu-63	1085[c]	10^3 to 0.1	*Pu-242	1161	10^5 to 1
Cu-65	1086[c]	10^3 to 0.1	Am-241	1056	10^5 to 1

[a]All data from ENDF/B-IV unless otherwise noted.
[b]Livermore Evaluated Data Library.
[c]ENDF/B-III.
*Materials presently contained in the 51/25 library currently in use at ORNL.

Table VI

Weighting Function Used for the LMFBR Processed Library

Functional Form[a]	Energy Limits
(1) Maxwellian Thermal Spectrum (300°K) $S_1(E) = C_1 E e^{-E/kT}$	10^{-5} eV to 0.125 eV
(2) "1/E" Slowing-Down Spectrum $S_2(E) = C_2(E)$	0.125 eV to 820.8 keV
(3) Fission Spectrum (Θ = 1.4 MeV) $S_3(E) = C_3 E^{1/2} e^{-E/\Theta}$	820.8 keV to 10.0 MeV
(4) "1/E" Spectrum $S_4(E) = C_4/E$	10.0 MeV to 12.57 MeV
(5) Velocity Exponential Fusion Peak (Ep = 14.07 MeV) (kT = 0.025 MeV) $S_5(E) = C_5 \exp\left\{-\frac{5}{kT}\left(E^{1/2} - E_p^{1/2}\right)^2\right\}$	12.57 to 15.57 MeV
(6) "1/E" Spectrum $S_6(E) = C_6/E$	15.57 to 17.333 MeV

[a]Constants are chosen to match values at region limits.

format is more flexible than the CCCC file in that all partial cross section information is retained (e.g., group-to-group transfer cross sections for discrete inelastic levels, group averaged cross sections for threshold reactions, etc.). This type of access to the entire data file is vital to do a definitive nuclear data sensitivity analysis.

Beginning with the 126 group library containing all nuclides of interest, the calculational flow to produce composition dependent self-shielded cross sections is illustrated in Fig. 2. Although no gamma-ray transport was involved in this analysis, this is the same path used to derive composition dependent neutron-gamma coupled sets.

PROCESSING PATH TO DERIVE COMPOSITION DEPENDENT COUPLED LIBRARIES

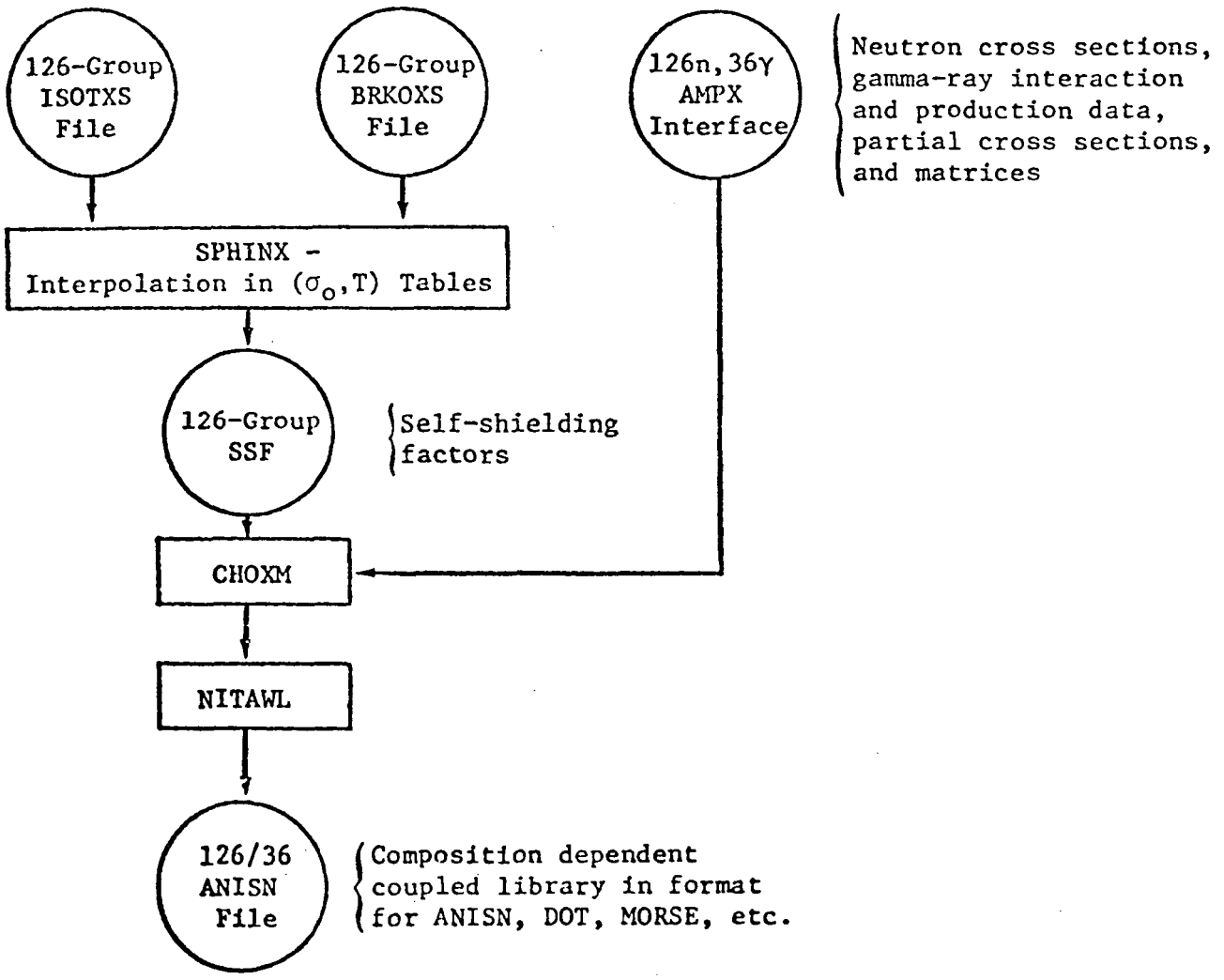

Fig. 2

As illustrated in Fig. 2, SPHINX is used to produce space-energy self-shielded neutron cross sections for a given reactor composition and temperature. For each energy group of each isotope in each zone, self-shielding factors are computed for total, fission, capture, and elastic cross sections. SPHINX also has a one-dimensional diffusion theory option which may be used to compute fluxes and collapse cross sections. This option was not exploited in the present analysis.

The function of CHOXM is to take the self-shielding factors generated by SPHINX and an infinite dilution neutron AMPX interface produced by MINX, and generate a self-shielded neutron AMPX interface for the specific problem of interest which was described in the SPHINX calculation. CHOXM can also combine a neutron interface, a gamma interface, and a photon production interface to produce a neutron-gamma coupled interface. Finally, the NITAWL module is used to convert data from master interface cross section formats to working library formats for codes like ANISN.

Figures 3 and 4 illustrate the self-shielded macroscopic total cross section for the ZPR-6/7 core and blanket. In the core, the 2.85 keV Na scattering resonance, the 28 keV Fe scattering resonance, and the 440 keV oxygen scattering resonance are clearly evident in addition to other resonances of Na and Fe in the 50-200 keV range. The blanket, being composed primarily of ^{238}U and Fe, reflects the 28 keV Fe resonance and the onset of fast fission in ^{238}U above 1 MeV. The curves for ZPR-6/6A are essentially identical to Figs. 3 and 4.

2. Flux and response calculations. Using the cross sections generated in the previous section, ANISN was used in the S_4, P_3 approximation to compute fluxes, adjoints, and responses for the three assemblies of interest. The total scalar flux at the core center of ZPR-6/7 is illustrated in Fig. 5. The flux has a fission spectrum shape (slightly degraded in energy) with structure corresponding to the cross section resonances in Fig. 3. The 2.85 keV Na and 28 keV Fe resonances are particularly noticeable. Figure 6 illustrates the flux spectra at the center of the uranium blanket. The spectrum in the blanket appears to contain

ORNL DWG 76-16127

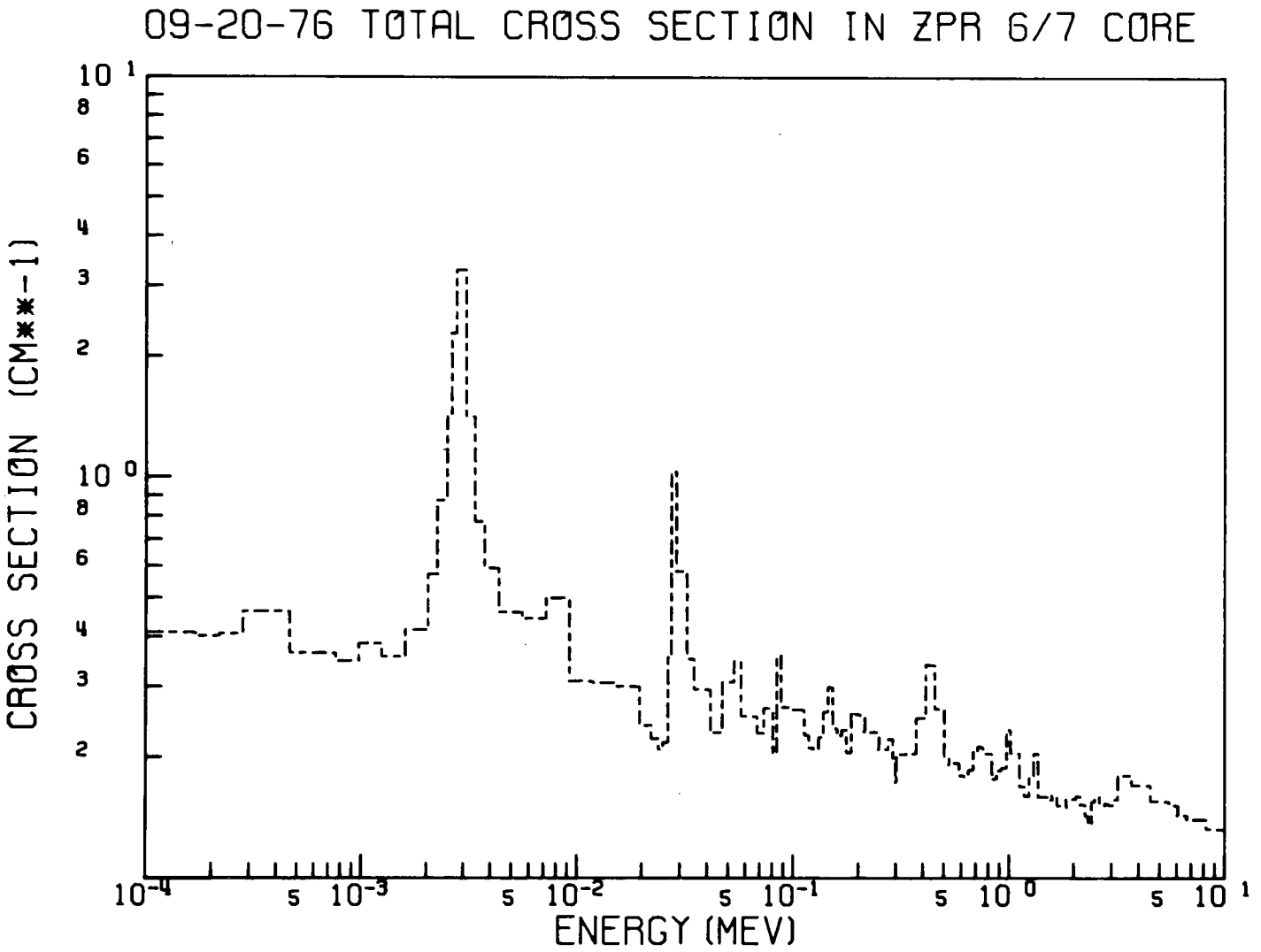

Fig. 3. The Macroscopic Total Cross Section at the Center of the ZPR-6/7 Core.

ORNL DWG 76-16121

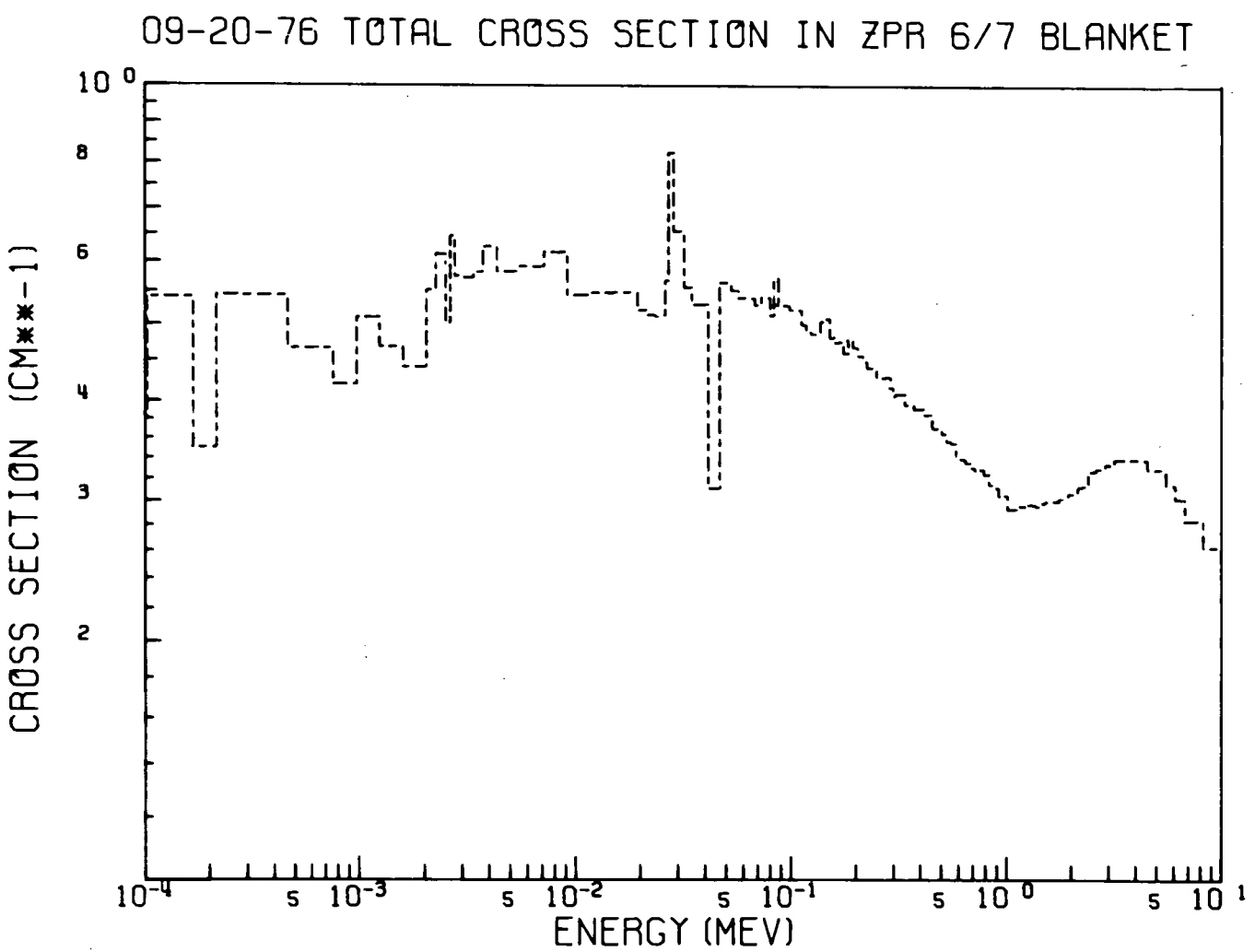

Fig. 4. The Macroscopic Total Cross Section at the Center of the ZPR-6/7 Blanket.

ORNL DWG 76-16124

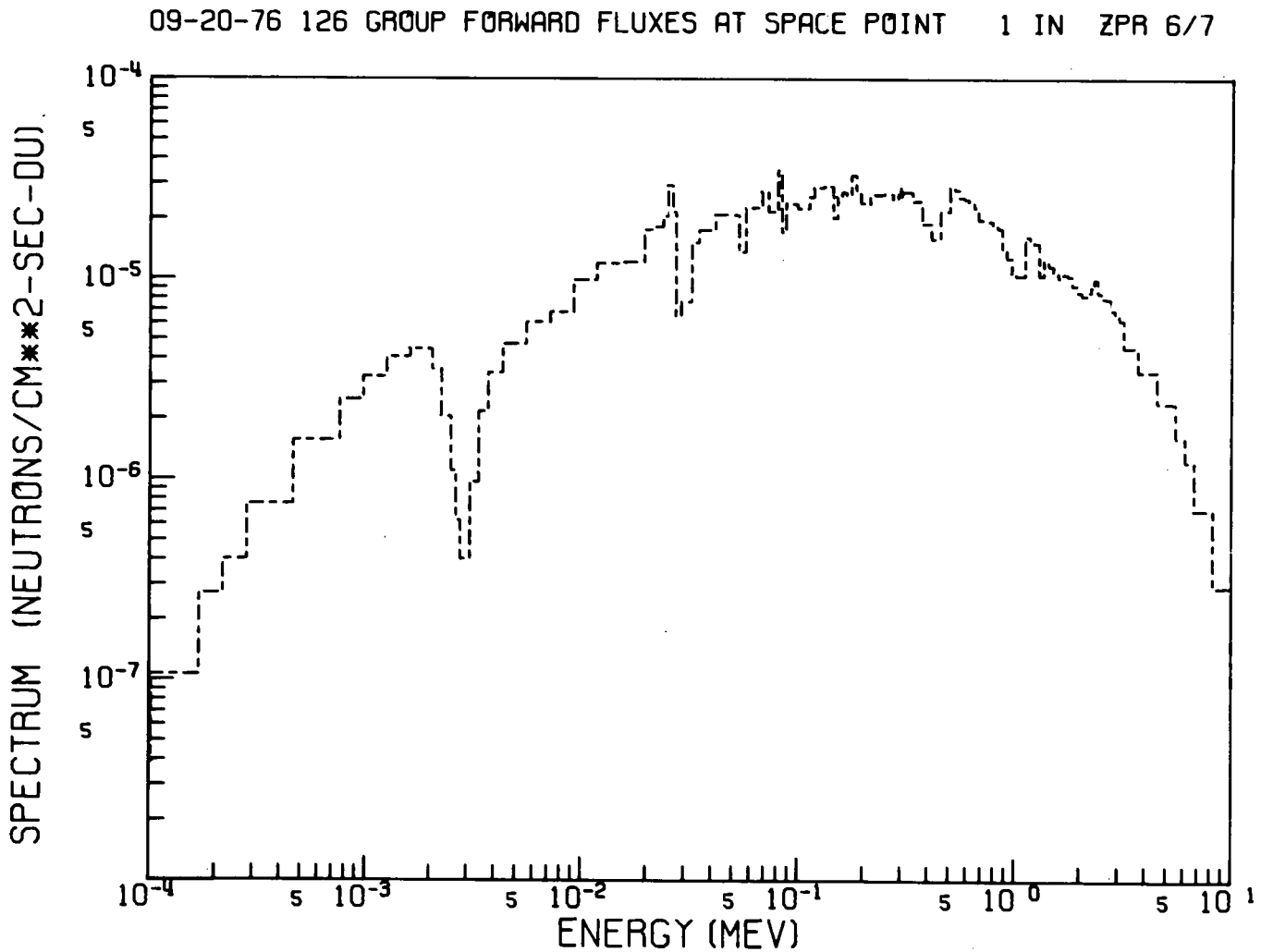

Fig. 5. Total Flux Spectrum at the Center of the ZPR-6/7 Core.

ORNL DWG 76-16118

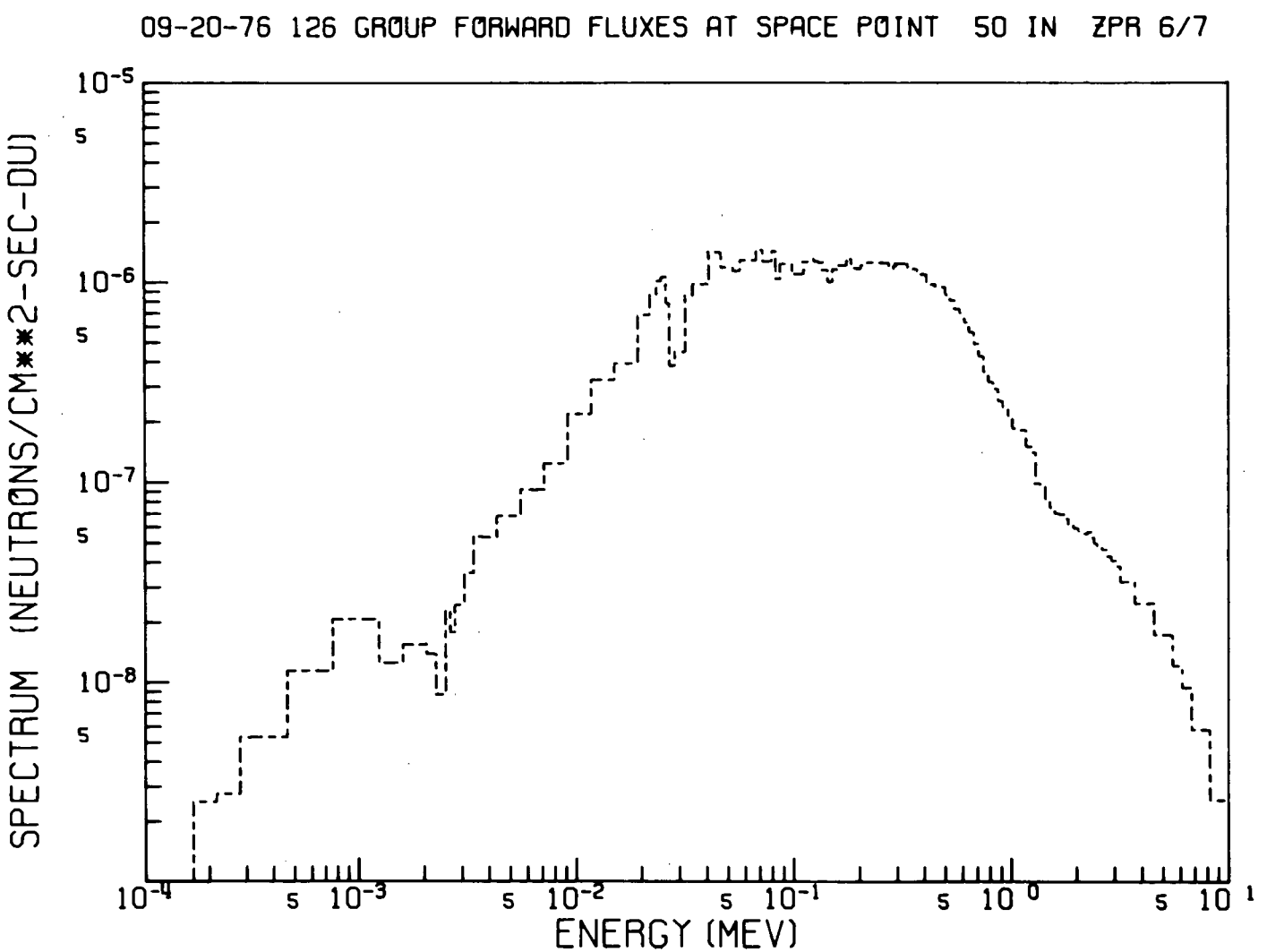

Fig. 6. Total Flux Spectrum at the Center of the ZPR-6/7 Blanket.

considerably fewer high and low energy neutrons; i.e., the spectrum is focussed more between ∿10 keV and 1 MeV as opposed to 700 eV to 5 MeV at the core center. Higher energy neutrons leaking from the core (with a χ/Σ_T spectrum) are quickly degraded in the ^{238}U-Fe blanket by the fission and inelastic reactions; lower energy neutrons are either reflected back toward the core or captured in the blanket. The ZPR-6/6A core central and blanket spectra are very similar to that for ZPR-6/7 (ZPR-6/7 spectra being just slightly softer). GODIVA has a fission type spectrum not displayed here. With these fluxes one is able to tabulate directly a number of parameters of interest. This is done below in Table VII.

Table VII

Performance Parameter Calculation/Experiment for ZPR-6/7, ZPR-6/6A, and GODIVA

	ZPR-6/7	ZPR-6/6A	GODIVA
$k_{corrected}$	0.9885	0.9999	1.0033
$\langle {}^{28}f/{}^{25}f \rangle \frac{C}{E}$		0.917	
$\langle {}^{28}c/{}^{25}f \rangle \frac{C}{E}$	1.030	1.007	
$\langle {}^{28}c/{}^{49}f \rangle \frac{C}{E}$	1.073		
$\langle {}^{28}f/{}^{49}f \rangle \frac{C}{E}$	0.961		

c - capture

f - fission

$\frac{C}{E}$ - calculation/experiment; multigroup cross sections do not include recent methods improvement in performing unresolved quadrature.

3. Adjoints, generalized sources, and generalized adjoints. The adjoint flux spectrum at the center of ZPR-6/7 is illustrated in Fig. 7. It is generally concave in shape, as a function of energy, and relatively energy independent compared to the real flux. (The graph for ZPR-6/6A is similar in shape and even more energy independent.) The adjoint increases above 1 MeV due to an increase in η ($\nu\sigma_f/\sigma_a$) for the fissile materials

ORNL DWG 76-16120

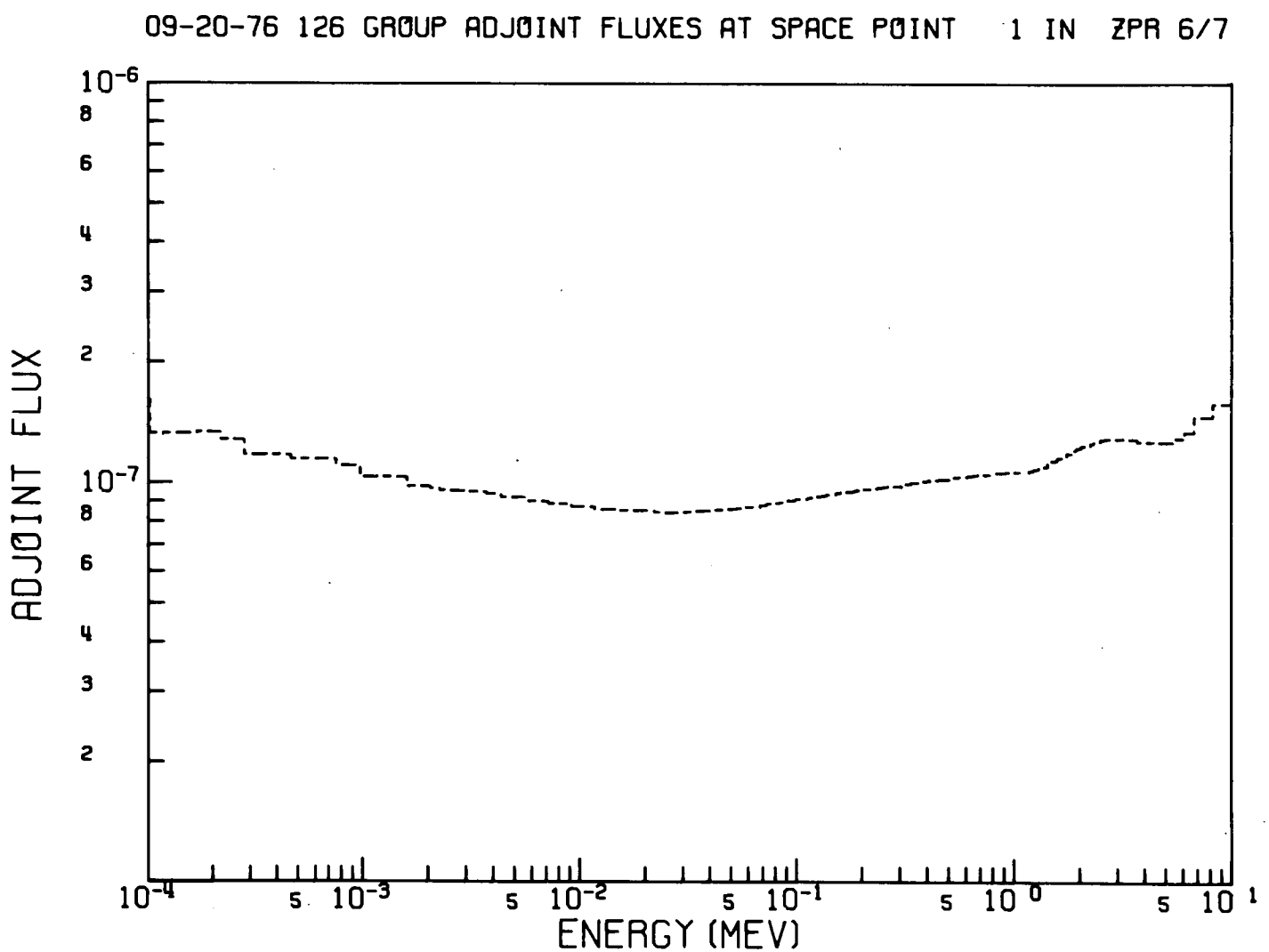

Fig. 7. Adjoint Flux Spectra at the Center of the ZPR-6/7 Core.

and the onset of threshold fission in the fertile materials. A cause of the increase at low energies is the fact that resonance self-shielding for the fertile materials is stronger than for the fissile materials. Figure 8 illustrates the adjoint at the center of the uranium blanket. The adjoint clearly favors higher energies as anticipated. Thresholds for fission and (n,2n) are clearly observable leading to increased importance with increasing energy. The ^{238}U capture cross section rapidly decreases with increasing energy also tending to a situation of increasing importance with increasing energy. Since the blanket for ZPR-6/6A is the same as that for ZPR-6/7, it is not surprising that the shape of the adjoint is very similar to that for ZPR-6/7.

The generalized adjoint source for $(^{28}c/^{49}f)_{central}$ in ZPR-6/7 and $(^{28}c/^{25}f)_{central}$ in ZPR-6/6A is given in Figs. 9 and 10, respectively. These sources are localized to the central interval and play a key role in establishing the spectral shape of the generalized adjoint functions near the center of the core. Since the energy-dependent sources for these generalized adjoints depend on differences between macroscopic group cross sections, it is possible that the energy-dependent source (and subsequently the generalized adjoint) is positive in one region and negative in another. Physically, a change in the flux can affect the numerator of the response rate ratio more than the denominator (or vice versa) in particular energy regions. In Fig. 9, the lower energy region (< 0.5 MeV) favors $^{239}Pu(n,f)$ while the higher energy region (< 3 MeV) is more dominated by $^{238}U(n,\gamma)$. The energy region above ~ 3 MeV contains many regions of oscillating sign and decreasing importance in the determination of the sensitivity profile since the neutron flux is very low. Figure 10 exhibits similar behavior.

Figures 11 and 12 present the generalized adjoint for the $(^{28}c/^{49}f)_{central}$ parameter at the center of ZPR-6/7 and at the center of the blanket region, respectively. The generalized adjoint, represented in part in Figs. 11 and 12, is orthogonal to the flux, represented in part in Figs. 5 and 6. It should be noted that the magnitude of the values in Fig. 12 are very small so that any physical interpretation derived from

ORNL DWG 76-16122

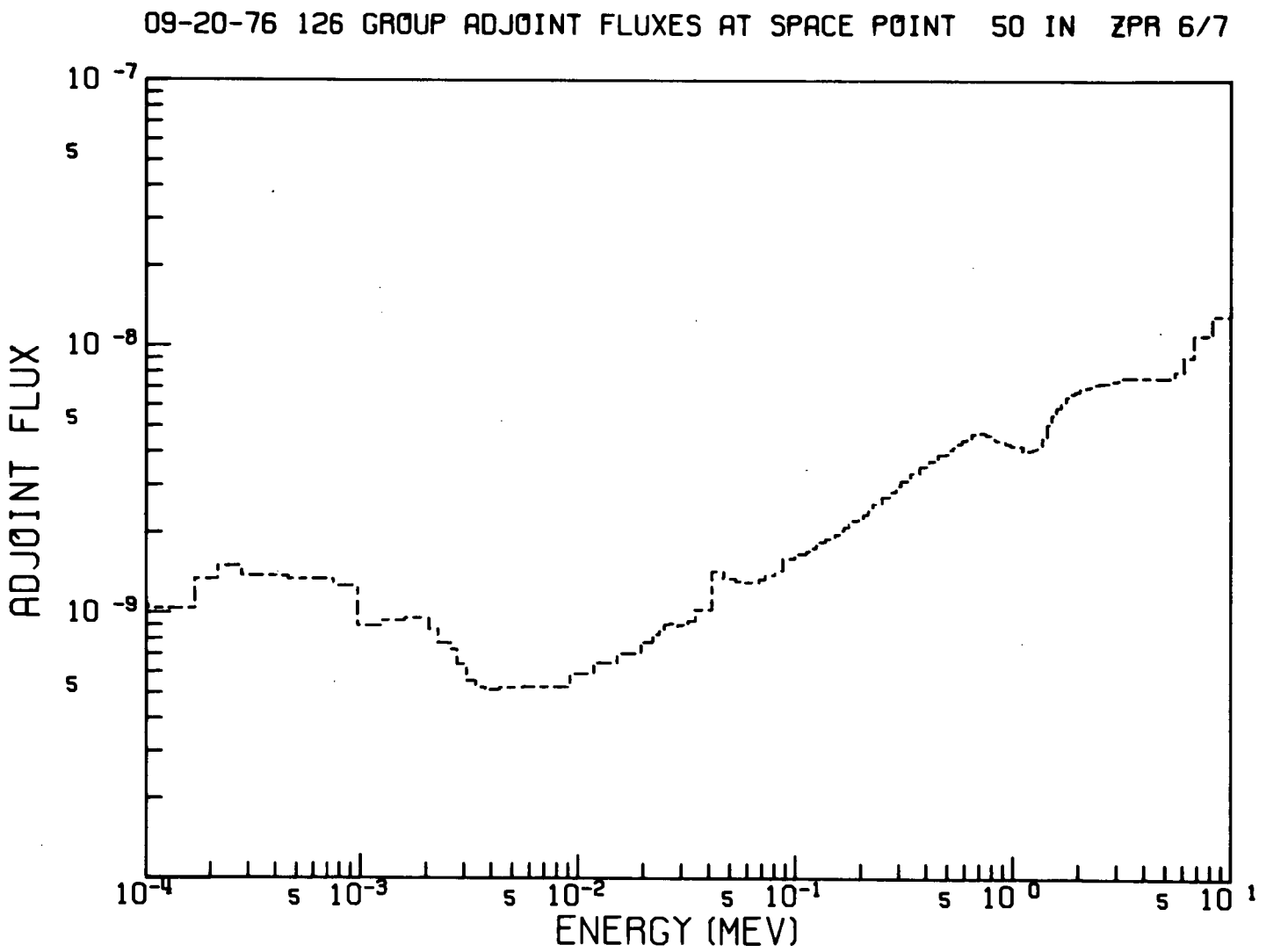

Fig. 8. Adjoint Flux Spectra at the Center of the ZPR-6/7 Blanket.

ORNL DWG 76-16123

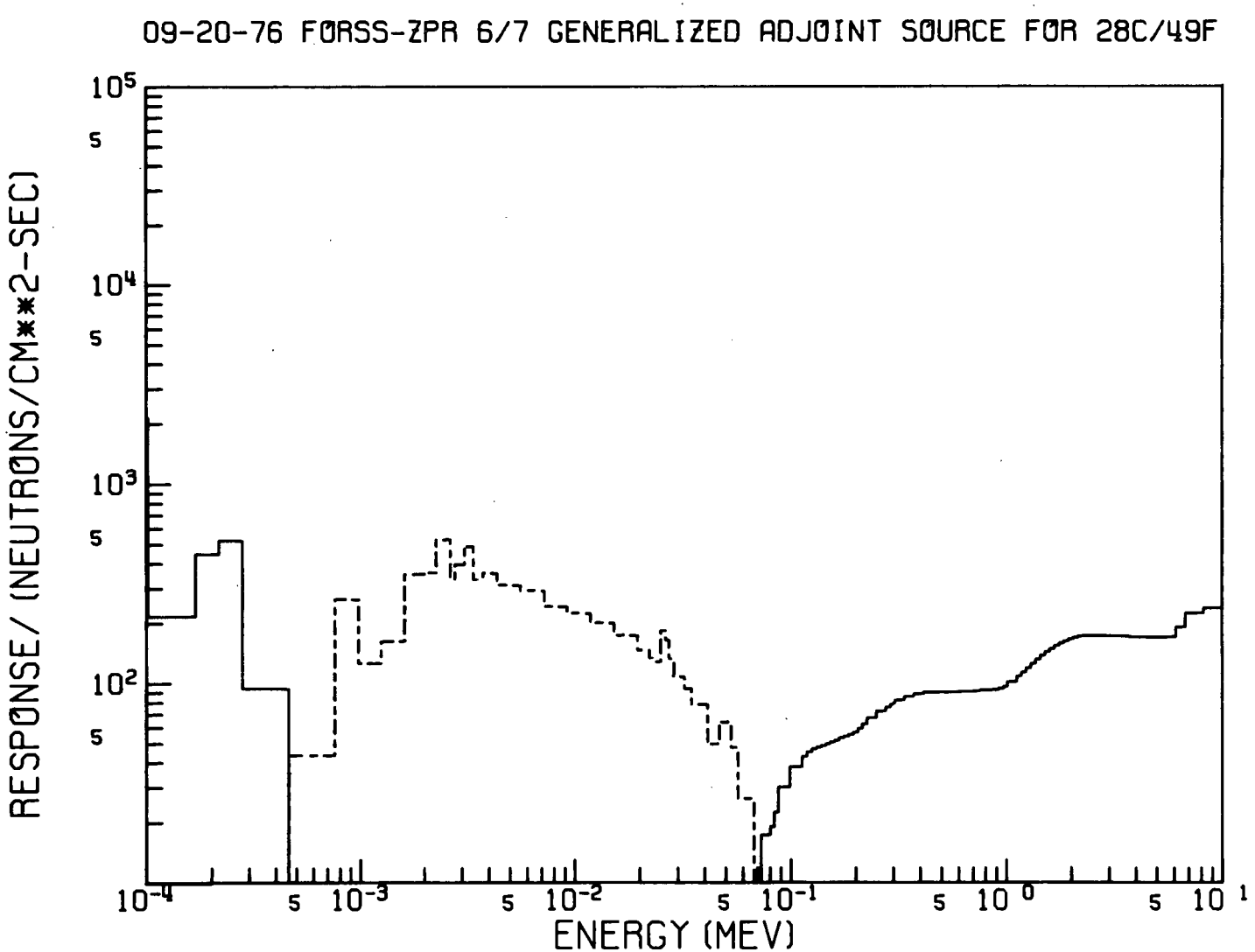

Fig. 9. Generalized Adjoint Source for the ^{238}U Capture/^{239}Pu Fission Central Reaction Rate Ratio in ZPR-6/7.

ORNL DWG 76-16119

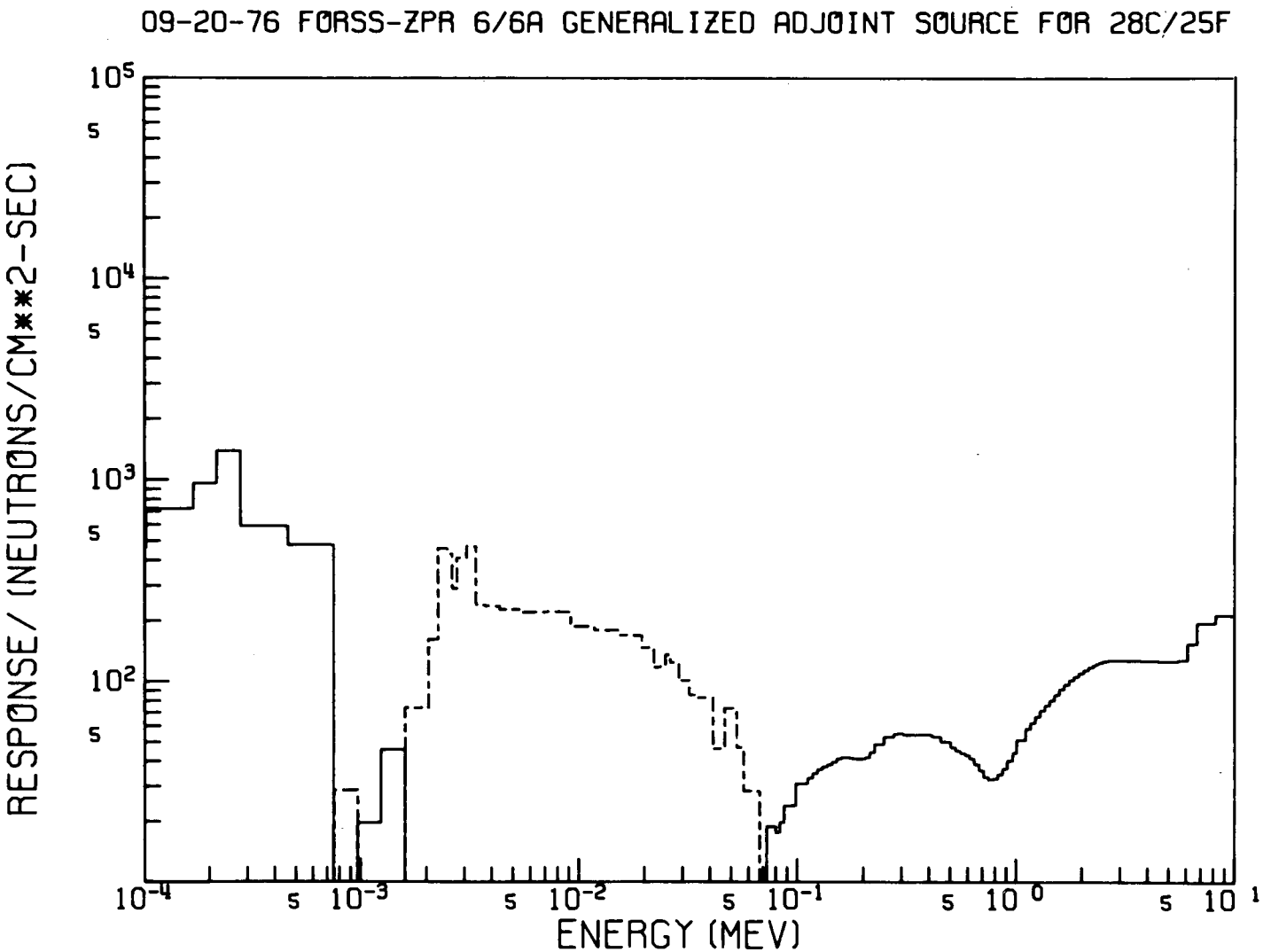

Fig. 10. Generalized Adjoint Source for the ^{238}U Capture/^{235}U Fission Central Reaction Rate Ratio in ZPR-6/6A.

ORNL DWG 76-16126

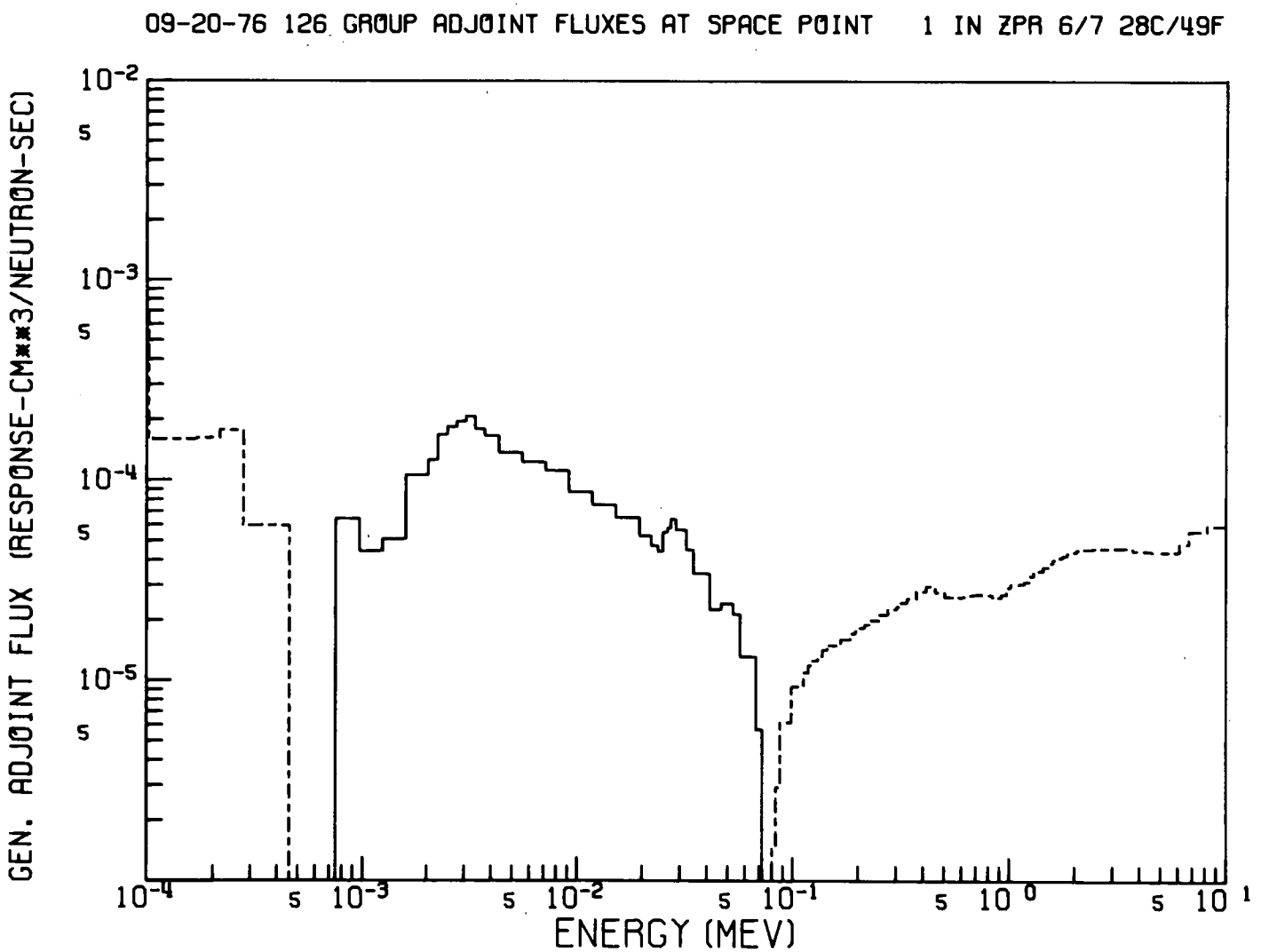

Fig. 11. Generalized Adjoint for the ^{238}U Capture/^{239}Pu Fission Ratio at the Center of the ZPR-6/7 Core.

ORNL DWG 76-16125

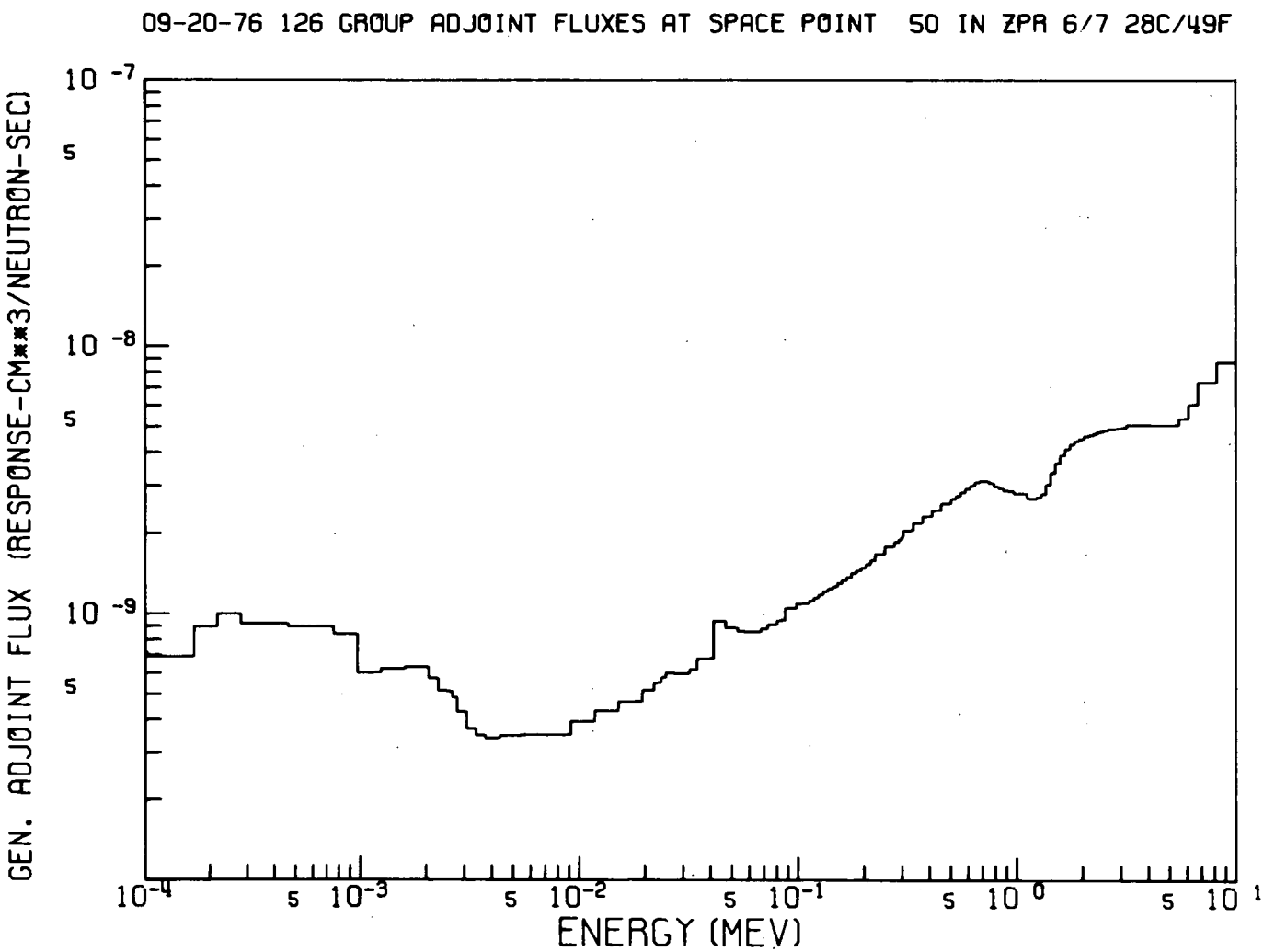

Fig. 12. Generalized Adjoint for the ^{238}U Capture/^{239}Pu Fission Ratio at the Center of the ZPR-6/7 Blanket.

the graph must be done with caution since the amount of ϕ^* contamination may be significant.

4. Energy dependent sensitivity profiles. Several important energy-dependent profiles are presented in Figs. 13-32. Comprehensive libraries[19] of energy dependent coefficients (126 energy groups including additional assemblies such as ZPR-3/56B, ZPR-3/11) in a computer retrievable format[34] have been documented and released for distribution by RSIC and NNCSC. Of particular note is the fine degree of detail observable in this group structure as well as the ability to generate sensitivity coefficients for any nuclear cross section in ENDF/B (e.g., sensitivity of k in ZPR-6/7 to the n'th level of inelastic scattering in ^{238}U; or even finer - to the ℓ'th component of the group-to-group matrix).

D. Verification of Sensitivity Profiles

The formulation, implementation, and numerical evaluation of Eqs. (25) and (27) is a sizeable task which requires detailed verification before general acceptance. We have proceeded in a number of directions which are reported below.

1. Hand Calculation. A two-group, two-nuclide (one fissionable, the other a scatterer), infinite medium problem is amenable to direct solution with no more than a desk calculator. Fluxes, adjoints, generalized sources and adjoints, and profiles were verified for k, reaction rate ratio, and worths to within machine precision.

2. The direct effect summed over all groups, zones, and reaction types is identically zero, provided that the H operators [Eq. (1)] are linear homogeneous multiples of the cross sections. The first term [Eq. (3)] summed over all energy groups and reaction types must be unity, the second [Eq. (4)] must be -1. Furthermore, $\bar{\nu}$-profiles for k summed over all reaction types, energy groups, zones etc. must be unity. The $\bar{\nu}$-profiles in this case represent the fraction of the fissions taking place in particular groups, zones, materials, etc. Many cases were examined confirming the results presented subsequently to high precision.

ORNL DWG 76-6894

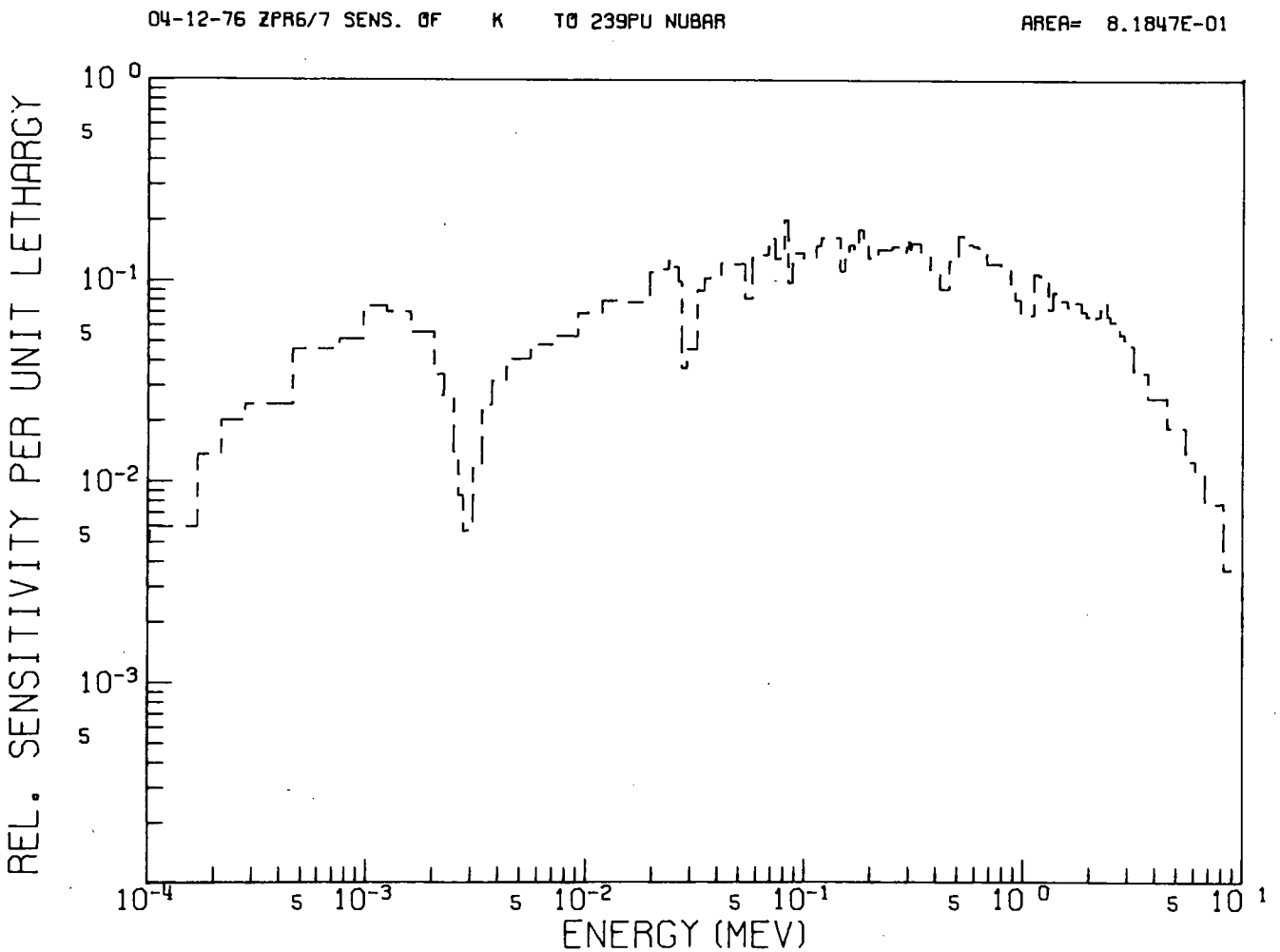

Fig. 13. Sensitivity of k in Assembly ZPR-6/7 to ^{239}Pu Neutron/Fission.

ORNL DWG 76-5557

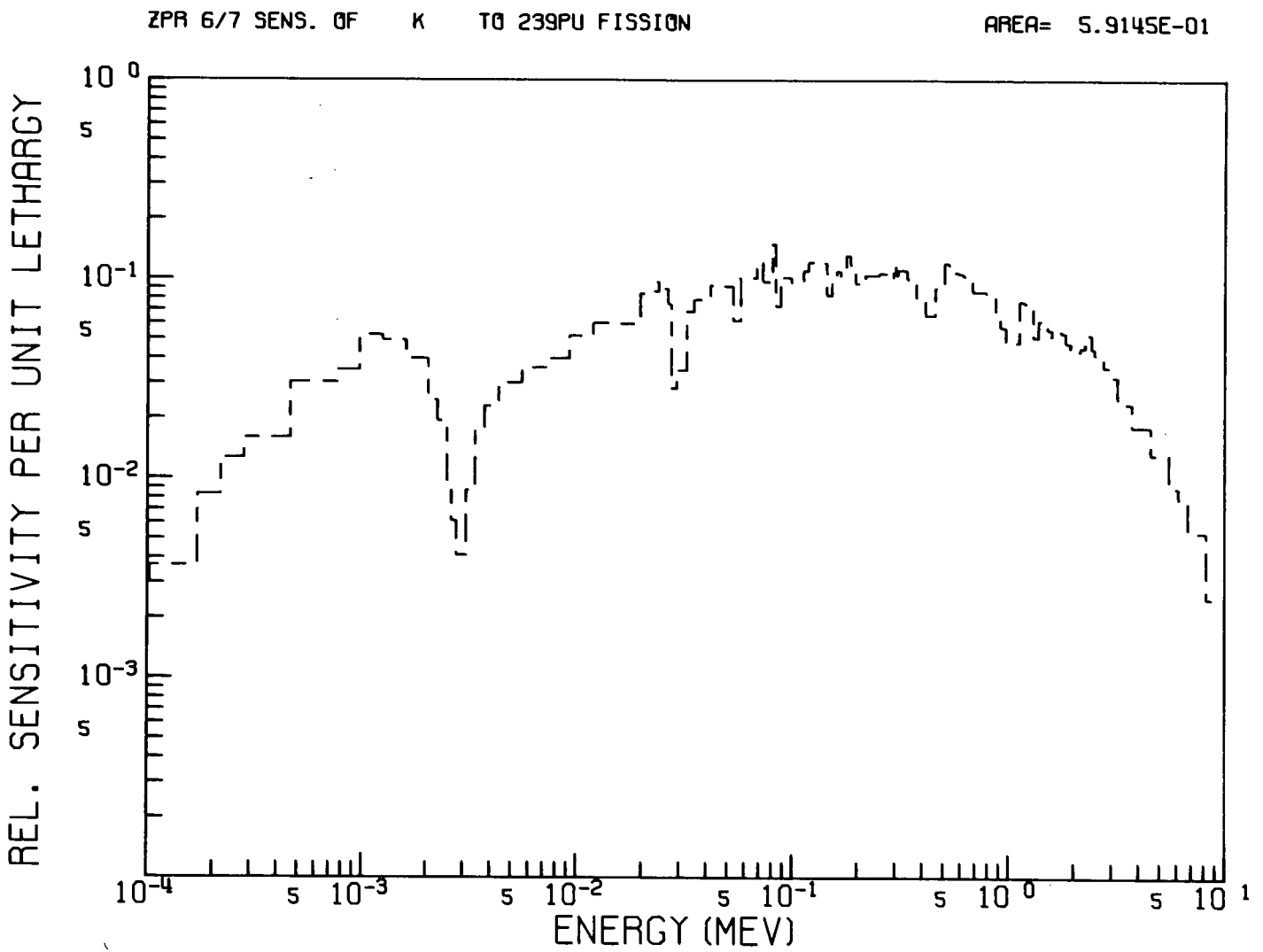

Fig. 14. Sensitivity of k in Assembly ZPR-6/7 to the ^{239}Pu Fission Cross Section.

ORNL DWG 76-5583

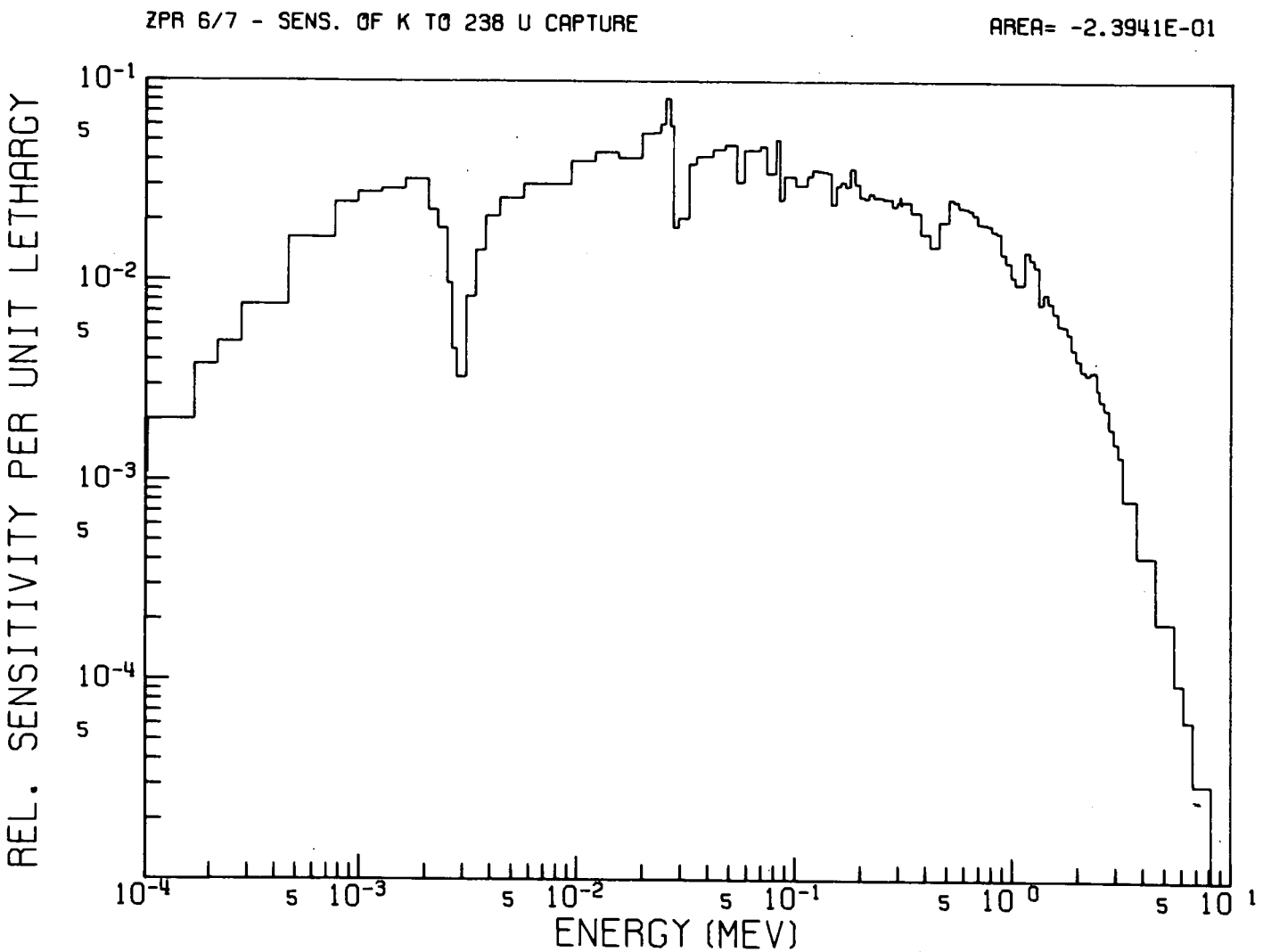

Fig. 15. Sensitivity of k in Assembly ZPR-6/7 to the ^{238}U Capture Cross Section.

ORNL DWG 76-6897

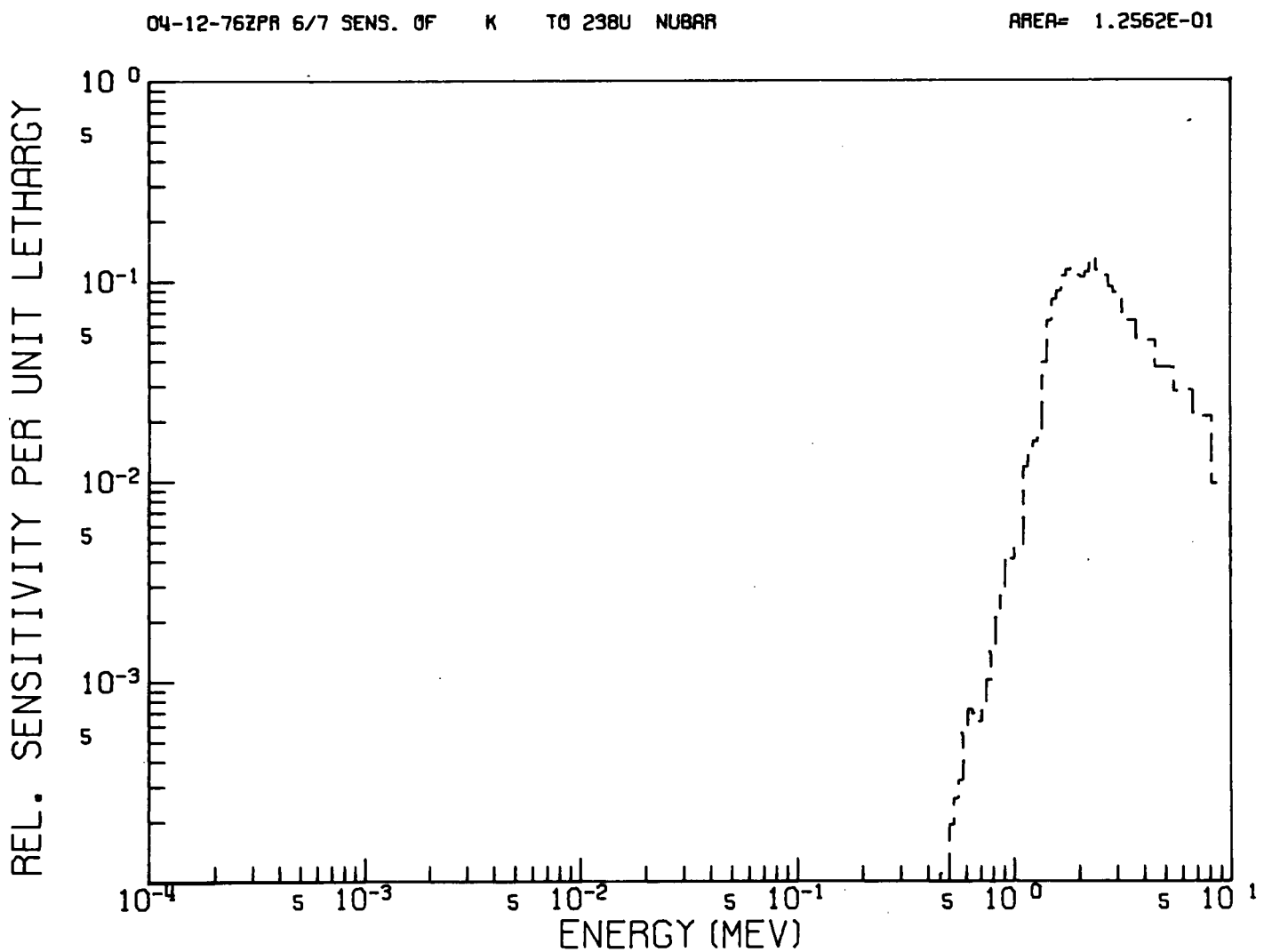

Fig. 16. Sensitivity of k in Assembly ZPR-6/7 to the Neutrons/Fission in ^{238}U.

ORNL DWG 76-5555

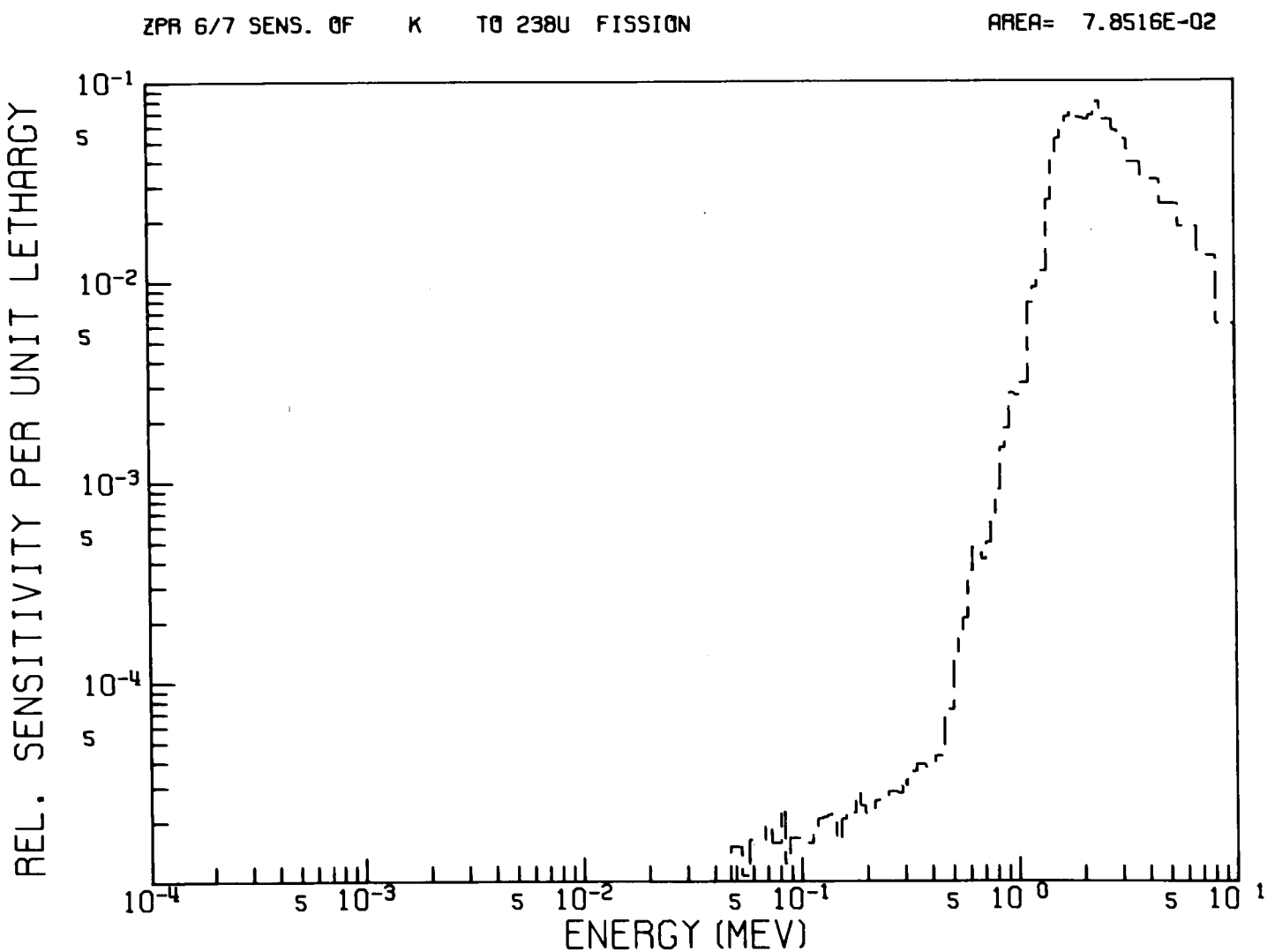

Fig. 17. Sensitivity of k in Assembly ZPR-6/7 to the ^{238}U Fission Cross Section.

ORNL DWG 76-6120

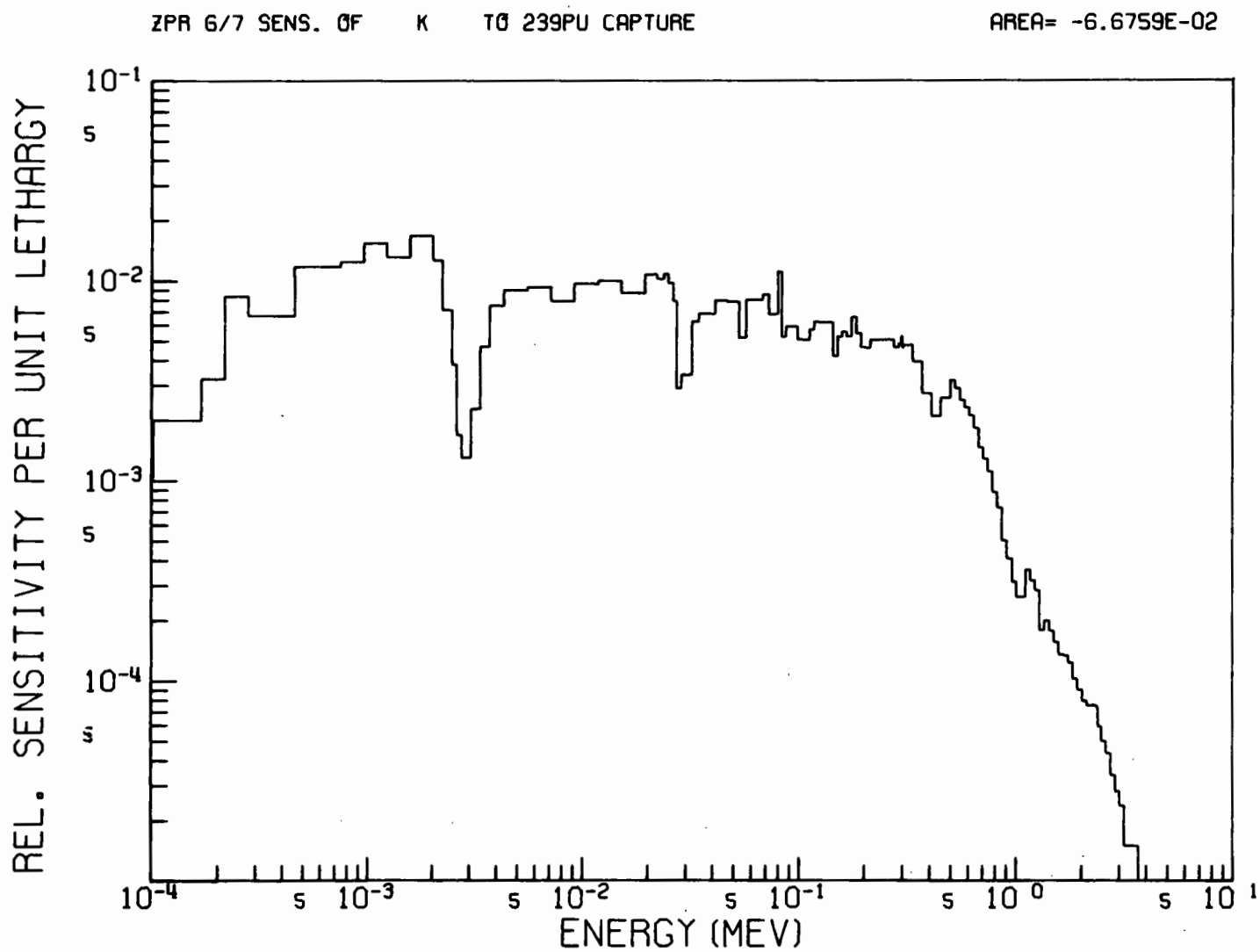

Fig. 18. Sensitivity of k in Assembly ZPR-6/7 to the ^{239}Pu Capture Cross Section.

ORNL DWG 76-5564

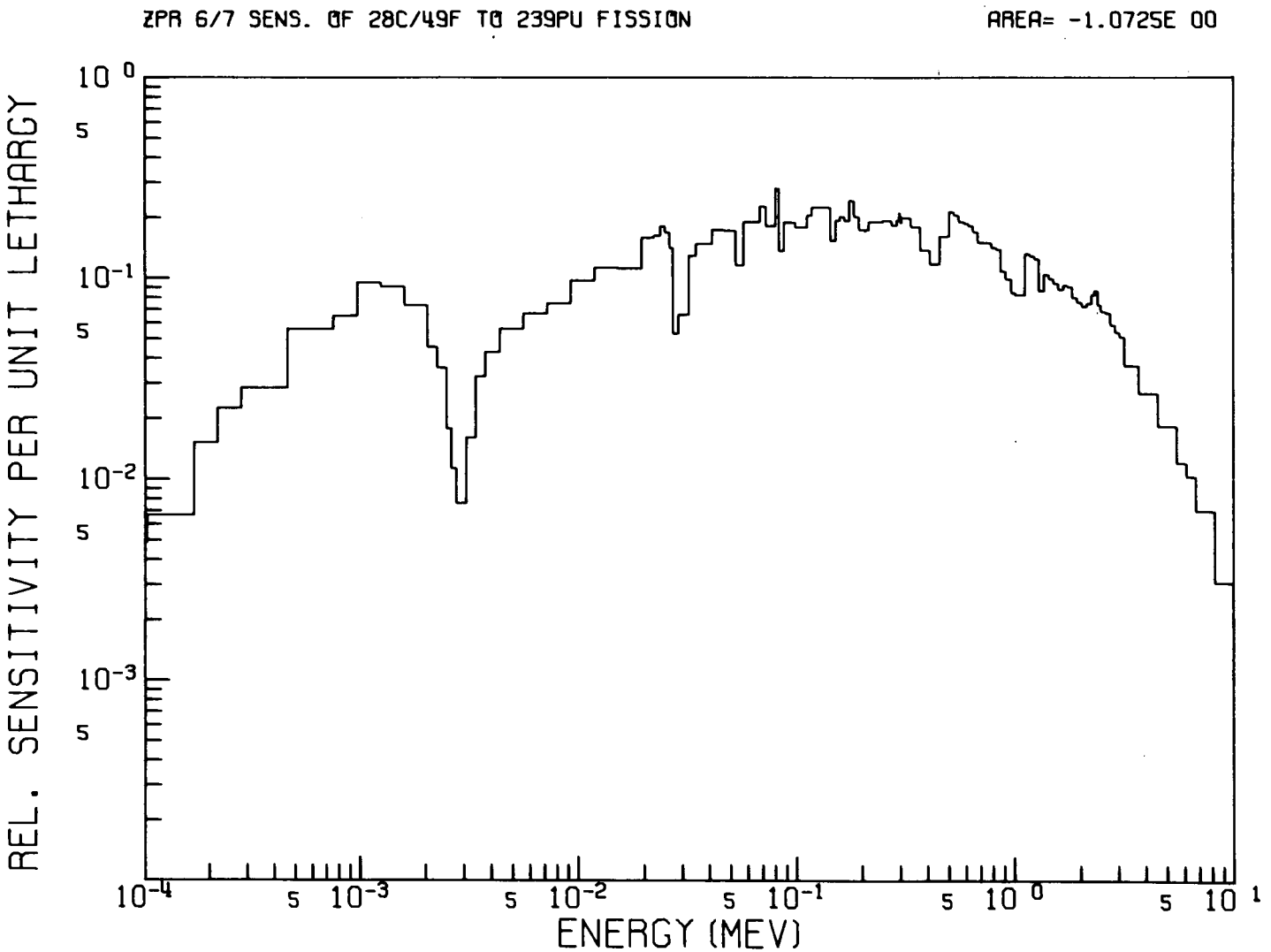

Fig. 19. Sensitivity of the ^{238}U Capture/^{239}Pu Fission Central Reaction Ratio in ZPR-6/7 to the ^{239}Pu Fission Cross Section.

ORNL DWG 76-5527

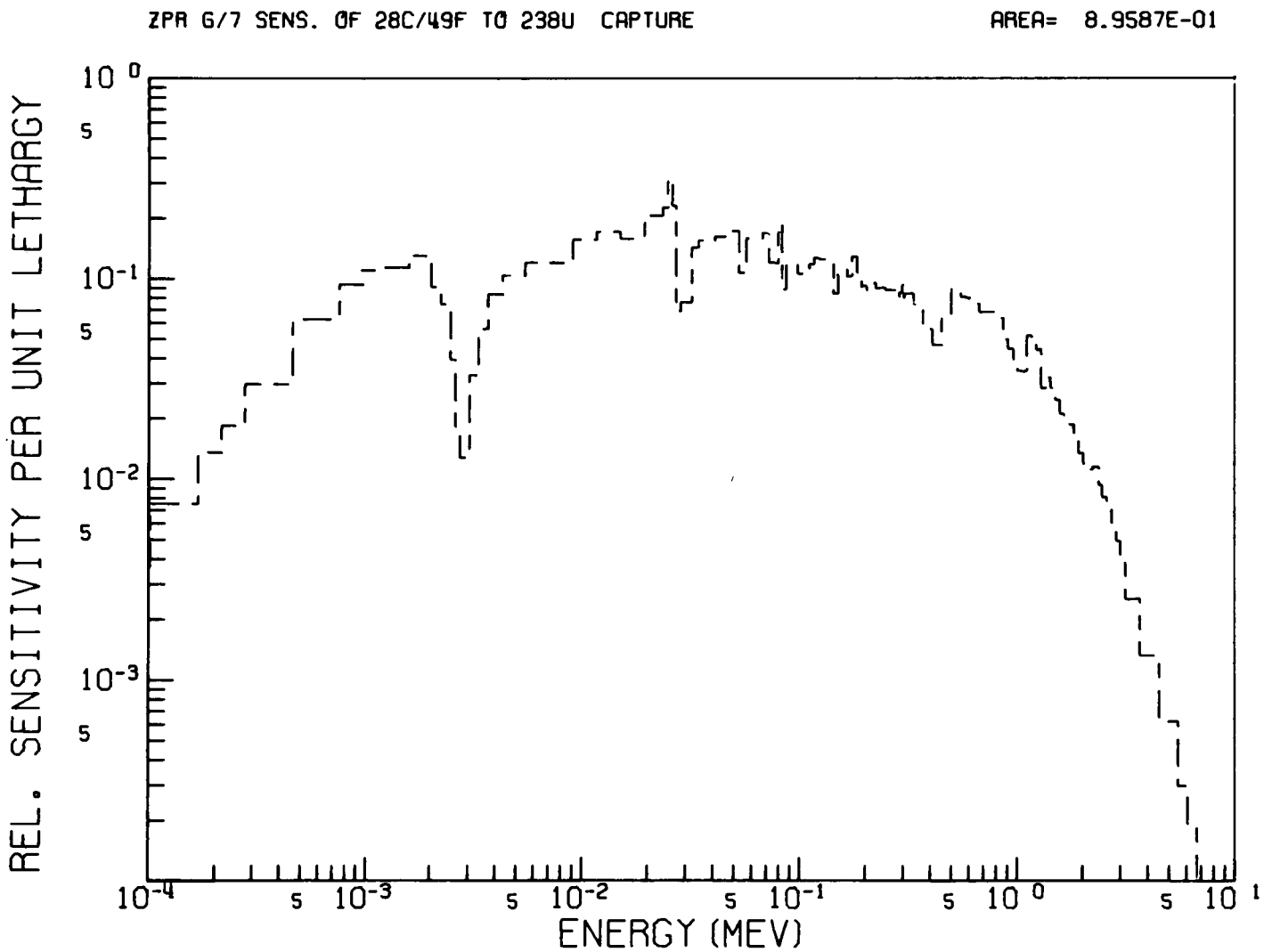

Fig. 20. Sensitivity of the ^{238}U Capture/^{239}Pu Fission Central Reaction Ratio in ZPR-6/7 to the ^{238}U Capture Cross Section.

ORNL DWG 76-6139

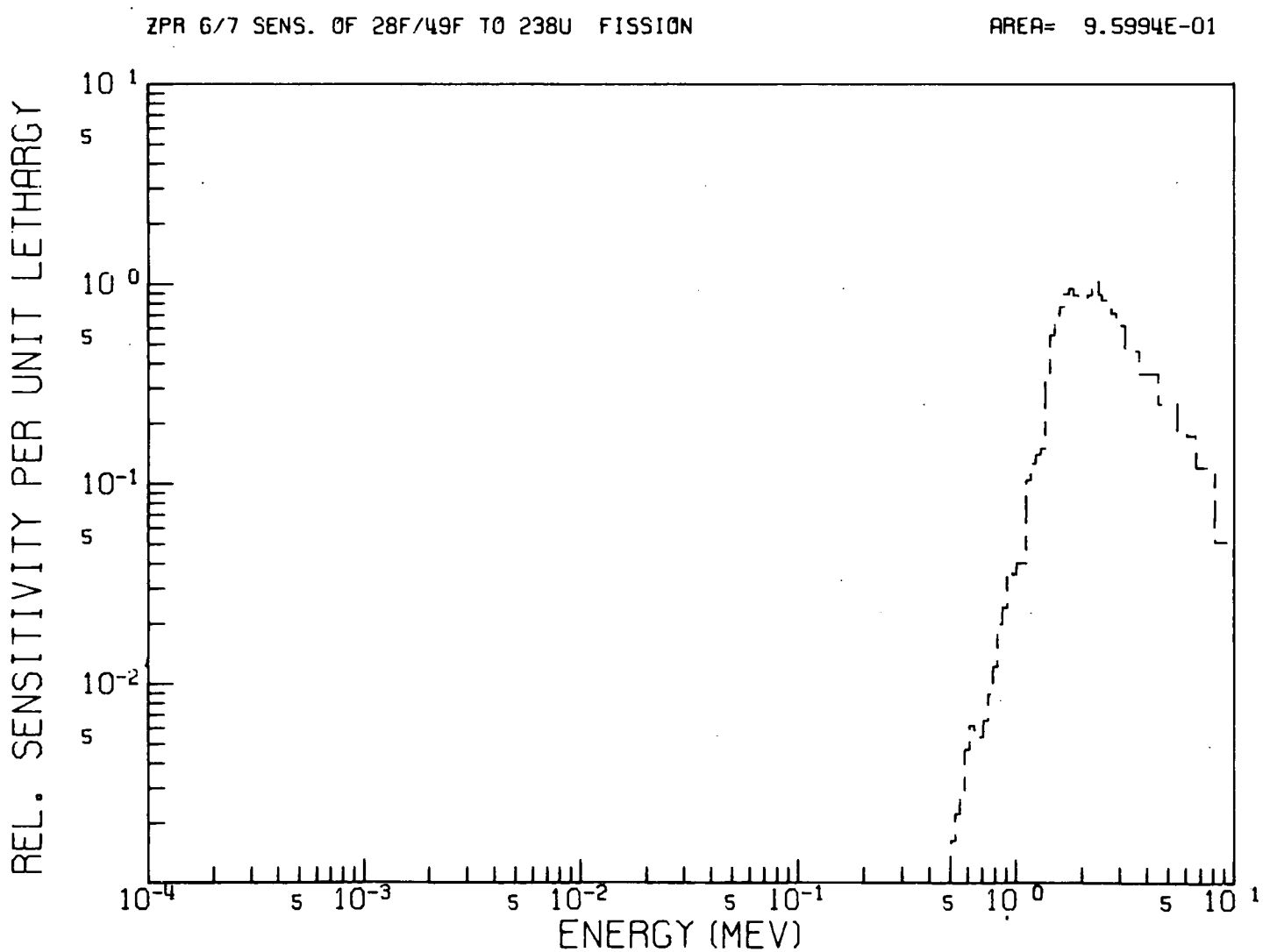

Fig. 21. Sensitivity of the ^{238}U Fission/^{239}Pu Fission Central Reaction Ratio in ZPR-6/7 to the ^{238}U Fission Cross Section.

ORNL DWG 76-6143

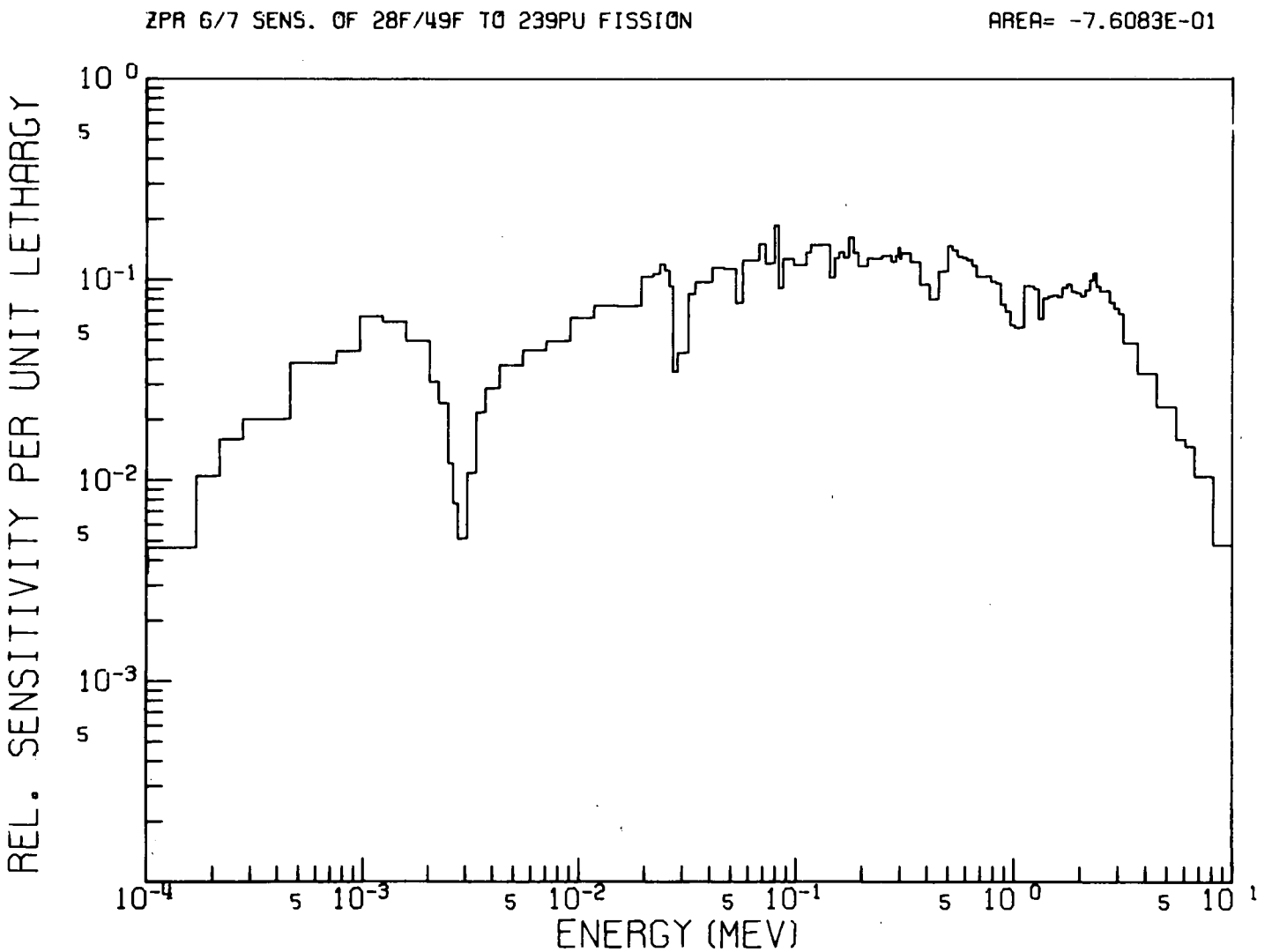

Fig. 22. Sensitivity of the ^{238}U Fission/^{239}Pu Fission Central Reaction Ratio in ZPR-6/7 to the ^{239}Pu Fission Cross Section.

ORNL DWG 76-5551

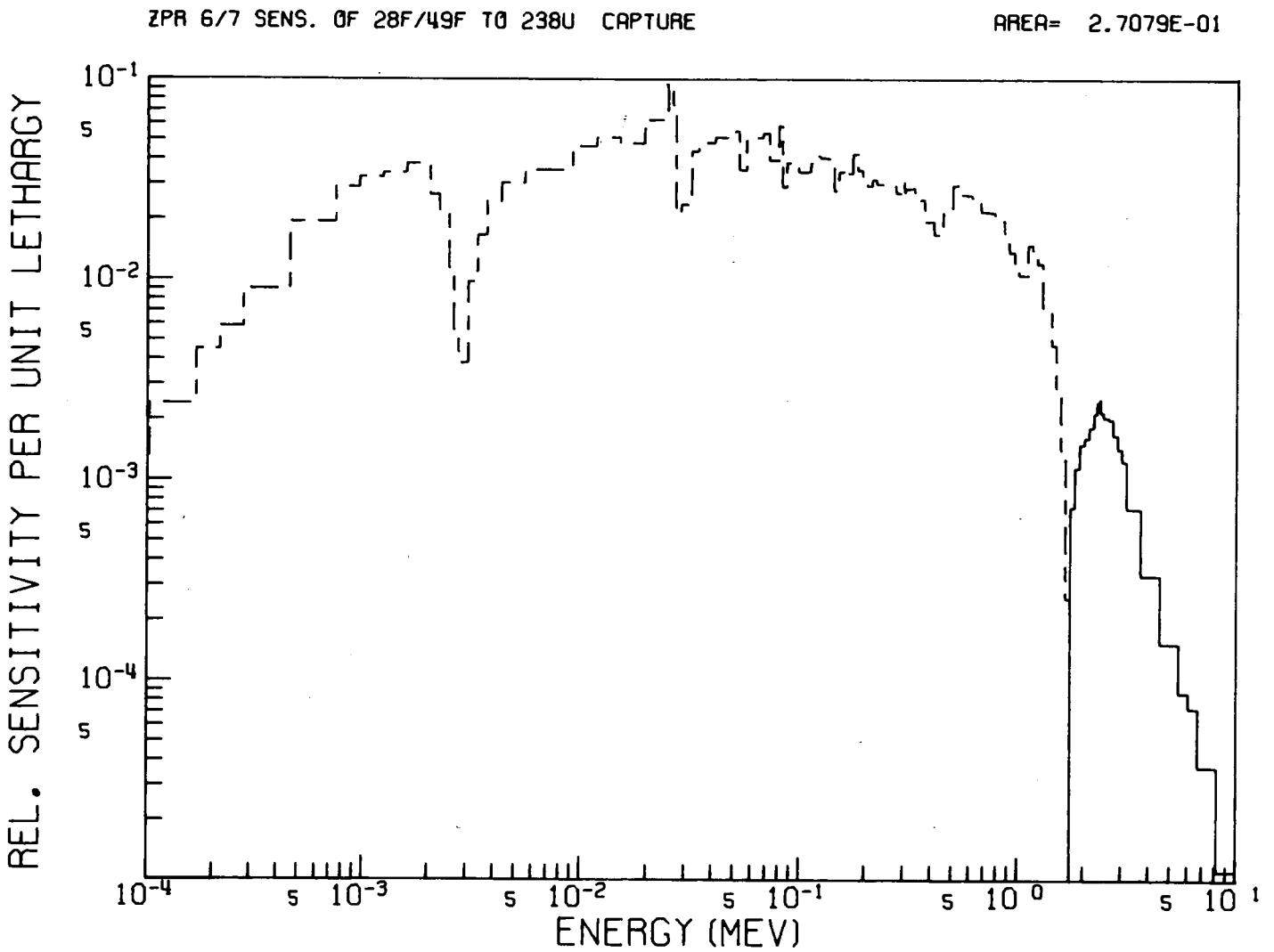

Fig. 23. Sensitivity of the ^{238}U Fission/^{239}Pu Fission Central Reaction Ratio in ZPR-6/7 to the ^{238}U Capture Cross Section.

ORNL DWG 76-6907

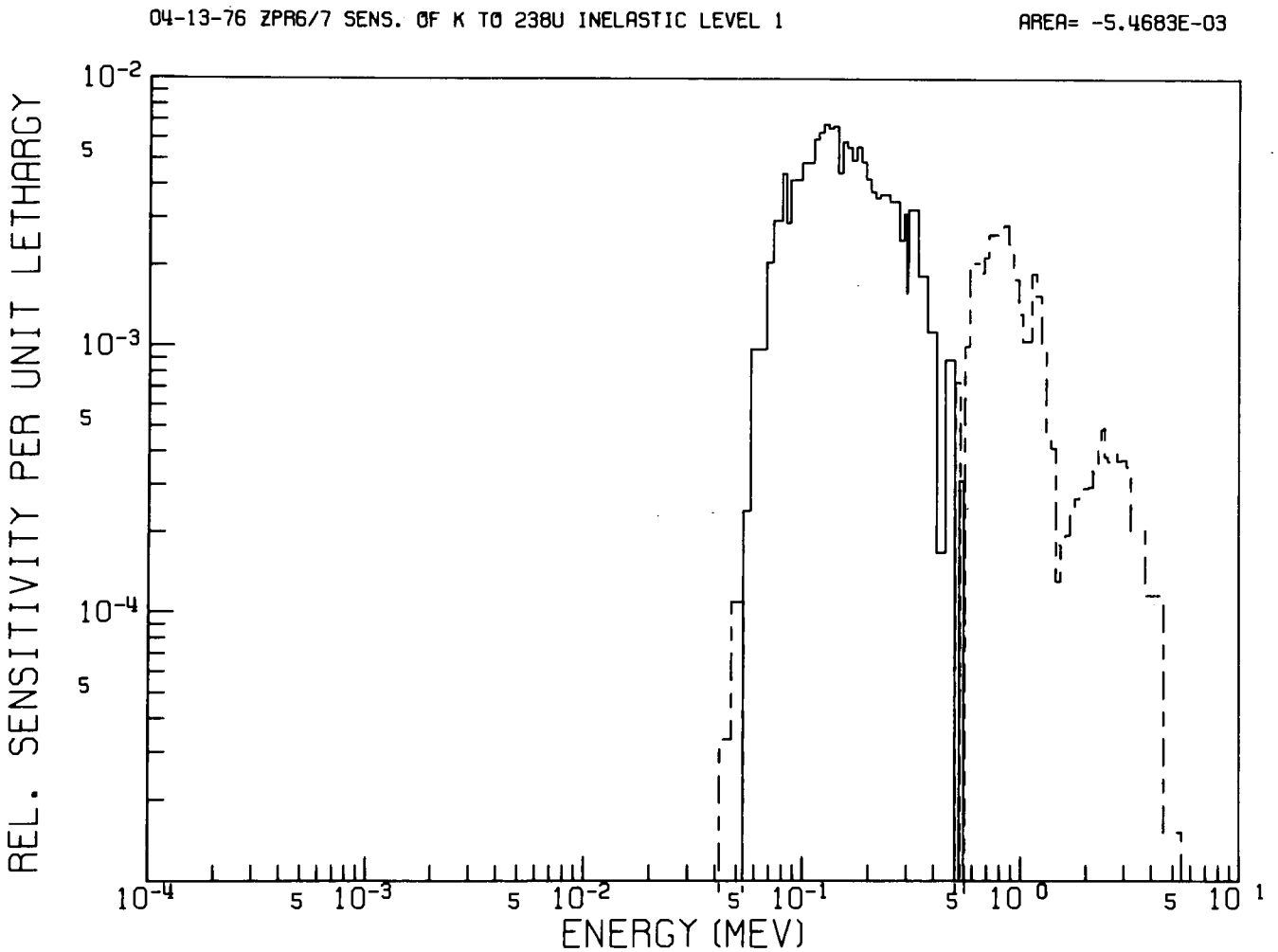

Fig. 24. Sensitivity of k in ZPR-6/7 to the First Level Inelastic Scattering in ^{238}U.

ORNL DWG 76-6889

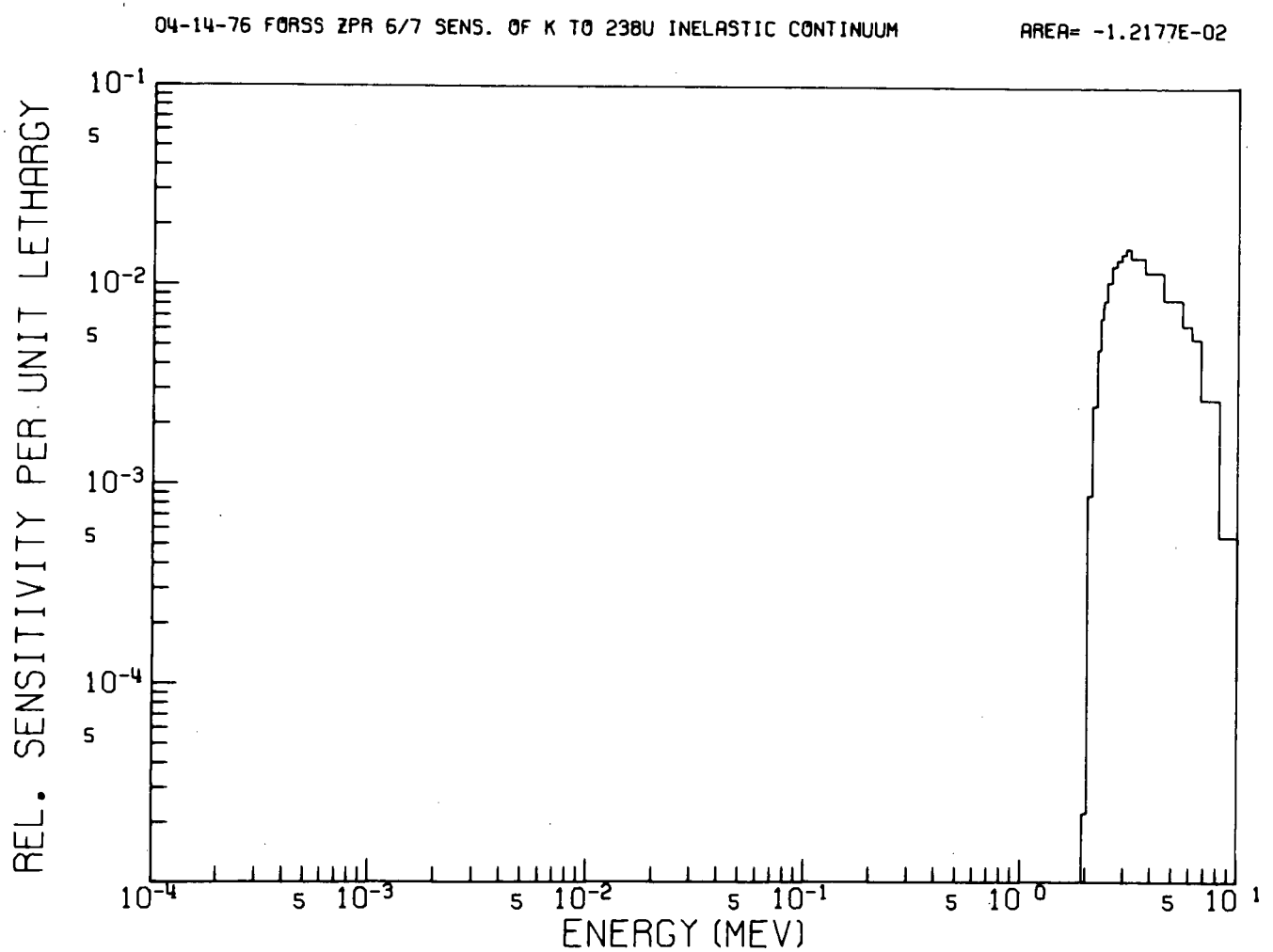

Fig. 25. Sensitivity of k in ZPR-6/7 to the Inelastic Continuum Cross Section of ^{238}U.

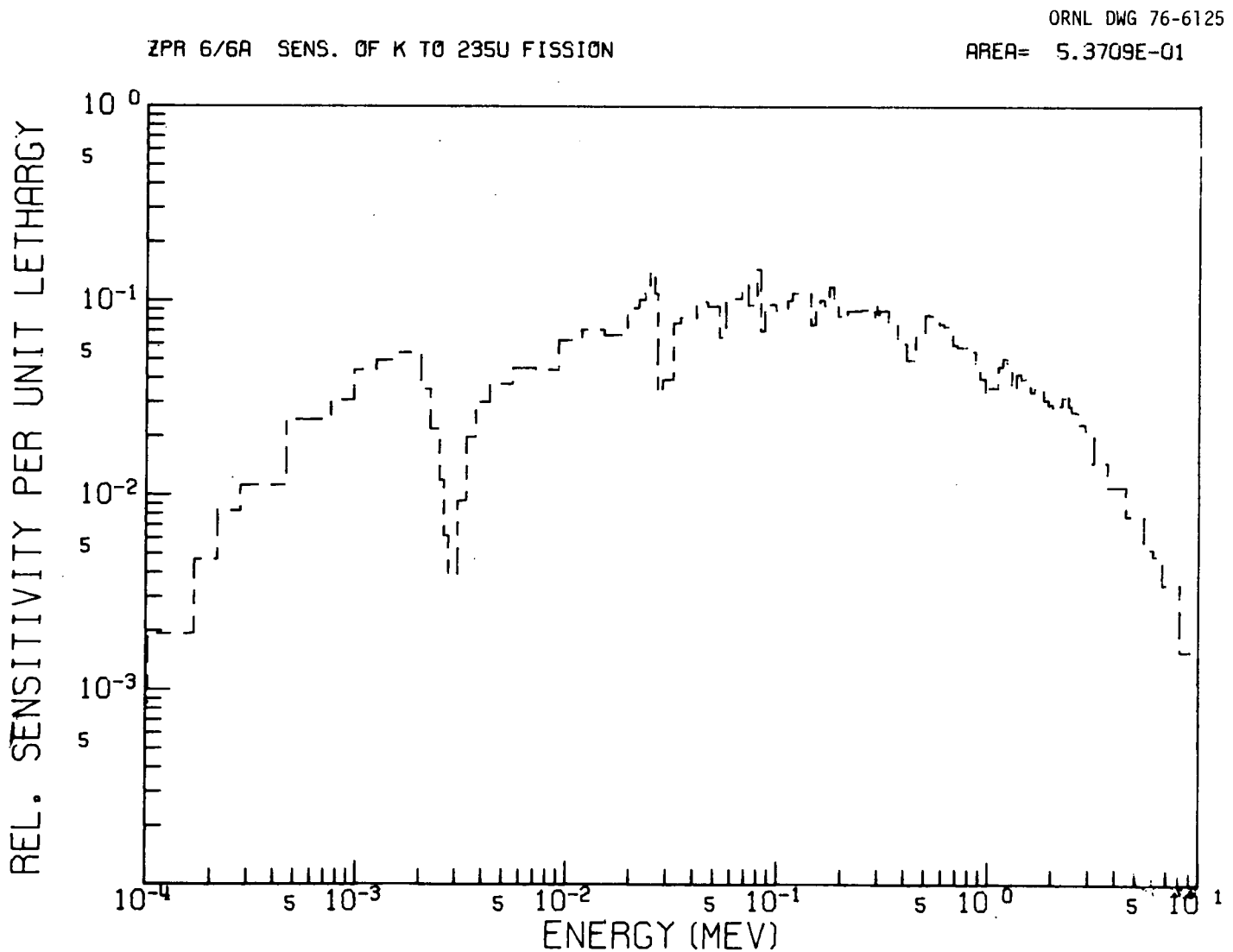

Fig. 26. Sensitivity of k in ZPR-6/6A to the ^{235}U Fission Cross Section.

ORNL DWG 76-6170

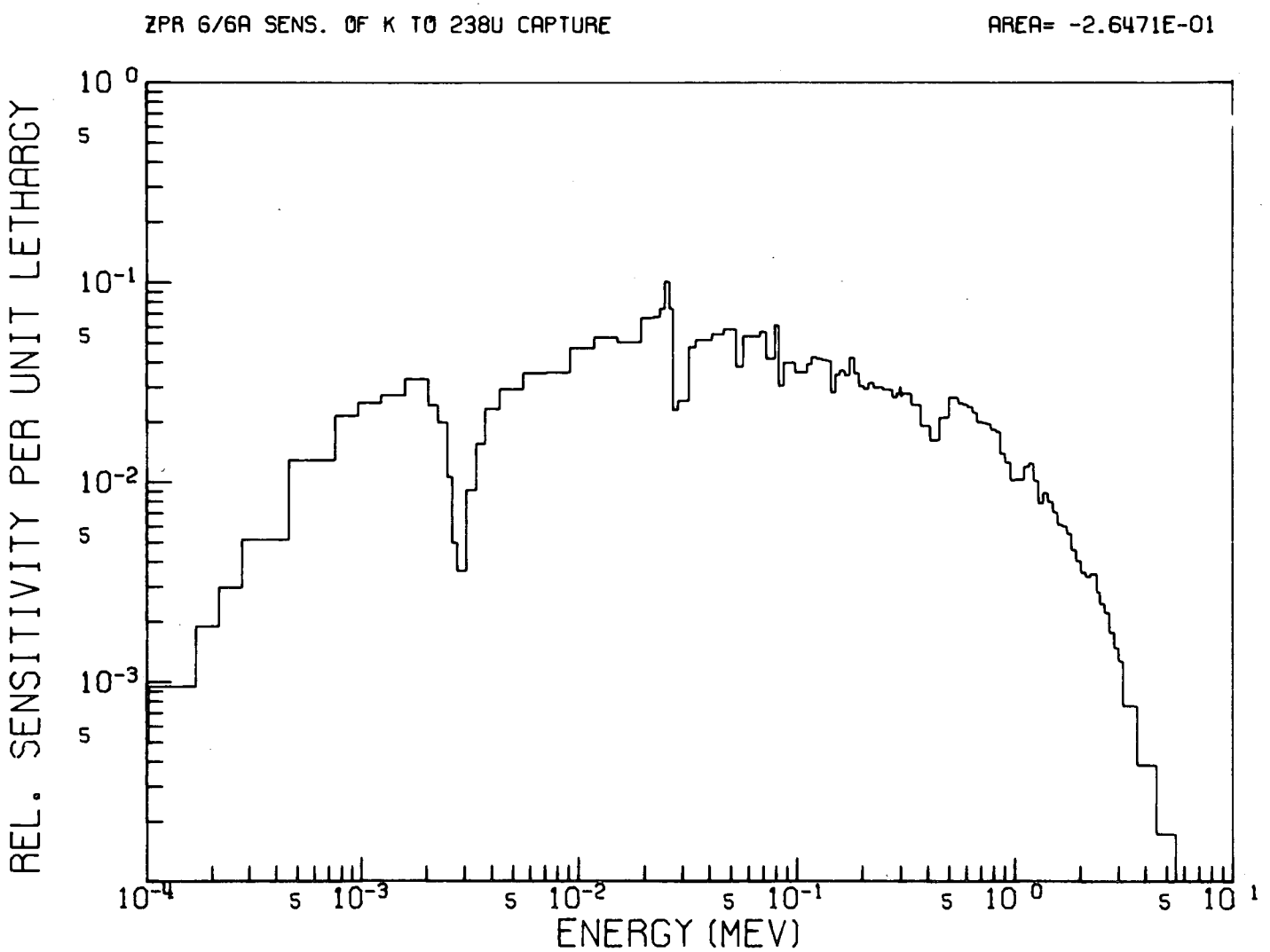

Fig. 27. Sensitivity of k in ZPR-6/6A to the ^{238}U Capture Cross Section.

ORNL DWG 76-5691

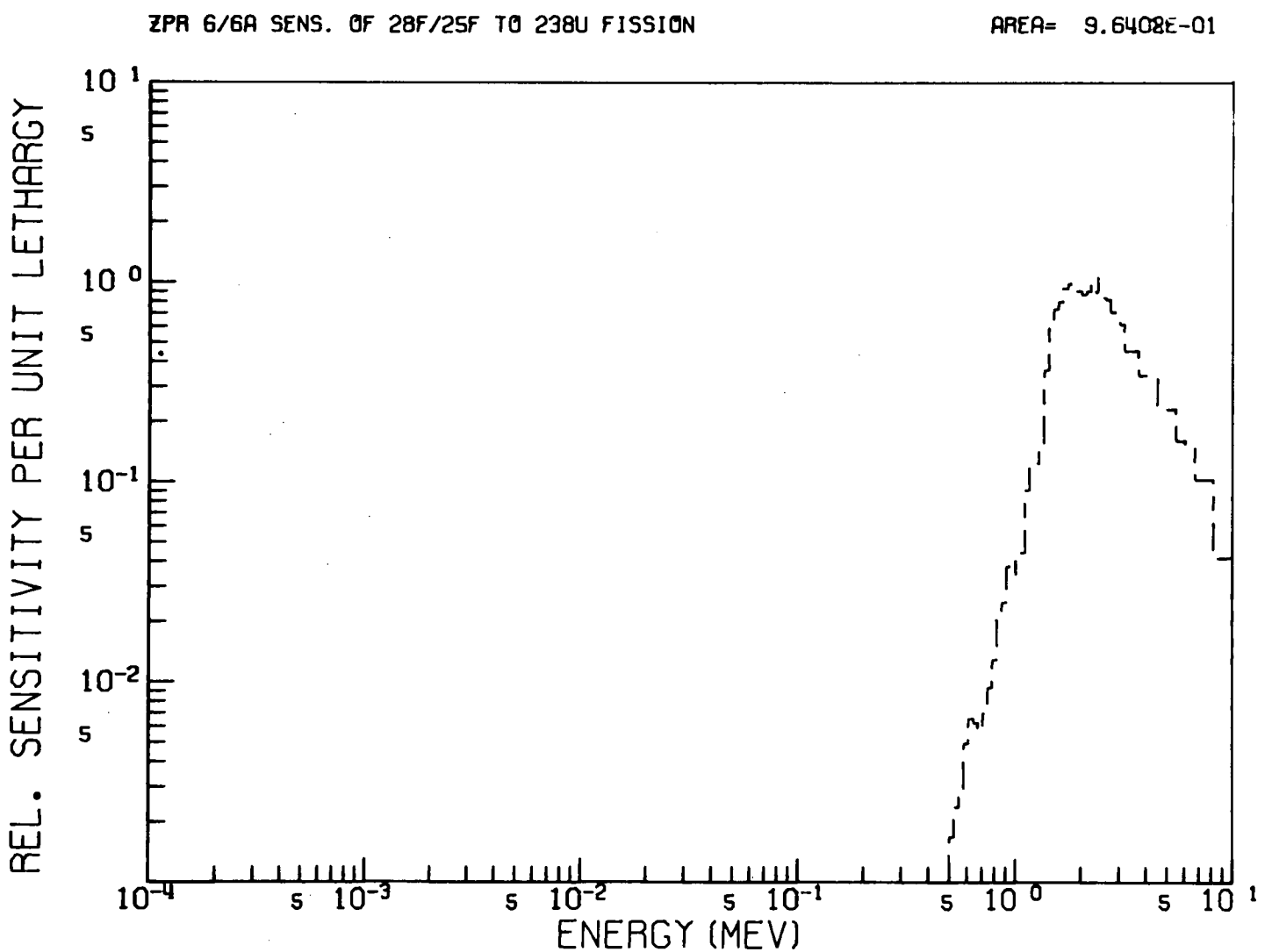

Fig. 28. Sensitivity of the ^{238}U Fission/^{235}U Fission Central Reaction Rate Ratio in ZPR-6/6A to the ^{238}U Fission Cross Section.

ORNL DWG 76-5525

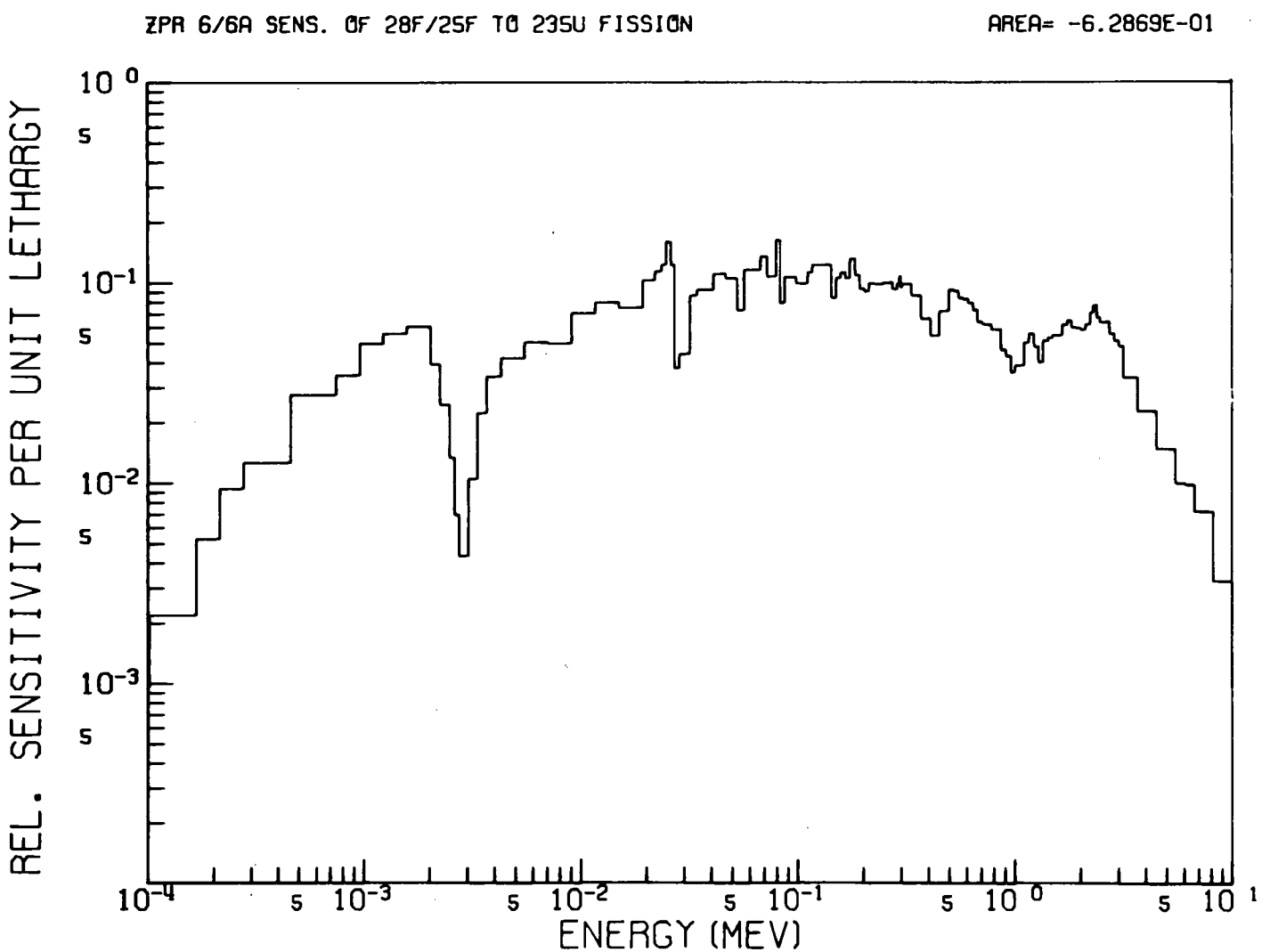

Fig. 29. Sensitivity of the ^{238}U Fission/^{235}U Fission Central Reaction Rate Ratio in ZPR-6/6A to the ^{235}U Fission Cross Section.

ORNL DWG 76-5645

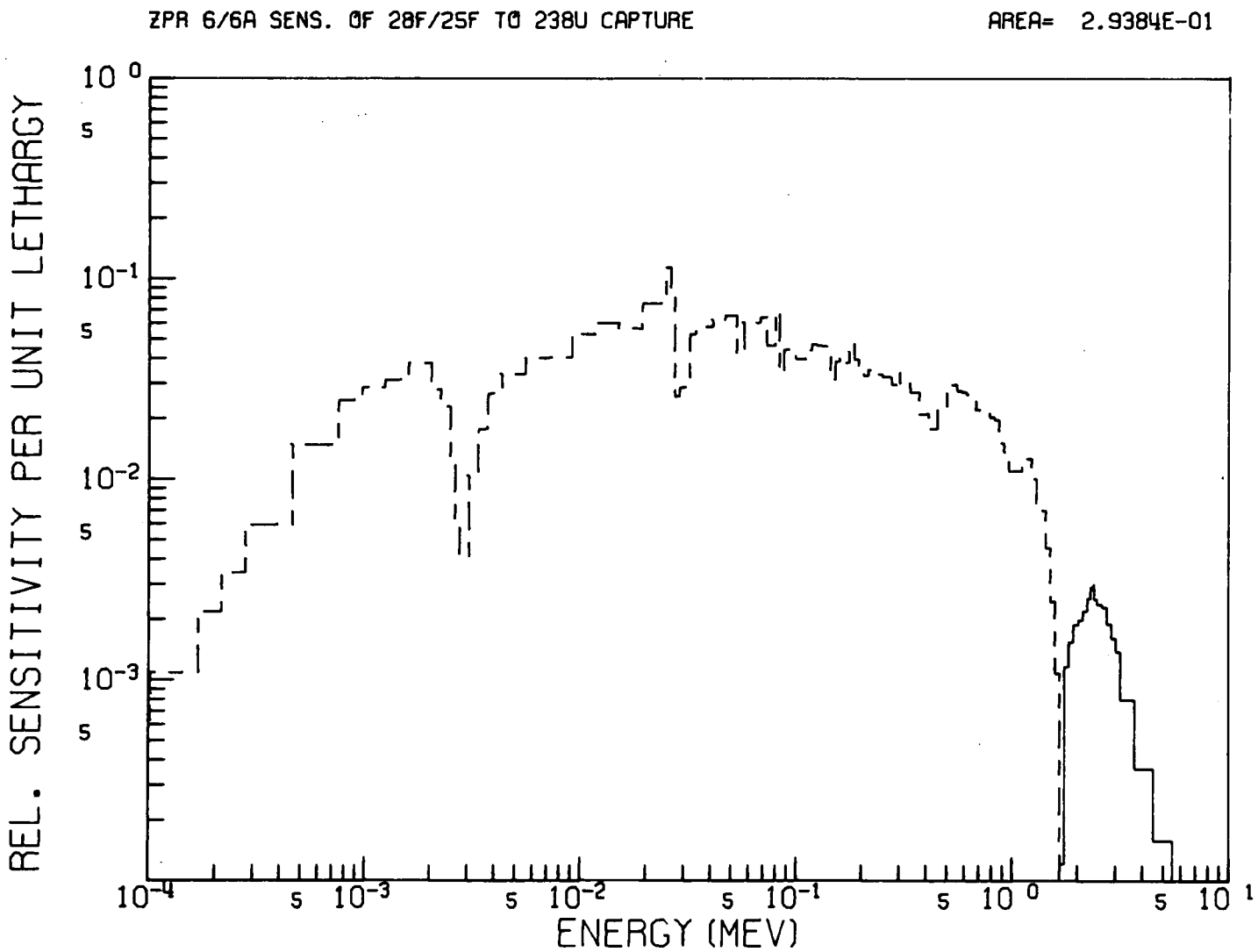

Fig. 30. Sensitivity of the ^{238}U Fission/^{235}U Fission Central Reaction Rate Ratio in ZPR-6/6A to the ^{238}U Capture Cross Section.

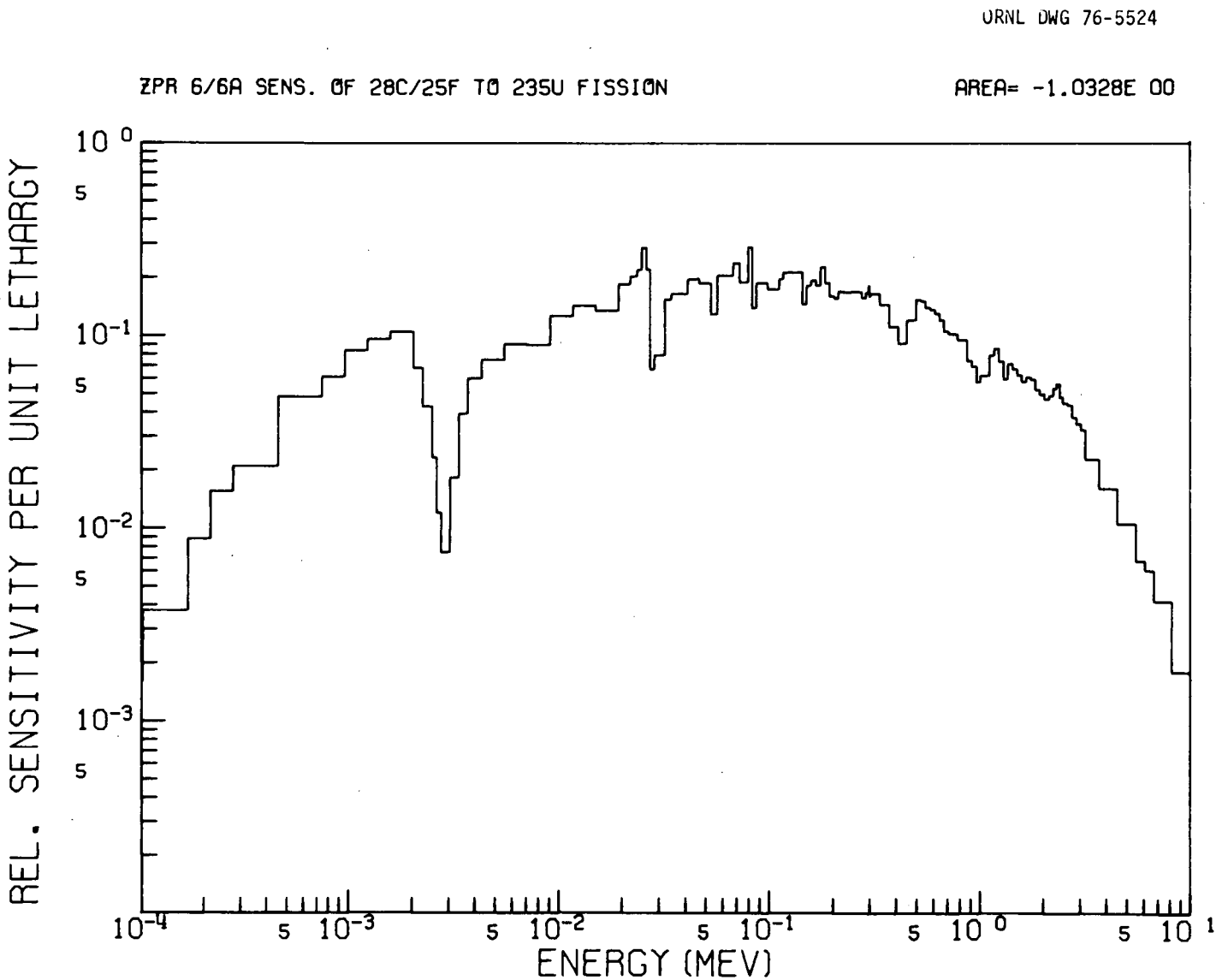

Fig. 31. Sensitivity of the ^{238}U Capture/^{235}U Fission Central Reaction Rate Ratio in ZPR-6/6A to the ^{235}U Fission Cross Section.

ORNL DWG 76-6066

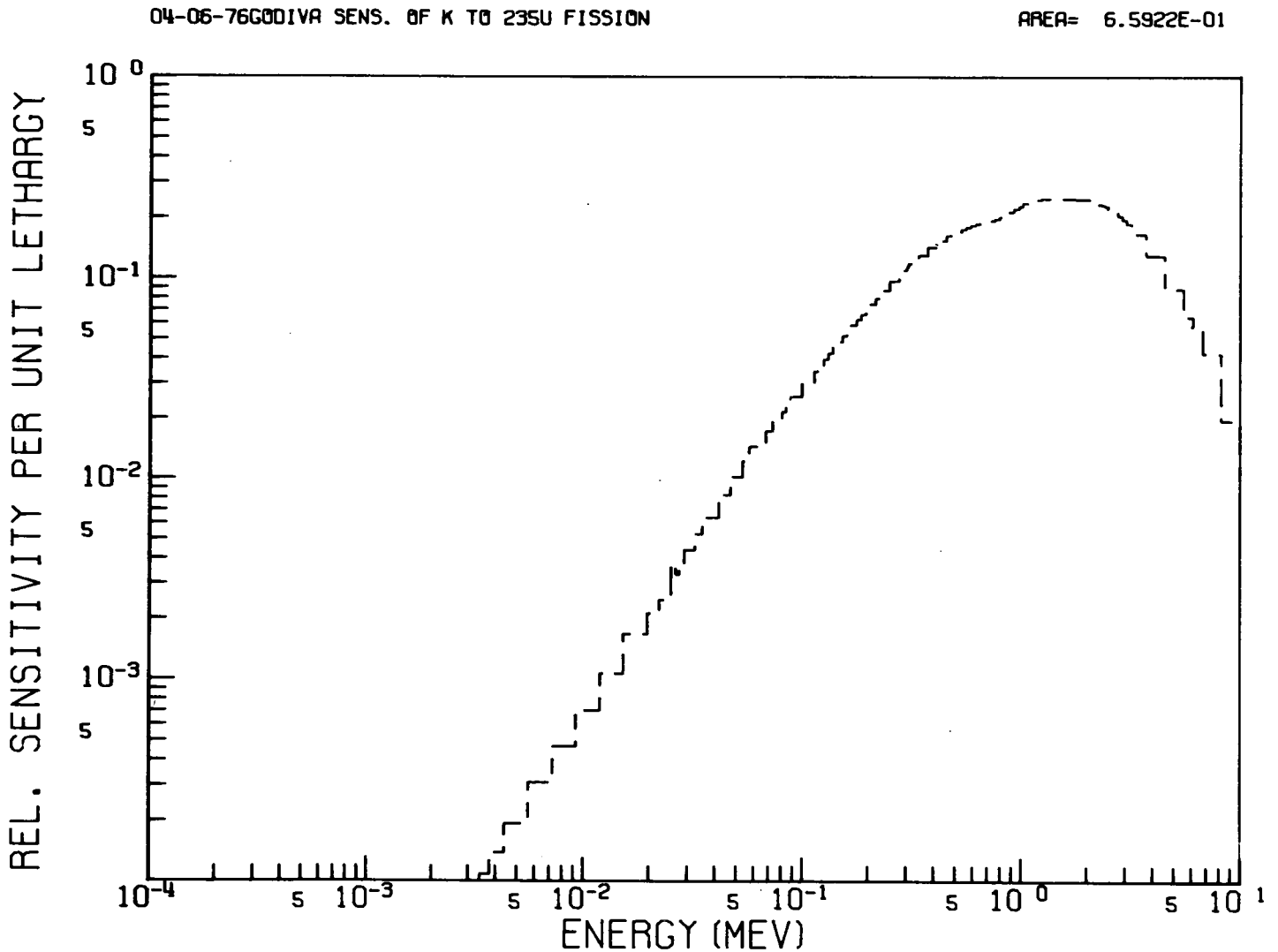

Fig. 32. Sensitivity of k in GODIVA to the ^{235}U Fission Cross Section.

3. A simple density change in a single material or all materials is easily recalculable using ANISN changing the density factors. The fractional change in response observed with direct recalculation should correspond to our estimated change using total profiles multiplied by the density change, for small perturbations. Such changes represent a simple sub-class of the more complicated changes discussed in #5 below.

4. Comparison with other work. Hummel[7] and Bohn[35] have published 12-group profiles for ZPR-6/7 using diffusion theory and VARI-I code.[36] In all cases for capture and fission the degree of agreement was excellent (better than one percent). For scattering reactions, observed discrepancies with Ref. 35 were clarified when ANL included the change in the diffusion coefficient in deriving profiles for elastic scattering.

5. Direct recalculation for realistic cross section changes. At the May, 1976, ENDF/B-V Task Force meeting, evaluators made "first-cut" estimations on what changes might be made in the cross sections for the principal isotopes [^{235}U(n,f), ^{238}U(n,γ), ^{239}Pu(n,f)] for version V relative to ENDF/B Version IV. Having coefficients from ORNL and ANL in hand, the following estimates were made based simply on evaluation of the scalar product

$$\frac{\delta R}{R} \simeq \frac{dR/R}{d\Sigma/\Sigma} \cdot \frac{\delta\Sigma}{\Sigma} \tag{63}$$

These calculations were rough estimates made using smoothed approximations to the changes the evaluators actually proposed simply for convenience (e.g., to align group boundaries). These estimates are included below in Table VIII.

Subsequent to that meeting, we re-estimated the changes (using the detailed 126 energy group sensitivity coefficients and including all of the evaluators proposed adjustments) and performed calculations with the proposed cross sections to verify our predictions for several of the important cases of interest. Table IX indicates that the preliminary estimates were quite reliable.

Table VIII

Impact of Proposed Cross Section Changes to ENDF/B-V on Fast Reactor Critical Analysis

Cross Section	Parameter	Percent Change	Assembly	C/E[a]
$^{25}\sigma_f$	k	-0.8	GODIVA	1.0033
	$^{28}c/^{25}f$	+0.7	ZPR-6/6A	1.007
	$^{28}f/^{25}f$	+0.4	ZPR-6/6A	0.92
$^{28}\sigma_c$	k	+0.12	ZPR-6/7	0.9885
	$^{28}c/^{49}f$	-0.4	ZPR-6/7	1.07
	$^{49}\rho$	-0.3	ZPR-6/7	1.2
	ρ(Na)	+0.4	ZPR-6/7	1.4
	k	$\sim$0	GODIVA	1.0033
$^{49}\sigma_f$	k	+0.06	ZPR-6/7	0.9885
	$^{28}c/^{49}f$	-0.09	ZPR-6/7	1.07
	$^{49}\rho$	+0.07	ZPR-6/7	1.2
	ρ(Na)	+0.08	ZPR-6/7	1.4

[a]Calculation (heterogeneous)/experiment using the original ENDF/B-IV data.

Table IX

Verification of Sensitivity Analysis Predictions for Preliminary ENDF/B-V Impact on Critical Experiment Calculations

	GODIVA (k)	ZPR-6/6A (k)	ZPR-6/7 (k)
Cross section Change	$^{235}U(n,f)$ (>200 keV)	$^{235}U(n,f)$ (>200 keV)	$^{239}Pu(n,f)$ (>200 keV)
ORNL calculation ENDF/B-IV (homogeneous Models)	1.0050	0.9926	0.9719
ORNL calculation ENDF/B-IV +Task Force	0.9961	0.9886	0.9734
Absolute Change	-0.0089	-0.0040	+0.0015
ORNL Sensitivity Analysis Prediction of Absolute Change	-0.0087	-0.0040	+0.0016

In view of the differences in the scattering reactions with the original ANL calculations and in order to investigate the limits of first order perturbation theory, we list in Table X results that would be obtained under the hypothetical increase in the sodium elastic scattering cross section by a factor of two.

VI. Multigroup Covariance Matrices

Only recently have standard formats and procedures been established within the ENDF/B system[37] for the processing of evaluated and correlated energy-dependent uncertainty information into a multigroup covariance matrix formulation. These covariance matrices were established[38] to permit systematic sensitivity investigations to propagate uncertainties and thereby determine, in a credible fashion, what cross-section measurements, evaluation, or processing methods most need further refinement.

Table X

Recalculation of ZPR-6/7 Performance Parameters Assuming the Na(n,n) Cross Section To Be Doubled and Comparison with Sensitivity Analysis Predictions

	ZPR-6/7 (k)	ZPR-6/7 ($^{28}f/^{49}f$)	ZPR-6/7 ($^{28}c/^{49}f$)
Cross Section Change	Na(n,n) (multiplied by 2)	Na(n,n) (multiplied by 2)	Na(n,n) (multiplied by 2)
ORNL Calculation ENDF/B-IV (homogeneous models)	0.9719	0.1500	1.0046
ORNL Calculation (sodium cross section multiplied by 2)	0.9805	0.1432	1.0246
Absolute[a] Change	+0.0086	-0.0068	+0.0200
Sensitivity Analysis Prediction of Absolute Change	+0.0087	-0.0072	+0.0281

[a]Note that comparisons of predictions of small relative changes are exaggerated here by tabulated predictions of absolute change. Also note these are macroscopic reaction rates (as opposed to microscopic rates on pg. 25) for the homogeneous model (as opposed to the heterogeneous values reported on pg. 25).

A. Formulation

The types of covariance representations permitted in ENDF/B-IV included:[37]

LB=0 absolute components correlated only within each E_k interval

$$\mathrm{Cov}(X_i,Y_j) = \sum_k P^{i;k}_{j;k} F_{XY,k} \tag{64}$$

LB=1 fractional components correlated only within each E_k interval

$$\mathrm{Cov}(X_i,Y_j) = \sum_k P^{i;k}_{j;k} F_{XY,k} X_i Y_j \tag{65}$$

LB=2 fractional components fully correlated over all E_k intervals (one table $F_{XY,k}$ as a function of energy)

$$\mathrm{Cov}(X_i,Y_j) = \sum_{k,k'} P^{i;k}_{j;k'} F_{XY,k} F_{XY,k'} X_i Y_j \tag{66}$$

LB=3 fractional components arbitrarily correlated between E_k and E_ℓ intervals

$$\mathrm{Cov}(X_i,Y_j) = \sum_{k,\ell} P^{i;k}_{j;\ell} F_{X,k} F_{Y,\ell} X_i Y_j \tag{67}$$

where X_i and Y_j represent cross sections X and Y evaluated at energies i and j, respectively, the F's ($F_{XY,k}$, $F_{XY,k'}$, $F_{X,k}$, and $F_{Y,\ell}$) represent uncertainty components, taken directly from the ENDF/B file describing the covariances of cross sections X and Y for specific energy intervals. These fractional components are defined assuming a multivariate normal distribution of cross section uncertainties; furthermore, multiple sections (e.g., $F^n_{XY,k}$) may be provided to identify specific types of experimental uncertainties associated with the complete covariance matrix.

The $F_{XY,k}$ and $F_{XY,k'}$ are taken from a single table of energy-dependent correlation information for reactions X and Y. The $F_{X,k}$ and $F_{Y,\ell}$ indicate that the covariance data for these reactions are taken from two independent tables, one for X and one for Y. The $P^{i,k}_{j,k'}$ is zero except for the case when energy i is contained within energy interval k and energy j is contained within energy interval k'. $Cov(X_i,Y_j)$ is then the covariance of cross section X at energy i and cross section Y at energy j. There is a fifth law (LB=4), but since it can be described as combinations of the first four, no data has yet been cast in this form for ENDF/B-IV.

This type of formulation (sums of quantities separable in X and Y) has the very desirable characteristic that if one assumes a flux model uncorrelated to the cross sections of interest, the multigroup covariance matrices are reduced to combinations of single integrals involving group fluxes and cross sections which can be calculated easily. In particular, for

LB=0,

$$Cov(X_G,Y_H) = \frac{\sum_n \sum_{k\varepsilon G} F^n_{XY,k}\ \phi^n_{G,k}\ \phi^n_{H,k}}{\phi_G\ \phi_H} \tag{68}$$

LB=1,

$$Cov(X_G,Y_H) = \frac{\sum_n \sum_{k\varepsilon G} F^n_{XY,k}\ \phi^n_{G,k}\ X^n_{G,k}\ \phi^n_{H,k}\ Y^n_{H,k}}{\phi_G\ \phi_H} \tag{69}$$

LB=2,

$$Cov(X_G,Y_H) = \frac{\sum_n \left(\sum_{k\varepsilon G} F^n_{XY,k}\ \phi^n_{G,k}\ X^n_{G,k}\right)\left(\sum_{k'\varepsilon H} F^n_{XY,k'}\ \phi^n_{H,k'}\ Y^n_{H,k'}\right)}{\phi_G\ \phi_H} \tag{70}$$

LB=3,

$$\mathrm{Cov}(X_G,Y_H) = \frac{\sum_n \left(\sum_{k\varepsilon G} F^n_{X,k}\ \phi^n_{G,k}\ X^n_{G,k}\right)\left(\sum_{k'\varepsilon H} F^n_{Y,k'}\ \phi^n_{H,k'}\ Y^n_{H,k'}\right)}{\phi_G\ \phi_H} \tag{71}$$

In general, the covariance matrix will be a sum of terms from any of the LB descriptions. The derivation of Eqs. (68-71) has been described previously;[37] the notation used here is:

$\mathrm{Cov}(X_G,Y_H)$ = Multigroup covariance of reaction X group G and reaction Y, group H.

ϕ_G = Multigroup flux per user group G.

$X^n_{G,k}$ = Multigroup cross section for reaction X for a super-group (G,k) constructed from the union of energy bounds for interval k (taken from subsection n) and those which were user input. $\phi^n_{G,k}$ is the flux for this group.

Note that this formalism is appropriate for infinitely dilute cross sections; uncertainties in resonance parameters are not addressed. The assumption is that uncertainties in the infinitely dilute cross sections are more severe than those in the self-shielding factor which, itself, is a ratio.

B. Results for Processed Uncertainty Files

Several quantities related to uncertainties in multigroup cross sections are processed from the pointwise ENDF/B data covariance file using the PUFF covariance file processing code.[24] Clearly, of interest, is the covariance matrix

$$\mathrm{Cov}(X_G,Y_H) = \left\langle (X_G - \overline{X}_G)(Y_H - \overline{Y}_H)\right\rangle \tag{72}$$

the covariance of reaction X, group G, and reaction Y, group H. (Angle brackets represent expectation values in this section.) The associated quantity, the relative covariance matrix is defined

$$\text{Rel Cov}(X_G,Y_H) = \text{Cov}(X_G,Y_H)/X_G Y_H \tag{73}$$

In this notation, the standard deviation is given by:

$$\text{Std. Dev}(X_G) = \sqrt{\text{Cov}(X_G,X_G)} \tag{74}$$

and the analogous relative quantity, the relative standard deviation, is

$$\text{Rel Std. Dev}(X_G) = \frac{\text{Std. Dev}(X_G)}{X_G} \tag{75}$$

It is reasonable to expect that in many cases the covariance matrix of energy-dependent cross sections is strongly diagonal, i.e., the magnitude of the matrix elements tend to be small for groups G and H widely displaced from each other in energy. However, since relative cross sections are often well known, this introduces large covariances between nearby group cross sections.

The correlation matrix is a quantity constructed by dividing the relative covariance matrix for X_G and Y_H by the respective relative standard deviations.

$$\text{Corr}(X_G,Y_H) = \frac{\left\langle (X_G - \overline{X}_G)(Y_H - \overline{Y}_H)\right\rangle}{\sqrt{\left\langle (X_G - \overline{X}_G)^2\right\rangle \left\langle (Y_H - \overline{Y}_H)^2\right\rangle}} \tag{76}$$

The correlation matrix is bounded by unity, i.e.,

$$|\text{Corr}(X_G,Y_H)| \leq 1 \tag{77}$$

When $\text{Corr}(X_G,Y_H) = 0$, the group cross sections are said to be totally uncorrelated; when $|\text{Corr}(X_G,Y_H)| = 1$, the group cross sections are termed fully correlated.

Figures 33 to 38 illustrate the covariance matrices for the important reactions with ^{238}U and ^{239}Pu in the ten-group processed form used to obtain the results given in this report. (The uncertainty files have also been processed and used in the 126-group format.) The underlying files of covariance data were based primarily on "external" methods of analysis which examine the scatter among existing data sets. These sets are assumed to represent fairly the statistical ensemble of hypothetical sets of measurements which could have been obtained in the experiments which form our present data base. In all cases the group cross sections obtained from ENDF/B-IV were taken as expectation values of the hypothetical ensemble. The "pointwise" covariance files were represented on convenient energy grids believed to be adequately fine to faithfully reproduce the broad-range behavior important for estimation of uncertainties in integral quantities.

The capture and fission covariance files were obtained as indicated in the SUR report,[39] essentially applying Eq. (72) directly to compiled sets of experimental cross sections. In cases for which only a few data sets exist or could be compiled, the ensemble variances were statistically poorly determined by the small sample; however, variance fluctuations from group to group may be unimportant after averaging over the reactor neutron spectrum. In cases for which many data sets were available, the method overestimates uncertainties because it does not correct for the distinction between the ensemble of hypothetical measurements and the ensemble of evaluations based on these measurements; the resulting covariance elements should be too large by a factor roughly equal to the number of "good" measurements available. Beyond this question, and often tending to make our estimates too small, is the fact that external methods like that of SUR cannot fully sense uncertainties (like those in standard cross sections) which influence more than one set of measurements and thus cannot be sensed in the scatter among their results. In the case of the ^{239}Pu uncertainty files it was possible to take the latter type of uncertainty partially into account.[40] Elements reflecting correlations between

ORNL DWG 76-16208

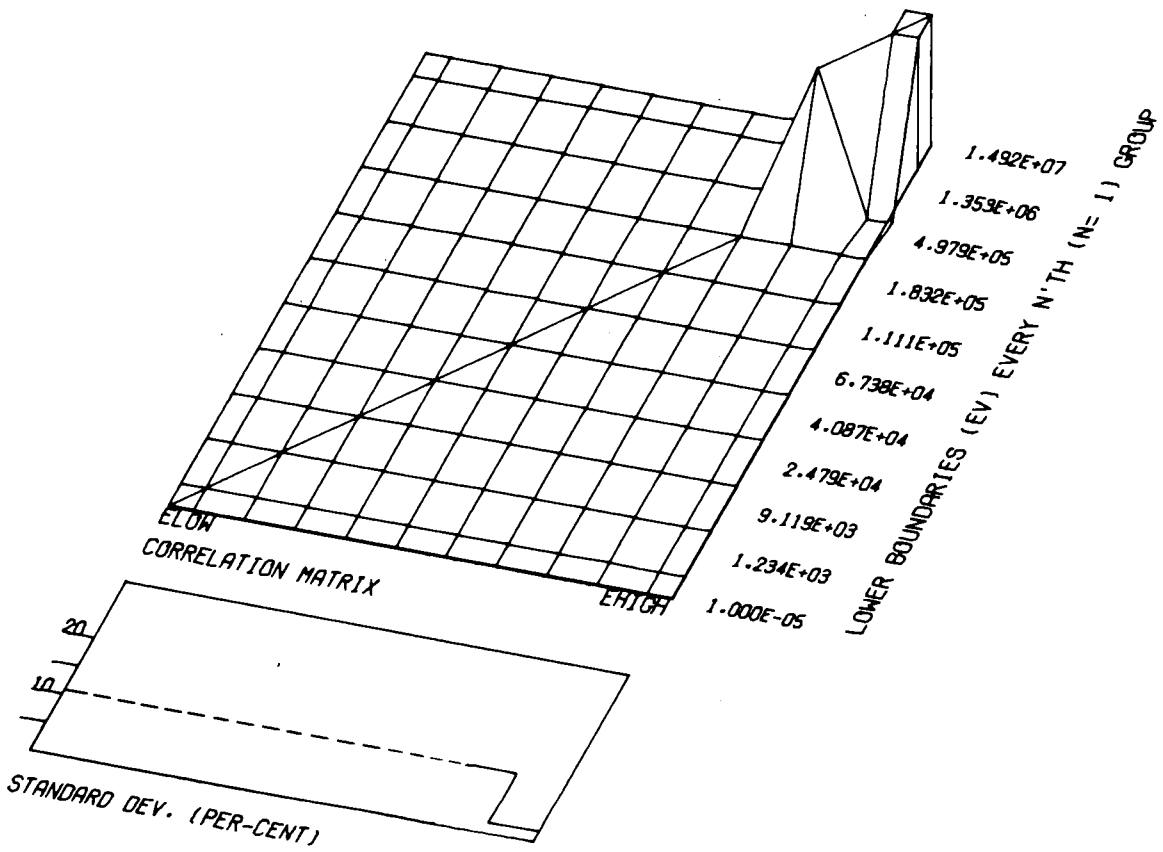

MAT'L 1262 10 GROUPS REACT 18 TO REACT 18

Fig. 33. Correlation Matrix and Standard Deviation for the $^{238}U(n,f)$ Cross Section.

ORNL DWG 76-16209

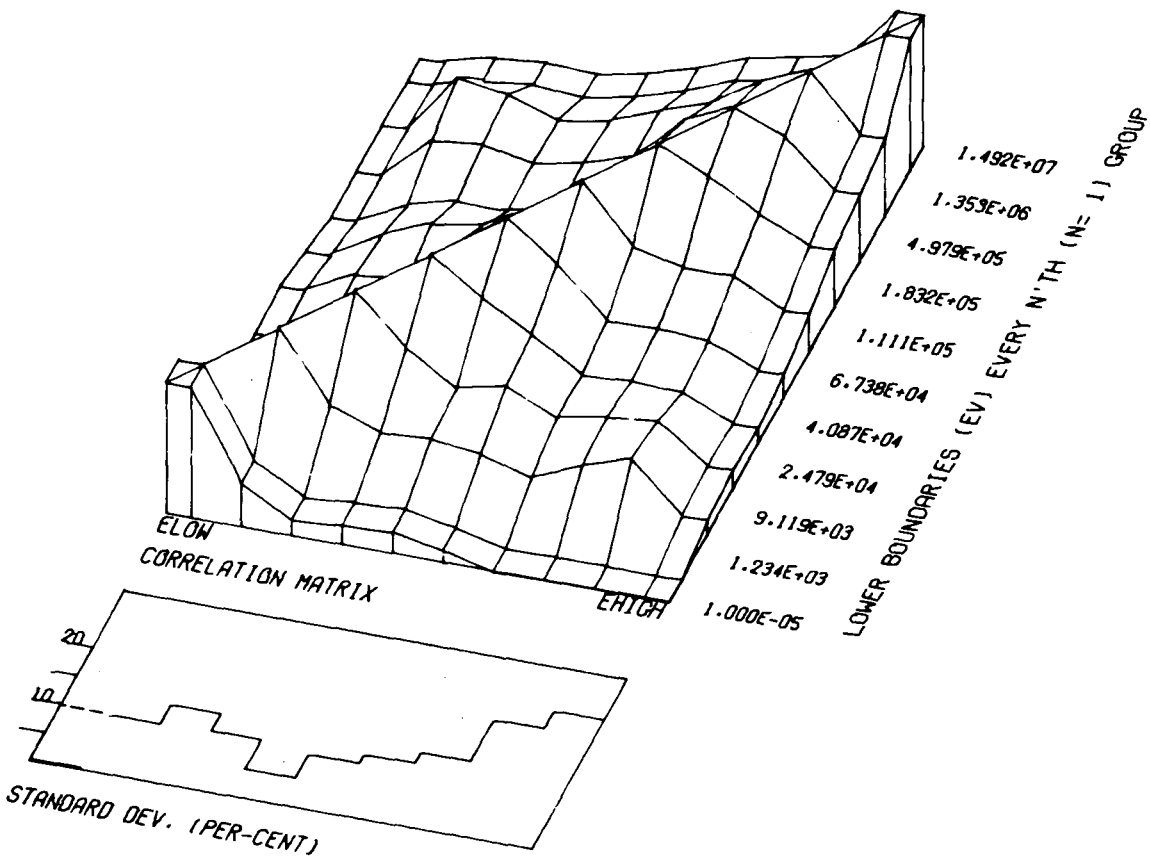

MAT'L 1262 10 GROUPS REACT 102 TO REACT 102

Fig. 34. Correlation Matrix and Standard Deviation for the $^{238}U(n,\gamma)$ Cross Section.

(NOTE: The sample means for the sets of measurements used to obtain this uncertainty matrix were not close to the ENDF/B-IV evaluated cross sections over the major portion of the energy spectrum, so the rms uncertainties for this case reflect primarily the real discrepancy between the sample mean and the evaluated cross sections. That is, for the considerable sample of measurement data selected for this particular covariance analysis the ENDF/B-IV evaluated cross section falls ~8% below the inferred ensemble average over the important energy region from 10-300 keV. A consistent evaluation based solely upon differential measurements would exacerabate the central $^{28}c/^{49}f$ discrepancy for ZPR-6/7 apparent in Tables II and VII. Proper handling of this difficulty is presently a major challenge to the reliability of the uncertainty analyses now made by FORSS (or any such system) if one assumes that adjustments to microscopic measurements may have already been included in ENDF/B-IV.

ORNL DWG 76-16210

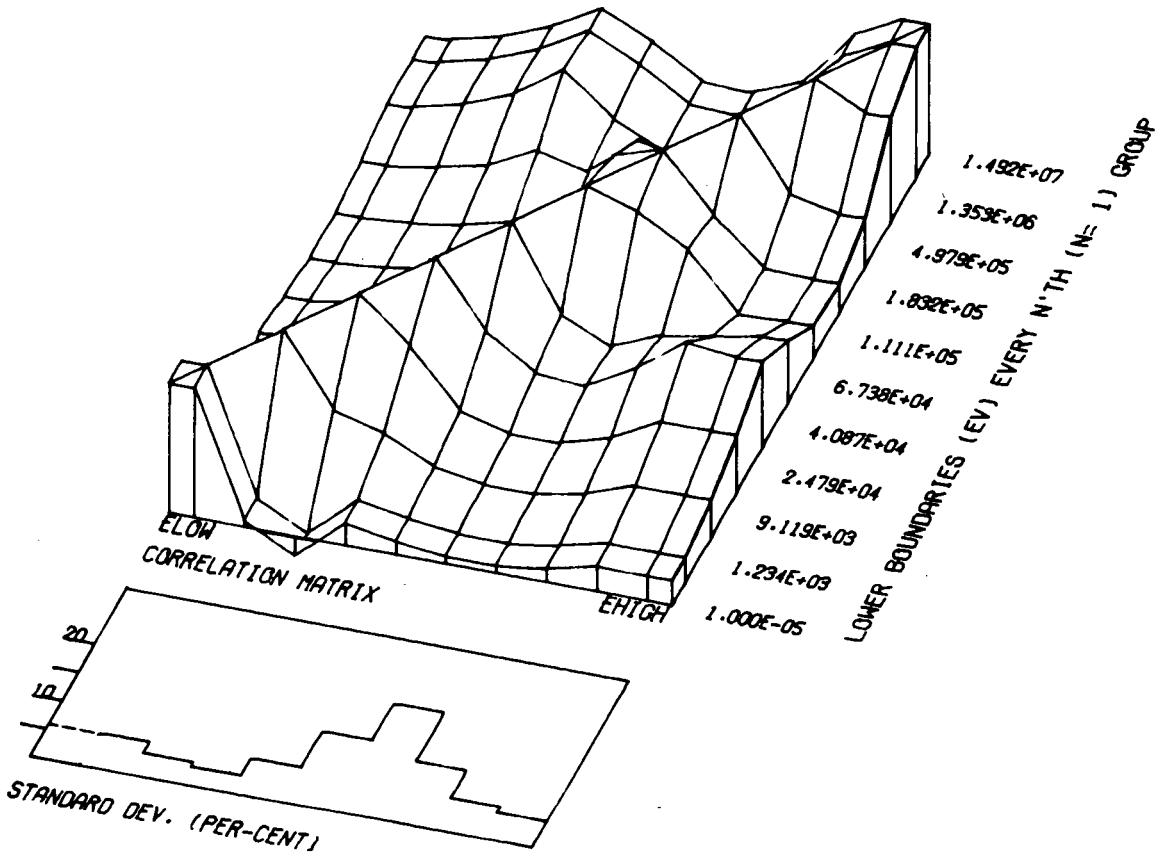

MAT'L 1264 10 GROUPS REACT 18 TO REACT 18

Fig. 35. Correlation Matrix and Standard Deviation for the $^{239}Pu(n,f)$ Cross Section.

ORNL DWG 76-16211

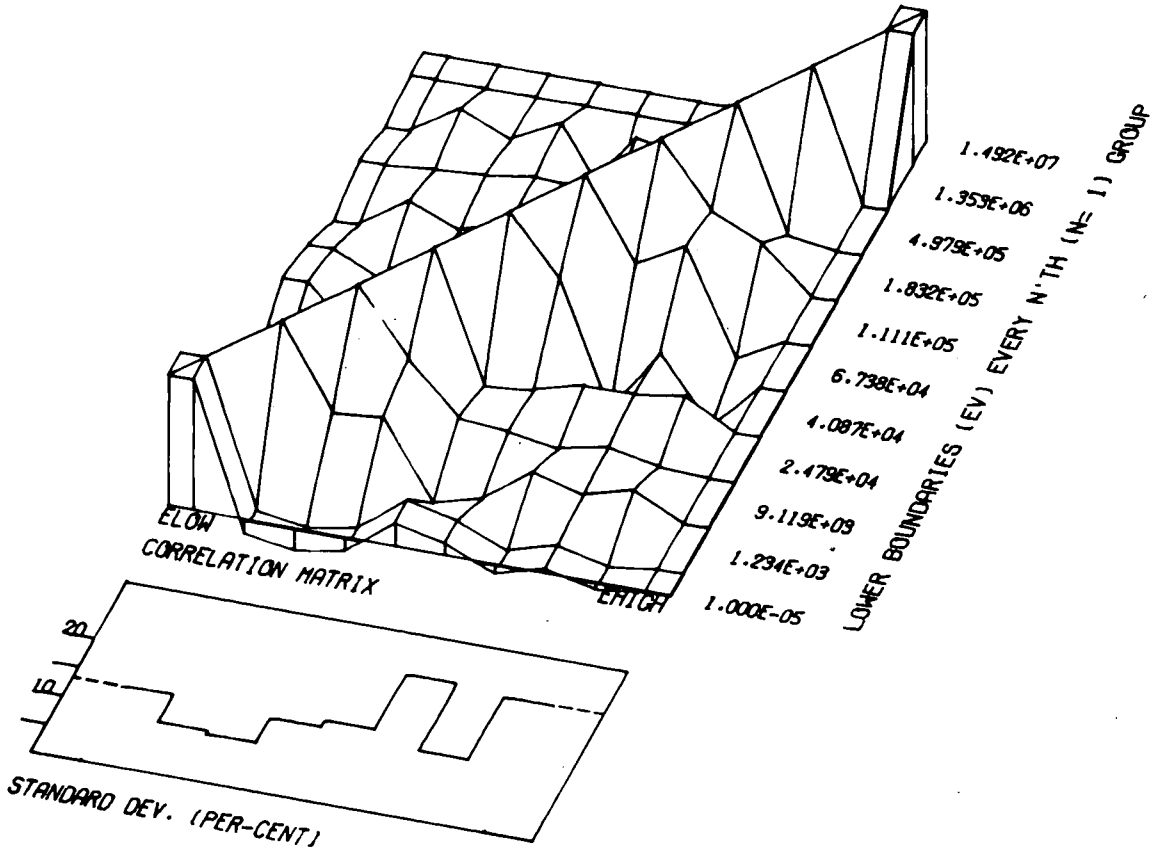

MAT'L 1264 10 GROUPS REACT 102 TO REACT 102

Fig. 36. Correlation Matrix and Standard Deviation for the $^{239}Pu(n,\gamma)$ Cross Section.

ORNL DWG 76-16212

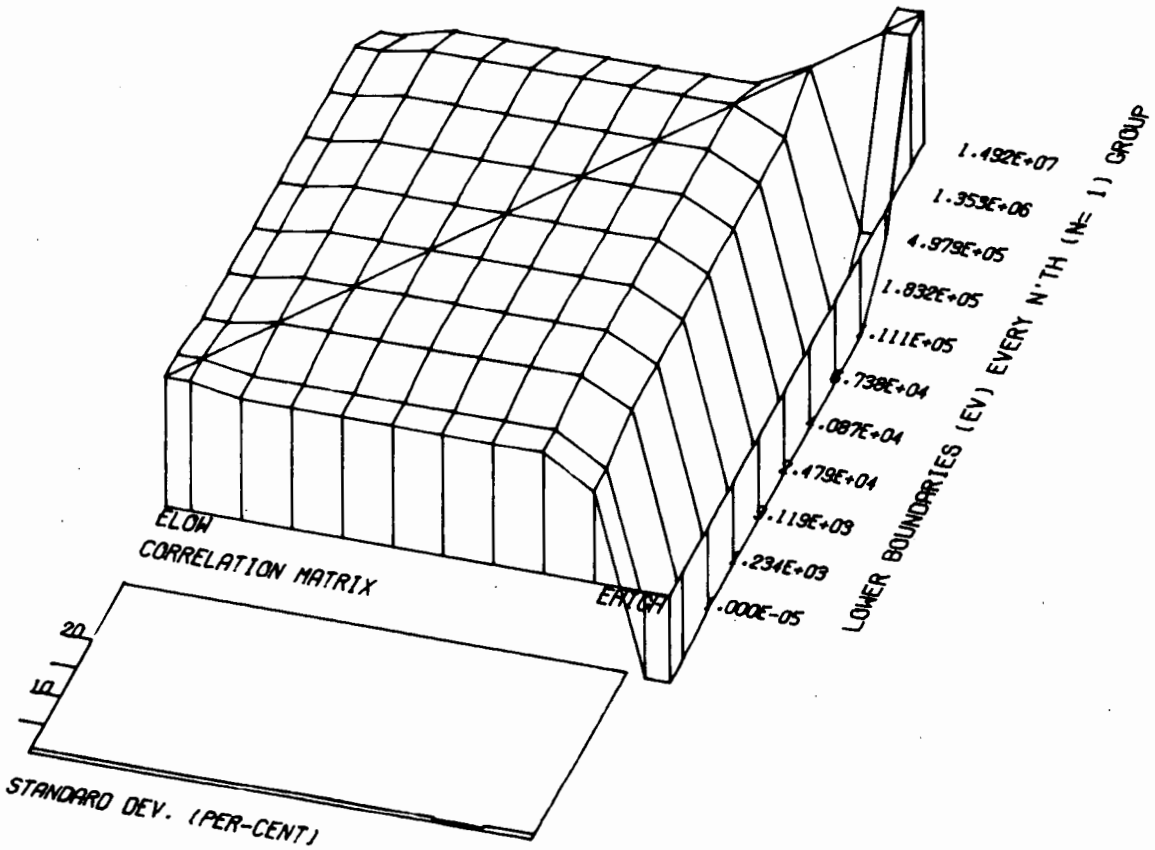

MAT'L 1264 10 GROUPS REACT 452 TO REACT 452

Fig. 37. Correlation Matrix and Standard Deviation for $^{239}Pu(\bar{\nu})$ Neutrons/Fission.

ORNL DWG 76-16213

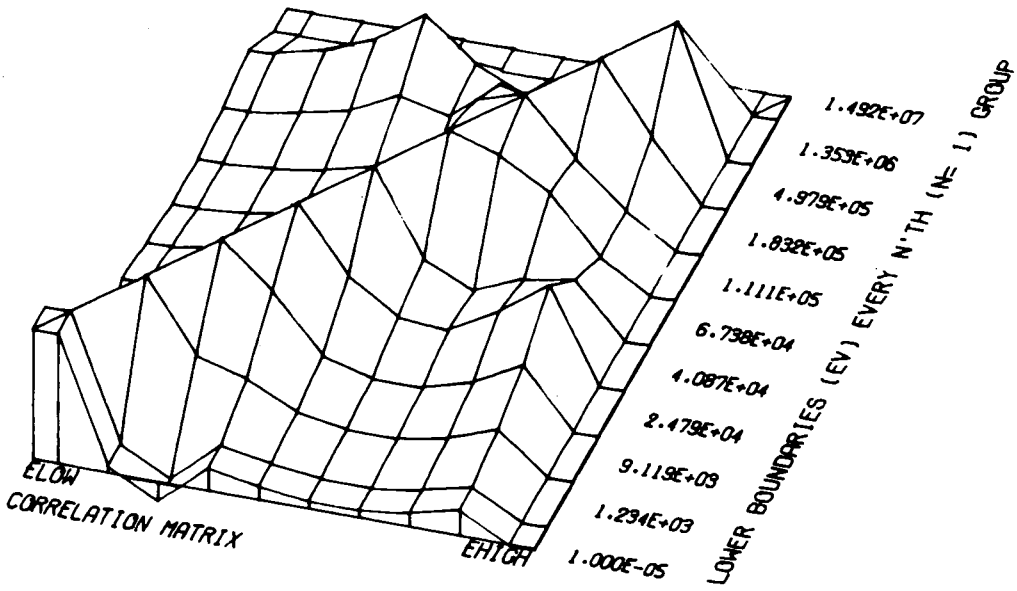

MAT'L 1264 10 GROUPS REACT 18 TO REACT 102

Fig. 38. Correlation Matrix Between $^{239}Pu(n,f)$ and $^{239}Pu(n,\gamma)$ Reactions

^{239}Pu capture and fission also take into account that most measurements of capture in that nuclide may be interpreted as capture/fission ratio measurements. In all cases the uncertainty files refer to the average cross sections for infinitely dilute material rather than the self-shielded cross sections, so the analyses below assumes that self shielding does not affect the relative covariance matrices. Some of the figure captions give additional details.

VII. Uncertainties Due Exclusively to Nuclear Data Uncertainties

Errors in calculated responses stem from three sources: (1) errors due to models, calculational methods, and approximations, (2) errors in data from measurements on the particular reactor system under consideration (densities, lengths, etc.), and (3) errors in fundamental physical constants, and in particular, nuclear cross sections.

Up to the present time, errors from the first source above (models, etc.) have been taken into account chiefly through the use of correction factors (e.g., diffusion to transport) when these are known. It is usually assumed that errors arising from the second source have been considered by the experimentalist and included in his report of the results and standard deviations of integral experiments. In this section only errors due to the third source, namely primary nuclear data, will be considered.

A calculational model for a performance parameter R_j of a given reactor implies the existence of a function $Q_j(\underline{\sigma})$ which maps the points lying in the space of nuclear data $\underline{\sigma}$ into points lying in the performance parameter space. Thus, the calculated value of R_j according to the model is given symbolically by

$$R_j^{calc} = Q_j(\underline{\sigma}) \tag{78}$$

Typically, the function $Q_j(\underline{\sigma})$ cannot be written explicitly but only parametrically by introducing the forward and adjoint fluxes. To date these have been calculated using a one-dimensional discrete ordinates transport model embodied in the ANISN code.[26]

Given the first-order partial derivatives of the above function $Q_j(\underline{\sigma})$ at the point $\underline{\sigma}^o$ of interest in nuclear data space, then for sufficiently small deviations about this point the first order result

$$\delta Q_j = \sum_i \left. \frac{\partial Q_j}{\partial \sigma_i} \right|_{\underline{\sigma}^o} \delta\sigma_i \tag{79}$$

will be valid. These partial derivatives are simply related to the relative sensitivity coefficients:

$$S_{ji} \equiv \frac{\sigma_i^o}{Q_j^o} \left. \frac{\partial Q_j}{\partial \sigma_i} \right|_{\underline{\sigma}^o} \tag{80}$$

Thus, to first order the relative or fractional changes are given in terms of the relative sensitivity coefficients by

$$\frac{\delta Q_j}{Q_j^o} = \sum_i S_{ji} \frac{\delta\sigma_i}{\sigma_i^o} \tag{81}$$

An expectation value based on an ensemble of cross-section sets clustered about $\underline{\sigma}^0$ and, in fact, having $\underline{\sigma}^0 = \langle\sigma\rangle$ as a mean, will yield a corresponding expectation value for the calculated value of the performance parameter of $\langle Q_j\rangle \equiv Q_j^0 \equiv Q_j(\underline{\sigma}^0)$.

Similarly the relative covariance matrix elements (and hence relative variances, relative standard deviations, and correlations) can be calculated for such an ensemble using the first order relation involving the relative sensitivity coefficients. The resulting relative covariance matrix elements are given by

$$\left\langle \left(\frac{Q_j - Q_j^0}{Q_j^0}\right) \left(\frac{Q_{j'} - Q_{j'}^0}{Q_{j'}^0}\right) \right\rangle \tag{82}$$

$$= \sum_{i,i'} S_{ji}\, S_{j'i'} \left\langle \left(\frac{\sigma_i - \sigma_i^0}{\sigma_i^0}\right) \left(\frac{\sigma_{i'} - \sigma_{i'}^0}{\sigma_{i'}^0}\right) \right\rangle$$

where the large brackets denote expectation value. Equation (82) can also be written

$$V_{jj'} = \sum_{i\,i'} S_{ji}\, S_{j'i'}\, W_{ii'} \tag{83}$$

where

$$V_{jj'} = \left\langle \left(\frac{Q_j - Q_j^0}{Q_j^0}\right) \left(\frac{Q_{j'} - Q_{j'}^0}{Q_{j'}^0}\right) \right\rangle = \text{Rel Cov}(Q_j, Q_{j'}) \tag{84}$$

is the relative covariance of the j and j' performance parameters and

$$W_{ii'} = \left\langle \left(\frac{\sigma_i - \sigma_i^0}{\sigma_i^0}\right) \left(\frac{\sigma_{i'} - \sigma_{i'}^0}{\sigma_{i'}^0}\right) \right\rangle \tag{85}$$

is the relative covariance of the i and i' nuclear cross sections.

The square root of the relative covariance element V_{jj} gives the relative standard deviation of the j'th performance parameter as calculated from the nuclear data base which is characterized by the cross-section covariances $W_{ii'}$. Equation (83) has been used to calculate such standard deviations from processed covariance files and sensitivity profiles generated by FORSS. Results of such calculations for the ZPR-6/7 benchmark assembly are given in Table XI. Based on our current covariance files, three quarters of the variance in k_{eff} is due to uncertainties in $^{239}Pu(n,f)$, the remainder being primarily the uncertainty in $^{238}U(n,\gamma)$. For the $^{28}c/^{49}f$ parameter, uncertainties in the variance are approximately evenly divided. Results for the central ^{238}U fission to ^{239}Pu fission ratio do not include the covariances arising from fission ratio measurements relative to ^{235}U. The standard deviations are all larger than estimates of required accuracies for nuclear design. With nuclear data uncertainties of this magnitude, it is appropriate to include integral information to improve significantly the quality of the calculated performance prediction.

Table XI

Uncertainties in ZPR-6/7 Performance Parameters Due to Nuclear Data

Performance Parameters	Relative Standard Deviations* (%)
Multiplication factor k	3.46
Central ^{238}U capture to ^{239}Pu fission ratio	8.57
Central ^{238}U fission to ^{239}Pu fission ratio	4.55

*The source of these uncertainties included the reactions $^{238}U(n,\gamma)$, $^{238}U(n,f)$, $^{239}Pu(n,\gamma)$, $^{239}Pu(n,f)$, and the yield $\bar{\nu}$ for this last reaction. Correlations were included in these calculations as shown in Figs. 33-38.

VIII. Uncertainties with Integral Experiments Taken Into Account

Many have recognized the desirability, and even the necessity, of incorporating the data from integral experiments with the basic nuclear data obtained from differential cross section measurements in order to make sufficiently precise predictions of integral performance parameters.[6,9-11] However, procedures for combining integral experiment evidence with the more basic problem independent data have often been too subjective for general acceptance or for maintaining adequate quality control of the calculational results.

Adjustment of the nuclear data base for improvement of performance parameter prediction has been suspect because of its problem-dependent nature, because such adjustments have often ignored differential data covariance information data, and because deficiencies due to methods approximations, engineering data, etc., are compensated by fictitious alterations to the base data set. On the other hand, the view that it is not necessary to understand individual sources of error since bias factors (C/E) can be applied from knowledge of related analyses is also dangerous, since these bias factors are problem, methods, and data dependent and should not be extrapolated outside of the range of applicability.

A complete treatment of the problem must deal explicitly with each of the components of the uncertainty: those due to deficiencies in calculational models, those due to uncertainties in the integral experiment measurements, and those due to the nuclear data base (discussed in Section VI). At ORNL, methods developed elsewhere[6] have been implemented to improve performance parameter predictions for a restricted class of fast reactor systems, by taking into account detailed nuclear data covariances as well as the large effect the adjustment has in altering the covariance matrix of the adjusted data relative to the original data. The effect of the altered covariance is to reduce the overall problem uncertainty. In addition, work is underway to include the correlations in the integral measurements and to consider more carefully uncertainties due to methods approximations.

A. General Development

The cross section and covariance adjustments are made using a systematic procedure developed by Gandini.[6] The group cross section σ_i^o is changed by the amount $\delta\sigma_i$ such that the j'th calculated response Q_j^o is changed by the amount δQ_j, which can be estimated with the use of sensitivity coefficients. This adjustment is made so that the revised calculated response $Q_j^o + \delta Q_j$ agrees consistently with the experimentally measured R_j^{exp}. At the same time, the revised cross sections $\sigma_i^o + \delta\sigma_i$ are kept consistent with the values σ_i^o which are determined by differential experiments.

To implement these changes a J+I dimensional vector representing the adjustments is formed:

$$\underline{y} \equiv \begin{pmatrix} y_1 \\ y_2 \\ \cdot \\ \cdot \\ \cdot \\ y_J \\ y_{J+1} \\ \cdot \\ \cdot \\ \cdot \\ y_{J+I} \end{pmatrix} = \begin{pmatrix} \delta Q_1/Q_1^o \\ \delta Q_2/Q_2^o \\ \cdot \\ \cdot \\ \cdot \\ \delta Q_J/Q_J^o \\ \delta\sigma_1/\sigma_1^o \\ \cdot \\ \cdot \\ \cdot \\ \delta\sigma_I/\sigma_I^o \end{pmatrix}$$

The first J components correspond to relative changes in the responses about the calculated values Q_j^o. The final I components correspond to relative changes in the cross sections about the values σ_i^o. The point in this y-space which agrees with experiment (exactly) is given by:

$$\underline{y}^{exp} = \begin{pmatrix} (R_1^{exp} - Q_1^o)/Q_1^o \\ (R_2^{exp} - Q_2^o)/Q_2^o \\ \vdots \\ (R_J^{exp} - Q_J^o)/Q_J^o \\ (\sigma_1^{exp} - \sigma_1^o)/\sigma_1^o \\ \vdots \\ (\sigma_I^{exp} - \sigma_I^o)/\sigma_I^o \end{pmatrix} \tag{87}$$

Note that recent measurements of the cross section data can be included in this formalism although in the present work we have not included such (i.e., $\sigma_i^{exp} \equiv \sigma_i^o$). Interpreting the previous discussion in the framework of this y-space, we want to find a point y which lies "as close as possible" to $\underline{y}^{exp}$ and at the same time remains in the vector subspace determined by the linear constraints of Eq. (79) which may be written for the $\underline{y}$-space as:

$$\mathcal{S}\,\underline{y} = 0 \tag{88}$$

where

$$\mathcal{S} \equiv (-\mathcal{I}, S) \tag{89}$$

$\mathcal{S}$ is the combined matrix made up of partitions including $\mathcal{I}$, the J-dimensional unit matrix and S, the JxI matrix of relative sensitivity coefficients S_{ji}; i.e.,

$$\mathcal{A}_{j\ell} = \begin{cases} -\delta_{j\ell} & \ell \leq J \\ S_{j,\ell-J} & \ell > J \end{cases} \tag{90}$$

The expression "as close as possible" implies the application of some particular distance-determining metric. Previous work[6,11] has shown that an optimal measure is provided by the inverse of the (J+I) x (J+I) relative covariance matrix

$$B_{\ell\ell'} \equiv \left\langle (y_\ell - y_\ell^{exp})(y_{\ell'} - y_{\ell'}^{exp}) \right\rangle \qquad \ell,\ell' = 1,\ I+J \tag{91}$$

The average is over an ensemble consistent with the experimental measurements and, in particular, satisfies the equation

$$\left\langle y_\ell - y_\ell^{exp} \right\rangle = 0 \tag{92}$$

The constraint represented by Eq. (88) can be modified in at least two ways which give greater generality with little additional computation. First, a constant bias may be added and, second, additional independent linear constraints and rows in the $\underline{y}$ vector may be added. The final form of this generalized constraint

$$\underline{\mathcal{A}}_0 + \mathcal{A}\,\underline{y} = 0 \tag{93}$$

is still linear. Hence, we have the following problem:

Minimize

$$r = (\tilde{\underline{y}} - \underline{y}^{exp})^T\, B^{-1}\, (\tilde{\underline{y}} - \underline{y}^{exp}) \tag{94}$$

subject to the linear constraint of Eq. (93) with $\underline{y} = \tilde{\underline{y}}$. The superscript T denotes the transpose; $\tilde{\underline{y}}$ is an estimator to the actual $\underline{y}$.

The solution to this system,

$$\tilde{\underline{y}} = \underline{y}^{exp} - B\mathcal{S}^T G^{-1}(\underline{\alpha}_0 + \mathcal{S}\underline{y}^{exp}) \tag{95}$$

has been reported using conventional Lagrangian multiplier techniques for minimization subject to constraints.[6] The matrix G is nothing more than

$$G = \mathcal{S} B \mathcal{S}^T \tag{96}$$

and G^{-1} merely its inverse. It is important to note that the matrix G is a square matrix of dimension J, the number of integral measurements, rather than the size I of the nuclear data vector which is considerably larger. Finally, in addition to new best estimates for both the nuclear data <u>and</u> integral experiment results, we can obtain estimates for the covariance matrix of both the integral measurements and nuclear data after information from both sets of data are synthesized. The covariance matrix $\tilde{B}$ for the data including both integral and differential measurements is simply related to the original covariance estimate B through

$$\tilde{B} = B - B\mathcal{S}^T G^{-1}\mathcal{S} B \tag{97}$$

This new covariance matrix constains important new information concerning correlations among the adjusted nuclear data which tend to substantially reduce the overall problem uncertainty for problems related to those for which the integral experimental results have been included in the analysis.

B. <u>Two Brief Examples</u>

Consider two integral experiments [k and central ($^{28}c/^{49}f$) for ZPR-6/7] and nuclear data uncertainties arising from $^{238}U(n,\gamma)$, $^{238}U(n,f)$, $^{239}Pu(n,\gamma)$, $^{239}Pu(n,f)$, and $^{239}Pu(\bar{\nu})$. Problem characteristics assumed are given in Table XII.

Table XII

Problem Characteristics for Nuclear Data and Integral Experiment Adjustment

ZPR-6/7 Parameter	k	$(^{28}c/^{49}f)_{central}$
Calculated value (homogeneous 1-D model)	0.9719	1.0046
Experimental value	0.9834	0.9336
$\frac{\text{experiment-calculation}}{\text{calculation}}$ %	1.183	-7.068
Assumed integral experiment uncertainties (%) (no correlations)	1.00	2.00
Energy group structure		
Uncertainty due exclusively to nuclear data (%)	3.457	8.569

ENERGY GROUP STRUCTURE (EV)

GROUP	ENERGY RANGE
1	1.4918E+07-- 1.3534E+06
2	1.3534E+06-- 4.9787E+05
3	4.9787E+05-- 1.8316E+05
4	1.8316E+05-- 1.1109E+05
5	1.1109E+05-- 6.7379E+04
6	6.7379E+04-- 4.0868E+04
7	4.0868E+04-- 2.4788E+04
8	2.4788E+04-- 9.1188E+03
9	9.1188E+03-- 1.2341E+03
10	1.2341E+03-- 1.0000E-05

One sees from Table XII that k is underpredicted while the central capture/fission ratio is substantially overpredicted. However, the nuclear data uncertainties according to our present files are large enough that taken alone, one cannot argue that a "real" discrepancy actually exists. The uncertainties taken for the integral experiments were assumed based upon discussions in the CSEWG Fast Reactor Data Testing Committee and need considerably more attention (as one will see in the next example). The sensitivity profiles calculated in the previous section indicate that there is little encouragement for modifying nuclear data other than those involved in the direct effect, i.e., ^{238}U capture and ^{239}Pu fission, when trying to resolve the discrepancy in the capture/fission ratio. Table XIII indicates the adjustments computed using the method described above without biases in the constraints. The "best" value for k [corresponding

Table XIII

Nuclear Data Adjustments for Consistency Between Differential and Integral Data (see Table XII)

GRØUP # IN LARGE GRØUP	ACTUAL GRØUP #	MATERIAL	REACTIØN	ØLD STD. DEVIATIØN %	DIFF. IN X-SECT %	% CHANGE/ ØLD STD. DEVIATIØN	ØLD CRØSS SECTIØNS	NEW CRØSS SECTIØNS	NEW STD. DEVIATIØN %
1	1	1262	18	1.9	-0.1	-0.066	4.872E-01	4.866E-01	1.9
2	2	1262	18	10.7	-0.1	-0.009	9.974E-03	9.964E-03	10.7
3	3	1262	18	0.0	0.0	0.000	8.982E-05	8.982E-05	0.0
4	4	1262	18	0.0	0.0	0.000	4.668E-05	4.668E-05	0.0
5	5	1262	18	0.0	0.0	0.000	4.016E-05	4.016E-05	0.0
6	6	1262	18	0.0	0.0	0.000	3.206E-05	3.206E-05	0.0
7	7	1262	18	0.0	0.0	0.000	0.000E-01	0.000E-01	0.0
8	8	1262	18	0.0	0.0	0.000	0.000E-01	0.000E-01	0.0
9	9	1262	18	0.0	0.0	0.000	3.956E-09	3.956E-09	0.0
10	10	1262	18	0.0	0.0	0.000	1.076E-04	1.076E-04	0.0
11	1	1262	102	22.6	-7.3	-0.322	4.459E-02	4.135E-02	21.5
12	2	1262	102	19.6	-12.5	-0.637	1.140E-01	9.982E-02	15.6
13	3	1262	102	12.3	-7.4	-0.606	1.207E-01	1.117E-01	10.0
14	4	1262	102	10.3	-5.2	-0.501	1.626E-01	1.542E-01	9.1
15	5	1262	102	8.8	-4.9	-0.558	2.098E-01	1.995E-01	7.5
16	6	1262	102	4.7	-2.4	-0.504	3.127E-01	3.053E-01	4.1
17	7	1262	102	9.9	-5.5	-0.553	4.002E-01	3.783E-01	8.5
18	8	1262	102	12.9	-8.7	-0.676	5.425E-01	4.951E-01	10.0
19	9	1262	102	9.6	-5.8	-0.604	8.824E-01	8.315E-01	7.9
20	10	1262	102	0.3	-0.0	-0.159	1.289E+00	1.288E+00	0.3
21	1	1264	18	4.6	0.0	0.003	1.891E+00	1.892E+00	3.9
22	2	1264	18	5.7	0.4	0.071	1.667E+00	1.674E+00	4.9
23	3	1264	18	10.6	1.1	0.107	1.520E+00	1.538E+00	7.6
24	4	1264	18	19.3	2.2	0.114	1.533E+00	1.567E+00	14.2
25	5	1264	18	12.8	1.5	0.119	1.589E+00	1.613E+00	9.1
26	6	1264	18	6.3	0.4	0.071	1.603E+00	1.610E+00	5.8
27	7	1264	18	3.2	0.3	0.087	1.469E+00	1.473E+00	2.8
28	8	1264	18	3.9	0.3	0.084	1.800E+00	1.805E+00	3.7
29	9	1264	18	5.9	0.6	0.094	2.847E+00	2.863E+00	5.7
30	10	1264	18	0.0	0.0	0.009	7.995E+00	7.995E+00	0.0
31	1	1264	102	0.0	0.0	0.000	6.925E-03	6.925E-03	0.0
32	2	1264	102	22.4	0.9	0.042	5.992E-02	6.049E-02	22.2
33	3	1264	102	11.3	1.2	0.110	1.690E-01	1.711E-01	8.7
34	4	1264	102	23.2	2.6	0.111	2.176E-01	2.232E-01	19.5
35	5	1264	102	13.5	1.3	0.098	2.982E-01	3.021E-01	10.1
36	6	1264	102	12.3	0.2	0.019	4.123E-01	4.132E-01	12.1
37	7	1264	102	7.9	0.9	0.116	4.402E-01	4.442E-01	7.8
38	8	1264	102	8.5	1.1	0.126	8.182E-01	8.269E-01	8.4
39	9	1264	102	13.2	2.2	0.166	2.260E+00	2.309E+00	13.1
40	10	1264	102	0.0	-0.0	-0.017	6.107E+00	6.107E+00	0.0
41	1	1264	452	1.0	0.1	0.108	3.254E+00	3.257E+00	1.0
42	2	1264	452	0.5	-0.1	-0.195	2.985E+00	2.982E+00	0.5
43	3	1264	452	0.8	-0.2	-0.221	2.916E+00	2.911E+00	0.8
44	4	1264	452	0.8	-0.2	-0.221	2.894E+00	2.889E+00	0.8
45	5	1264	452	0.8	-0.2	-0.221	2.886E+00	2.880E+00	0.8
46	6	1264	452	0.8	-0.2	-0.221	2.881E+00	2.876E+00	0.8
47	7	1264	452	0.8	-0.2	-0.221	2.878E+00	2.873E+00	0.8
48	8	1264	452	0.8	-0.2	-0.221	2.876E+00	2.871E+00	0.8
49	9	1264	452	0.8	-0.2	-0.221	2.874E+00	2.869E+00	0.8
50	10	1264	452	0.8	-0.2	-0.206	2.873E+00	2.869E+00	0.8

to these adjustments if 0.9878 (raised) and that for the capture/fission ratio is 0.9438 (reduced)]. The uncertainties in these estimates are substantially reduced relative to those tabulated in Table XII, i.e., $\delta k/k$ is 0.82% (compared to 3.45%) and $\delta[(^{28}c)/(^{49}f)]/[(^{28}c)/(^{49}f)]$ is 1.76% compared to 8.60%. A statistical test of the residual r indicates that the adjustments indicated in Table XIII are plausible if the input covariance data are realistic. Table XIII indicates that the best way to achieve consistency between the differential and integral data is to make substantial reductions to the capture cross section of ^{238}U. This conclusion is predicated, of course, on our original estimates for the uncertainty of ^{238}U and on the assumption that there is no larger uncertainty in the measurement of $(^{28}c)/(^{49}f)$. However, the covariance data for ^{238}U capture cross section has the implicit assumption of normality ($\pm$ errors equally likely) which is, perhaps, not applicable for the ^{238}U evaluation. However, if the ^{239}Pu fission uncertainty estimates are realistic, most adjustment schemes (which are statistically reasonable) lead one to the conclusion that the ^{238}U capture cross section must be lowered. On the other hand, if there were additional errors in the integral experiments, this conclusion would by no means be required. In this connection, note in Table I that there seems to be no discrepancy implied in the C/E for $^{28}c/^{49}f$ for ZPR-6/6A.

The substantial reduction in the uncertainties predicted for the integral parameters using the adjusted set results from the impact of the procedure on the cross section covariance matrix. In Figs. 39 and 40 we show the cross section covariance matrix before and after the inclusion of ZPR-6/7 integral data for k and for $(^{28}c/^{49}f)$. As is seen from the standard deviations, also given in columns 5 and 10 of Table XIII, the knowledge of the individual group cross sections has not improved much. At most, the standard deviations in a few groups have been reduced by about 30%, well within the accuracy with which we can estimate such quantities at the moment. It is evident from Figs. 39 and 40 that broad positive correlations between the ^{28}c cross section and ^{49}c and ^{49}f have been introduced as well as smaller broad negative correlations between ^{239}Pu $\bar{\nu}$ and the cross sections. A detailed examination of the

ORNL DWG 76-16205

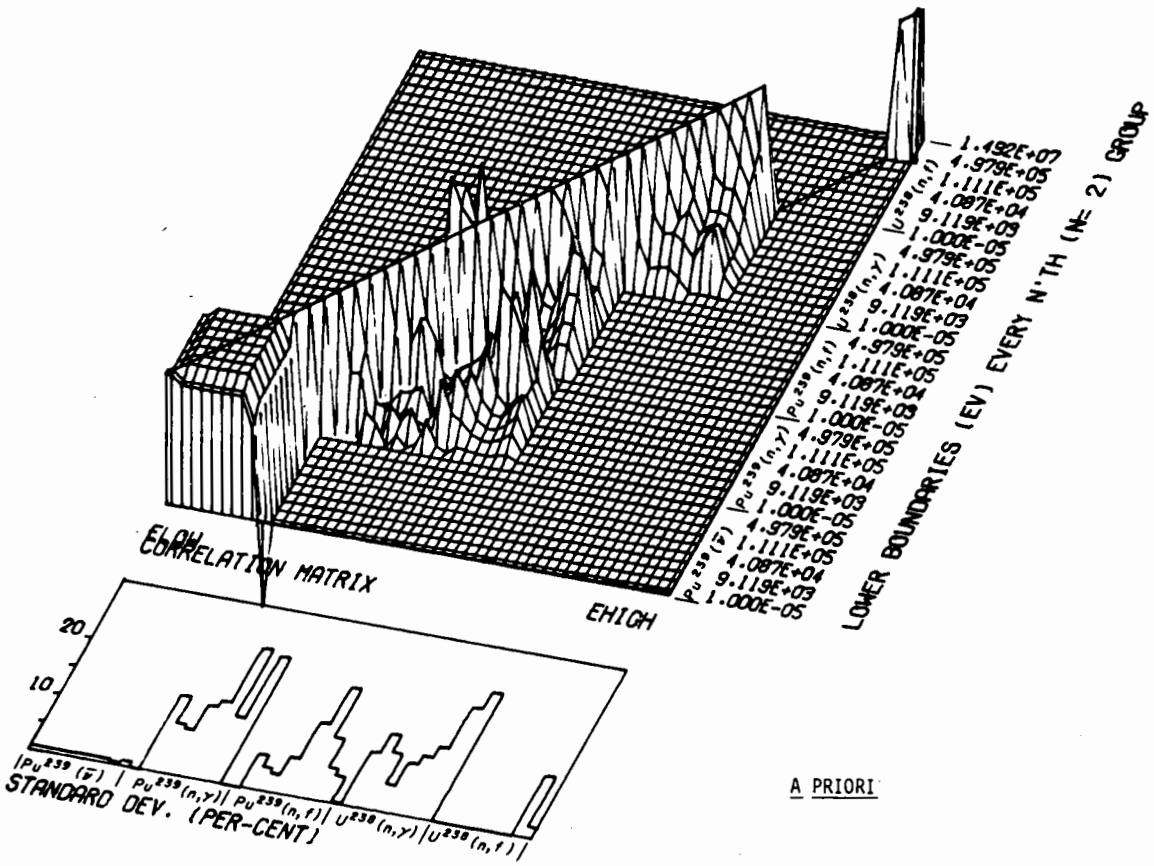

MAT'L 1262 50 GROUPS REACT 18 TO REACT 18

Fig. 39. Cross Section Covariance Matrix Before Inclusion of ZPR-6/7 Integral Data for k and $^{28}c/^{49}f$. This figure condenses the information presented in Figs. 33-38 for each of the five reaction types in ten energy groups. The upper part of the drawing gives the correlation matrix while the lower part illustrates the relative standard errors of the cross section for each group as given in Table XIII.

ORNL DWG 76-16206

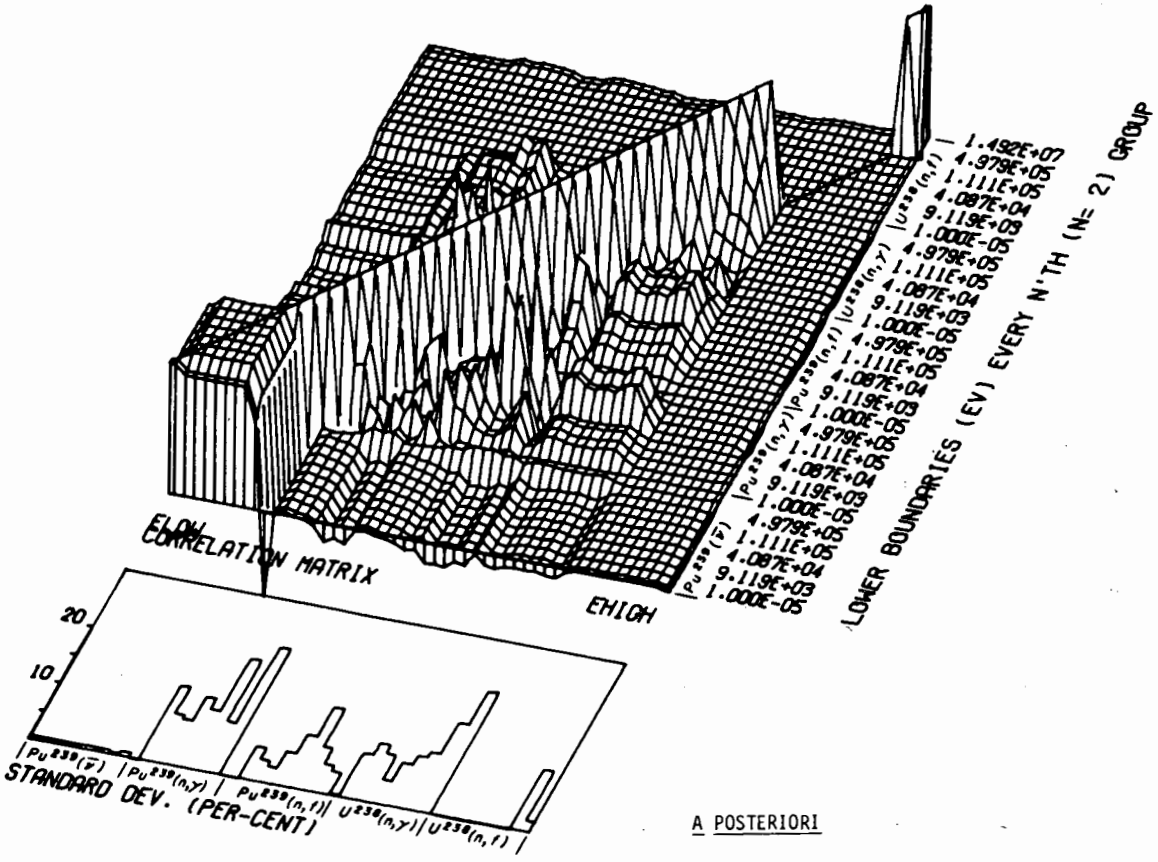

MAT'L 1262 50 GROUPS REACT 102 TO REACT 102

Fig. 40. Cross Section Covariance Matrix After Inclusion of ZPR-6/7 Integral Data for k and $^{28}c/^{49}f$. Presented is the cross section covariance matrix for the five indicated reaction types in ten energy groups resulting from the adjustment procedure. The upper part of the drawing gives the correlation matrix while the lower plots the relative standard errors of the cross sections for each group as given in Table XIII. Note that the inclusion of the integral information reduces the diagonal elements a little and makes broad changes of small magnitude in the correlation pattern.

correlation matrix of the cross sections as a function of energy reveal that although the elements close to the diagonal have not changed appreciably, substantial reductions in the magnitude of the off-diagonal elements has occurred including some sign reversals. This effect is not clearly evident in Figs. 39 and 40 but it results in a substantial improvement in the accuracy with which the integrated cross sections over the ZPR-6/7 spectrum are now predicted.

In order to analyze in greater detail the impact of the adjustment procedure on the accuracy of the integral parameters, we show in Table XIV a partition by reaction type of the relative variance projected for ZPR-6/7 k and (^{28}c/^{49}f). The elements of each array represent the contribution of the corresponding portions of the data covariance matrix to the output relative variance for the indicated parameters. These arrays are obtained by folding the data covariance matrix with the sensitivity coefficients and collapsing the result for each reaction type over the complete energy range. The major conclusions from this partition are:

1. The major contribution to the variance in the integral parameters come from ^{28}c and ^{49}f as previously mentioned.

2. With the adjusted set large cancellations of the contribution to the uncertainties of ^{29}c and ^{49}f occur in the correlations between these two cross sections. In the input data set, these correlations were set to zero although in general we could expect to be able to predict positive correlations due to uncertainties in common methods used to determine the flux, i.e., correlations introduced by cross section standards.

3. From the partition, using the overall sensitivity coefficients given in Table II, we may extract an effective uncertainty for each cross section. (This would be an effective fully correlated uncertainty as weighted by the sensitivities for ZPR-6/7.) The effective uncertainty in ^{28}c went down from 7 to 4.4% and for ^{49}f from 5.3

Table XIV

Partitions by Reaction Type of Relative Variance Projected for ZPR-6/7 k and $^{28}c/^{49}f$ Parameters. The elements in each array below represent the contribution of the corresponding portions of the data covariance matrix to the output relative variance for the indicated parameter; a sum of the elements shown gives the computed relative variance. The values without parentheses are 10^4 times the contributions computed using a posteriori data base which includes some information from integral experiments. The values shown with parentheses are the corresponding nonzero partitions based on a priori data set.

Type	^{28}f	^{28}c	^{49}f	^{49}c	$^{49}\bar{\nu}$	Sums of Partitions (Relative variance x 10^4)	
				Results for k			
^{28}f	0.02 (0.02)					Diagonal	4.5(13.1)
^{28}c	0.01	1.09 (2.85)				Off-Diagonal	-3.8(-1.1)
^{49}f	-0.04	-3.26	3.04 (9.87)			Total	0.7(12.0)
^{49}c	0.00	0.26	-0.51 (-1.14)	0.10 (0.11)			
$^{49}\bar{\nu}$	0.00	0.16	-0.44	0.01	0.22 (0.24)		
				Results for Central $^{28}c/^{49}f$			
^{28}f	0.00 (0.01)					Diagonal	25.2(72.4)
^{28}c	0.00	15.06 (39.45)				Off-Diagonal	-22.1(1.0)
^{49}f	0.01	-22.13	10.17 (32.91)			Total	3.1(73.4)
^{49}c	0.00	-0.46	0.44 (1.04)	0.02 (0.02)			
$^{49}\bar{\nu}$	0.00	0.01	0.00	0.00	0.00 (0.00)		

to 2.9%. This improvement comes in large part from the effect of the adjustment on the far off diagonal elements of the covariance matrix of the cross sections as a function of energy. In the adjusted set the effective correlation of the ^{28}c and ^{49}f is 0.89, instead of zero in the input matrix. This large correlation is responsible for the dramatic improvement in the accuracy predicted for the integral parameters as seen in Table XIV from the sums of the contribution to the variance of the partitions for the diagonal and off-diagonal elements. Another way of stating this result is to say that for ZPR-6/7, accurate prediction of k and $^{28}c/^{49}f$ requires a knowledge of the relative cross sections of ^{28}c and ^{49}f.

4. In this example we assumed that the experimental uncertainties in k and $^{28}c/^{49}f$ were uncorrelated, an obvious oversimplification. It is interesting to note that using the input cross section covariance matrix, a correlation coefficient of -0.94 is predicted between the computed k and $^{28}c/^{49}f$. This correlation coefficient is very consistent with the original underprediction of k and overprediction of the ratio $^{28}c/^{49}f$. With the adjusted set this correlation coefficient is now reduced to -0.34.

As a second example, consider the same example as given in Table XII with the following changes: the capture/fission ratio experimental value is raised 3% and the uncertainty in it is raised to 3.5%. With just these changes alone and all other nuclear data, as in the previous example, another adjustment was made with results as shown in Table XV. Note that with this set of assumptions, the required adjustments to ^{238}U capture are clearly reduced and substantial adjustments are required to the ^{239}Pu σ_f and σ_c cross sections. Simple examples such as these suggest strongly that we develop reasonably reliable estimates for the uncertainties (and their correlations) as well as the nominal values for all the experimental results if we wish to improve our confidence in the prediction of performance parameters.

Table XV

Summary Table for the Problem of Table XII with the ($^{28}c/^{49}f$) Experiment Raised 3% and Its Uncertainty Raised to 3.5%[a]

GROUP # IN LARGE GROUP	ACTUAL GROUP #	MATERIAL	REACTION	OLD STD. DEVIATION %	DIFF. IN X-SECT %	% CHANGE/ OLD STD. DEVIATION	OLD CROSS SECTIONS	NEW CROSS SECTIONS	NEW STD. DEVIATION %
1	1	1262	18	1.9	-0.0	-0.002	4.872E-01	4.871E-01	1.9
2	2	1262	18	10.7	-0.0	-0.000	9.974E-03	9.973E-03	10.7
3	3	1262	18	0.0	0.0	0.000	8.982E-05	8.982E-05	0.0
4	4	1262	18	0.0	0.0	0.000	4.668E-05	4.668E-05	0.0
5	5	1262	18	0.0	0.0	0.000	4.016E-05	4.016E-05	0.0
6	6	1262	18	0.0	0.0	0.000	3.206E-05	3.206E-05	0.0
7	7	1262	18	0.0	0.0	0.000	0.000E-01	0.000E-01	0.0
8	8	1262	18	0.0	0.0	0.000	0.000E-01	0.000E-01	0.0
9	9	1262	18	0.0	0.0	0.000	3.956E-09	3.956E-09	0.0
10	10	1262	18	0.0	0.0	0.000	1.076E-04	1.076E-04	0.0
11	1	1262	102	22.6	-2.6	-0.114	4.459E-02	4.345E-02	21.7
12	2	1262	102	19.6	-4.3	-0.221	1.140E-01	1.091E-01	16.4
13	3	1262	102	12.3	-2.6	-0.211	1.207E-01	1.176E-01	10.5
14	4	1262	102	10.3	-1.8	-0.176	1.626E-01	1.597E-01	9.3
15	5	1262	102	8.8	-1.7	-0.192	2.098E-01	2.062E-01	7.7
16	6	1262	102	4.7	-0.8	-0.173	3.127E-01	3.101E-01	4.2
17	7	1262	102	9.9	-1.9	-0.188	4.002E-01	3.928E-01	8.8
18	8	1262	102	12.9	-3.0	-0.229	5.425E-01	5.264E-01	10.7
19	9	1262	102	9.6	-1.9	-0.203	8.824E-01	8.653E-01	8.3
20	10	1262	102	0.3	-0.0	-0.052	1.289E+00	1.289E+00	0.3
21	1	1264	18	4.6	0.6	0.135	1.891E+00	1.903E+00	3.9
22	2	1264	18	5.7	0.8	0.149	1.667E+00	1.681E+00	4.9
23	3	1264	18	10.6	2.2	0.204	1.520E+00	1.553E+00	7.6
24	4	1264	18	19.3	3.9	0.200	1.533E+00	1.592E+00	14.3
25	5	1264	18	12.8	2.6	0.207	1.589E+00	1.631E+00	9.1
26	6	1264	18	6.3	0.8	0.120	1.603E+00	1.615E+00	5.8
27	7	1264	18	3.2	0.5	0.146	1.469E+00	1.475E+00	2.8
28	8	1264	18	3.9	0.4	0.106	1.800E+00	1.807E+00	3.7
29	9	1264	18	5.9	0.5	0.086	2.847E+00	2.861E+00	5.7
30	10	1264	18	0.0	0.0	0.029	7.995E+00	7.995E+00	0.0
31	1	1264	102	0.0	0.0	0.000	6.925E-03	6.925E-03	0.0
32	2	1264	102	22.4	0.8	0.035	5.992E-02	6.040E-02	22.2
33	3	1264	102	11.3	2.1	0.188	1.690E-01	1.726E-01	8.7
34	4	1264	102	23.2	3.8	0.164	2.176E-01	2.259E-01	19.5
35	5	1264	102	13.5	2.6	0.191	2.982E-01	3.059E-01	10.2
36	6	1264	102	12.3	0.7	0.057	4.123E-01	4.152E-01	12.1
37	7	1264	102	7.9	0.5	0.059	4.402E-01	4.423E-01	7.8
38	8	1264	102	8.5	0.4	0.052	8.182E-01	8.218E-01	8.4
39	9	1264	102	13.2	0.6	0.044	2.260E+00	2.273E+00	13.1
40	10	1264	102	0.0	0.0	0.004	6.107E+00	6.107E+00	0.0
41	1	1264	452	1.0	0.0	0.003	3.254E+00	3.254E+00	1.0
42	2	1264	452	0.5	-0.0	-0.006	2.985E+00	2.985E+00	0.5
43	3	1264	452	0.8	-0.0	-0.007	2.916E+00	2.916E+00	0.8
44	4	1264	452	0.8	-0.0	-0.007	2.894E+00	2.893E+00	0.8
45	5	1264	452	0.8	-0.0	-0.007	2.886E+00	2.885E+00	0.8
46	6	1264	452	0.8	-0.0	-0.007	2.881E+00	2.881E+00	0.8
47	7	1264	452	0.8	-0.0	-0.007	2.878E+00	2.878E+00	0.8
48	8	1264	452	0.8	-0.0	-0.007	2.876E+00	2.875E+00	0.8
49	9	1264	452	0.8	-0.0	-0.007	2.874E+00	2.874E+00	0.8
50	10	1264	452	0.8	-0.0	-0.006	2.873E+00	2.873E+00	0.8

[a]Output values were: k (best estimate) = .9835 ± .86% and $^{28}c/^{49}f$ (best estimate) = .9723 ± 2.5%.

IX. Inverse Problem

The general objective of the "Inverse Problem" of reactor sensitivity theory is to provide quantitative guidance[41-43] to data acquisition, data evaluation, and associated data-processing code development programs by giving estimated accuracy requirements on various multigroup nuclear data to meet pre-determined design constraints and error margins.

The inverse problem is formulated here following the development reported by Usachev[42] as follows: Given (1) specified reactor systems with particular performance parameter accuracy requirements (e.g., 1/2% in k for CRBRP, etc.), (2) the sensitivity coefficients (as determined by FORSS, for example) of the performance parameters with respect to the broad group cross sections (the required accuracy of which are to be determined), (3) a matrix which gives the correlations between the group cross sections according to the various experimental methods by which these cross sections are determined, and (4) a cost function which gives the cost of an experimental program to determine by various experimental methods the group cross sections of interest, $\sigma_1, \sigma_2 \ldots \sigma_n$, to within an accuracy specified by the standard deviations $x_1, x_2 \ldots x_n$, what are the optimum standard deviations of the experimentally determined broad group cross sections which will give a minimum cost to the experimental program and at the same time satisfy the accuracy requirements of the design performance parameters. As now formulated, only differential experiments are included.

Let us represent the variable output standard deviation of the cross sections by the diagonal matrix X and the cost function by C(X). Let D be the correlation matrix and S^r the sensitivity coefficient vector of performance parameter r. Then the problem stated mathematically is

$$\begin{aligned} &\text{Minimize:} \quad C(X) \\ &\text{Subject to:} \quad \tilde{S}^r X D X S^r \leq V_r \\ &\qquad X_{ii} \geq 0 \end{aligned} \tag{98}$$

where $\sim$ indicates the transposed matrix, and V_r is the maximum value allowed by the constraint on the variance of the r'th performance parameter.

This is a non-linear programming problem with non-linear (quadratic) inequality constraints. Solutions are found by the module NUTCRACKER, which uses a modification of EXCOST, a code for non-linear optimization subject to non-linear constraints.[44]

The following typifies the results of applying the method using as typical the sensitivity coefficients obtained for the reactor benchmark ZPR-6/7. The following were assumed: (1) Relative standard deviations of the calculated multiplication factor k and the calculated central reaction-rate ratio of ^{238}U-capture to ^{239}Pu-fission were not to exceed 0.5% and 2%, respectively. (2) five types of experimental data were proposed for measurement: four reaction cross sections, ^{238}U-fission and -capture and ^{239}Pu-fission and -capture, and the neutron yield per ^{239}Pu-fission, $\bar{\nu}$. Each of these five was given a common ten-group structure. The correlation coefficients for these fifty quantities were calculated using the ORNL FORSS code system for covariance files generated to describe existing measurements. (3) The sensitivity coefficients were calculated with FORSS for a ten-group, one-dimensional model of ZPR-6/7 (collapsed with uniform weight from the 126 group profiles reported above). (4) The cost function was estimated with a sum of fifty terms, each term varying as the reciprocal of the square of a variable standard deviation and corresponding to one of the five nuclear data types and to one of the ten energy groups. For each group the cost of halving the present value of a standard deviation (as evaluated from covariance files) was assumed to be the same for each particular reaction cross section type. The group-dependent cost coefficients were determined from cost estimates of measuring ^{238}U cross section data provided by G. deSaussure.[45]

The energy-dependent results are presented in Table XVI along with energy-independent results of two earlier studies for comparison. If the four cross sections and $\bar{\nu}$ are to be remeasured so as to force the two design parameters to have standard deviations of 0.5% and 2% respectively,

Table XVI. Required Relative Standard Deviations in Percent to Achieve Design Accuracy at Minimum Experimental Cost[a]

Group Upper Energy (eV)	$^{238}U(n,f)$	$^{238}U(n,\gamma)$	$^{239}Pu(n,f)$	$^{239}Pu(n,\gamma)$	$^{239}Pu(\bar{\nu})$	Cost Parameter[e]
1.4918+7	1.1(1.9)	11.0(22.6)	1.2(4.6)	b	1.8(1.0)	429
1.3534+6	11.3(10.7)	3.8(19.6)	1.2(5.7)	64.8(22.4)	0.2(0.5)	277
4.9787+5	b	2.6(12.3)	2.1(10.6)	49.8(11.3)	0.3(0.8)	277
1.8316+5	b	2.1(10.3)	3.6(19.3)	84.1(23.2)	0.3(0.8)	196
1.1109+5	b	2.1(8.8)	3.2(12.8)	70.4(13.5)	0.3(0.8)	237
6.7379+4	b	1.3(4.7)	1.7(6.3)	38.2(12.3)	0.4(0.8)	237
4.0866+4	b	2.2(9.9)	1.0(3.2)	7.2(7.9)	0.4(0.8)	236
2.4788+4	b	2.2(12.9)	1.1(3.9)	6.1(8.5)	0.4(0.8)	301
9.1188+3	b	1.7(9.6)	1.5(5.9)	5.4(13.2)	0.3(0.8)	264
1.2341+3	b	b	b	b	0.3(0.8)	217
Usachev[c] (Ref. 42)	1.6-2.6	1.4-2.9	0.6-2.2	4.4-6.7	0.5	
Bohn[d] (Ref. 46)	5	2	1	7	1	

[a]Current estimated accuracies are in parentheses.
[b]Evaluation incomplete or does not apply.
[c]These accuracies ensure a determination of k_{eff} to within 1% and of breeding ratio to within 2%.
[d]For target accuracies of approximately 0.5% in k_{eff}, 5% on breeding ratio and control rod worths, and 10 to 15% in Doppler and sodium void coefficients.
[e]Cost parameter C_g gives the cost contribution $(C_g\, x_i^o/x_i)^2$ for variable standard deviation x_i and actual standard deviation x_i^o.

then, neglecting errors from other sources, this can be done with the least expense by measuring the group cross sections and $\bar{\nu}$ to within the uncertainties shown. Note that these particular results do not take credit for the current estimated accuracies which are in parentheses; i.e., where the accuracy requirements for a given cross section has already been satisfied, the calculation should be repeated with the cross section eliminated as a variable.

Based on our estimated correlations and standard deviations associated with the above nuclear data, a conclusion to be drawn from the table is that design accuracy goals [3,47] of 0.5% in k and 2% in the central $^{28}c/^{49}f$ ratio in conventional mixed oxide LMFBR cores (neutronic behavior similar to ZPR-6/7) are unlikely to be attained in the next 5-10 years if the nuclear data is based only on microscopic measurements and the level of effort on the most crucial cross sections is not increased dramatically. Incorporation of the results of the integral experiments is required either directly or indirectly in calculating reactor performance.

X. Conclusions

This paper presents the first results of applying FORSS to the analysis of fast reactor benchmarks. The sensitivities of performance parameters for the ZPR-6/6A, ZPR-6/7, and GODIVA CSEWG fast reactor benchmarks to various important partial cross sections have been computed and used in an attempt to reconcile current calculation/experiment discrepancies and quantify uncertainties. The first two assemblies are characteristic of LMFBR spectral environments while the latter has been used extensively to verify high energy cross section data for the uranium isotopes. The importance of the fission and capture cross sections of uranium and plutonium (as well as $\bar{\nu}$) was particularly evident and quantified in relation to other reaction types. The sensitivities were computed using transport theory in 126 energy groups. Comprehensive libraries of energy dependent coefficients (including additional assemblies such as ZPR-3/56B, ZPR-3/11, and profiles for individual reaction types, e.g., each individual inelastic level) in a computer retrievable format were documented and released for distribution by RSIC and NNCSC.

Multigroup covariance files for $^{238}U(n,f)$, $^{238}U(n,\gamma)$, $^{239}Pu(n,f)$, $^{239}Pu(n,\gamma)$, and $^{239}Pu(\bar{\nu})$ based upon data compilations and procedures developed by deSaussure, Difillipo, Peelle, and Perez were generated. These covariance matrices were folded with the sensitivity coefficients described above resulting in one standard deviation estimates for k, central ^{238}U capture/^{239}Pu fission and central ^{238}U fission/^{239}Pu fission for ZPR-6/7 (and designs with similar neutronic behavior) of 3.5, 8.6, and 4.6 percent respectively. Comparison of calculation and measurement indicates that k is underpredicted for ZPR-6/7 while the central capture/fission ratio is substantially overpredicted. However, the nuclear data uncertainties are large enough that taken alone, it is difficult to argue that a "real" discrepancy actually exists.

Inclusion of integral measurements in the uncertainty estimation process introduces correlations (heretofore unknown) in the covariance data which reduce the overall uncertainty for designs with similar neutronic sensitivities. Using the measurements in ZPR-6/7 for k and central ^{238}U capture/^{239}Pu fission with assigned uncorrelated one standard deviation (1σ) uncertainties (random and systematic) of 1 and 2 percent resulted in (1σ) calculations of the same parameters for similar systems (large LMFBR cores) of 0.82% and 1.8% respectively (compared to 3.5% and 8.6%) when the integral data is included in a cross section adjustment procedure which made changes of less than one standard deviation to the basic multigroup file. Elimination of any significant downward adjustment in the ^{238}U capture cross section can be effected only by significant upward revision in the reported ZPR-6/7 capture/fission ratio and/or its uncertainty so as to ameliorate the existing 7% calculated overprediction. Changes in k may be accounted for without resort to large changes in the ^{238}U capture cross section by including additional reaction types (e.g., ^{238}U inelastic) in the adjustment process.

The theory behind the "inverse problem" of reactor sensitivity theory (i.e., the determination of the accuracy required of multigroup nuclear data to ensure at minimum cost a given accuracy in calculated reactor performance parameters) was reviewed and coding developed to apply the

solution technique to a sample problem of interest. Based on our estimated correlations and standard deviations associated with the above nuclear data, design accuracy goals of 0.5% in k and 2% in the central $^{28}c/^{49}f$ ratio in conventional mixed oxide LMFBR cores (neutronic behavior similar to ZPR-6/7) are unlikely to be attained in the next 5 to 10 years if the nuclear data is based only on microscopic measurements and the level of effort on the most crucial cross sections is not increased dramatically. In fact, presently estimated uncertainties for $^{238}U(n,\gamma)$ and $^{239}Pu(n,f)$ need be reduced by factors of approximately four for important energy ranges. Incorporation of the results of the integral experiments is required either directly or indirectly in projecting reactor performance.

References

1. C. R. Weisbin, E. M. Oblow, F. R. Mynatt, and G. F. Flanagan, "The FORSS Sensitivity Analysis Code System," Trans. Am. Nucl. Soc., 22, 792 (1975).

2. J. Y. Barré, "Influence of Nuclear Data Uncertainties on Some Fast Reactor Characteristic Parameters - First Results - ^{239}Pu," EURFNR-409 (January 1967).

3. P. Greebler et al., "Implications of Nuclear Data Uncertainties to Reactor Design," Second International Conference on Nuclear Data for Reactors, Helsinki (June 1970).

4. L. N. Usachev et al., "Nuclear Data Sources and Their Implications on the Design of Fast Reactors," Applications of Nuclear Data in Science and Technology Symposium, Paris, 1973.

5. Koichi Maki et al., "Effect of Uncertainty in Nuclear Constants on Nuclear Characteristics Sensitivity Analysis of Nuclear Constants for the Core of the Monji Reactor," JAPFNR-78 (May 1972).

6. A. Gandini, "Nuclear Data and Integral Measurements Correlation for Fast Reactors," Parts I, II, and III, RT/FI(73)5, RT/FI(73)22, and RT/FI(74)3 (1973 and 1974).

7. H. Hummel and W. M. Stacey, Jr., "Sensitivity of A Fast Critical Assembly to Uncertainties in Input Data Determined by Perturbation Theory," Nucl. Sci. Eng., 54, 35 (1974).

8. D. R. Harris et al., "Consistency Among Differential Nuclear Data and Integral Observations: The ALVIN Code for Adjustment for Sensitivity Calculations, and for Identification of Inconsistent Data," LA-5987 (May 1975).

9. C. Campbell and J. Rowlands, "The Relationship of Microscopic and Integral Data," IAEA-CN-26/116 (June 1970).

10. J. Rowlands et al., "The Production and Performance of the Adjusted Cross Section Set FGL5," Physics of Fast Reactors, Tokyo (October 1975).

11. J. B. Dragt, "Statistical Considerations on Techniques for Adjustment of Differential Cross Sections with Measured Integral Parameters," RCN-122 (August 1970).

12. E. M. Oblow, "Sensitivity Theory from a Differential Viewpoint," Nucl. Sci. Eng., 59, 187 (1976); see also, E. M. Oblow, "Reactor Cross-Section Sensitivity Studies Using Transport Theory," ORNL-TM-4437 (April 1974).

13. W. M. Stacey, Jr., "Variational Estimates and Generalized Perturbation Theory for the Ratios of Linear and Bilinear Functionals," J. Math. Phys., 13, 1119 (1972); see also, W. M. Stacey, Jr., "Variational Estimates of Reactivity Worths and Reaction Rate Ratios in Critical Nuclear Reactors," Nucl. Sci. Eng., 48, 444 (1972).

14. L. N. Usachev, "Perturbation Theory for the Breeding Ratio and for Other Number Ratios Pertaining to Various Reactor Processes," J. Nucl. Energy, Pts. A/B 18, 571 (1964).

15. A. Gandini, "A Generalized Perturbation Method for Bilinear Functionals of the Real and Adjoint Neutron Fluxes," J. Nucl. Energy 21, 755 (1967).

16. F. R. Mynatt, "Methods for Calculating Neutron and Gamma-Ray Attenuation," Weapons Radiation Shielding Handbook, Chapter 3 (1968).

17. P. N. Stevens, "Use of the Discrete Ordinates S_n Method in Radiation Shielding Calculations," Nucl. Eng. Design, 13, 395 (1970).

18. D. E. Bartine, E. M. Oblow, and F. R. Mynatt, "SWANLAKE - A Computer Code Utilizing ANISN Radiation Transport Calculations for Cross Section Sensitivity Analysis," ORNL-TM-3809 (1973).

19. J. H. Marable, J. L. Lucius, and C. R. Weisbin, "Compilation of Sensitivity Profiles for Several CSEWG Fast Reactor Benchmarks," ORNL/TM-5560 (ENDF-234) (1976).

20. "ENDF-202 Cross Section Evaluation Working Group Benchmark Specifications," BNL-19302 (ENDF-202) (November 1974).

21. J. E. White, R. Q. Wright, L. R. Williams, and C. R. Weisbin, "Data Testing of the 126/36 Neutron-Gamma ENDF/B-IV Coupled Library for LMFBR Core and Shield Analysis," Trans. Am. Nucl. Soc., 23, 507 (June 1976).

22. C. R. Weisbin, P. D. Soran, R. E. MacFarlane, D. R. Harris, R. J. LaBauve, J. S. Hendricks, and J. E. White, "MINX, A Multigroup Interpretation of Nuclear Cross Sections from ENDF/B," Los Alamos Scientific Laboratory (to be published); see also, Trans. Am. Nucl. Soc., 16, 127 (1973).

23. N. M. Greene, J. L. Lucius, L. M. Petrie, W. E. Ford, III, J. E. White, R. Q. Wright, "AMPX: A Modular Code Systen for Generating Coupled Multigroup Neutron-Gamma Libraries from ENDF/B," ORNL/TM-3706 (March 1976).

24. C. R. Weisbin, E. M. Oblow, J. Ching, J. E. White, R. Q. Wright, and J. D. Drischler, "Cross Section and Method Uncertainties: The Application of Sensitivity Analysis to Study Their Relationship in Radiation Transport Benchmark Problems," ORNL-TM-4847 (ENDF-218) (August 1975)1 see also, RSIC Code Collection PSR-93.

25. N. C. Paik, W. Davis, M. B. Yarbrough, and D. Petros, "Physics Evaluations and Applications Quarterly Progress Report for Period Ending July 31, 1974," WARD-XS-3045-7 (and continuing -10) (November 1974).

26. W. W. Engle, Jr., "A User's Manual for ANISN, A One-Dimensional Discrete Ordinates Transport Code with Anisotropic Scattering," K-1693, Computing Technology Center, Oak Ridge Gaseous Diffusion Plant (1967).

27. W. A. Rhoades and F. R. Mynatt, "The DOT III Two-Dimensional Discrete Ordinates Transport Code," ORNL-TM-4280 (September 1973).

28. D. R. Vondy, T. B. Fowler, and G. W. Cunningham, "VENTURE: A Code Block for Solving Multigroup Neutronics Problems Applying the Finite-Difference Diffusion-Theory Approximation to Neutron Transport," ORNL-5062 (October 1975).

29. R. L. Childs, D. E. Bartine, and W. W. Engle, Jr., "Perturbation Theory and Sensitivity Analysis for Two-Dimensional Shielding Calculations," Trans. Am. Nucl. Soc., 21, 542 (June 1975).

30. INTEXP is a modification of the AMARA program to include a posteriori estimate of covariance matrices and conform with the interfaces in the FORSS System. See also, A. Gandini and M. Petilli, "AMARA: A Code Using the Lagrange Multiplier Method for Nuclear Data Adjustment," private communication, M. Salvatores (1975).

31. J. H. Marable, C. R. Weisbin, and E. M. Oblow, "The Nuclear Data Accuracy Required to Meet Specified Reactor Performance Goals," paper submitted to American Nuclear Society Winter Meeting, 1976; combined with another paper with same title as this report (July 1976).

32. C. R. Weisbin, R. W. Roussin, J. E. White, and R. Q. Wright, "Specification for Pseudo-Composition Independent Fine-Group and Composition-Dependent Fine- and Broad-Group LMFBR Neutron-Gamma Libraries at ORNL," ORNL-TM-5142 (ENDF-224) (December 1975).

33. B. M. Carmichael, "Standard Interface Files and Procedures for Reactor Physics Codes, Version III," LA-5486-MS (February 1974).

34. J. L. Lucius and C. R. Weisbin, "Interface Specifications for Sensitivity Profiles (SENPRO) and Covariance Files (COVERX)," Presentation to the Committee on Computer Code Coordination, Los Alamos Scientific Laboratory (May 1976).

35. E. M. Bohn, I. K. Olson, and K. E. Freese, "A Compilation of Cross Section Sensitivity Coefficients for ZPR-6/6A, ZPR-6/7, and ZPR-3/48," ZPR-TM-240 (May 1976).

36. W. M. Stacey, Jr., and J. Regis, VARI-1D: A One-Dimensional Variational Sensitivity Code," FRA-TM-57 (May 1973).

37. F. Perey, Format Modifications 73-7, minutes of the CSEWG Meeting, December 1973 (Enclosures 6 and 12), S. Pearlstein, Editor, Brookhaven National Laboratory; see also, F. G. Perey, "Estimated Uncertainties in Nuclear Data - An Approach," Proceedings of a Conference on Nuclear Cross Section and Technology, Volume II, edited by R. A. Schrack and C. D. Bowman, p. 842 (October 1975).

38. F. G. Perey, "The Estimated Data Covariance Files of ENDF/B - Their Uses," minutes of the CSEWG Meeting, June 17-19, 1974 (enclosure 10), S. Pearlstein, Editor, Brookhaven National Laboratory.

39. F. C. Difillipo, "SUR, A Program to Generate Error Covariance Files," ORNL/TM-5223 (March 1976). The data in this report were derived from discussions with G. deSaussure, R. B. Perez, R. Gwin, and R. W. Peelle; the principles behind the procedures described are discussed in F. G. Perey, G. deSaussure, and R. B. Perez, "Estimated Data Covariance Files for Evaluated Cross Sections - Examples for ^{235}U and ^{238}U," Advanced Reactors: Physics, Design, and Economics, Edited by Kallfelz and Karam, Pergamon Press, p. 578 (1975).

40. R. Gwin, ORNL private communication (March 1976).

41. S. M. Zaritsky et al., "Nuclear Data Requirements for the Calculation of Fast Reactors," DNDC(CCP)-174 (January 1972).

42. L. N. Usachev and Yu. G. Bobkov, "Planning an Optimum Set of Microscopic Experiments and Evaluations to Obtain a Given Accuracy in Reactor Parameter Calculations," INDC(CCP) 19U (February 1972).

43. Yu. G. Bobkov, L. T. Pyataitskaya, and L. N. Usachev, "Planning of Neutron Data Experiments and Evaluations for Reactors," INDC(CCP)-46/L (1974).

44. Kenneth E. Cross, "A Gradient Projection Method for Constrained Optimization," Report K-1746 (May 30, 1968), Union Carbide Corp., Nuclear Division Computing Technology Center, Oak Ridge, Tenn.

45. G. deSaussure, ORNL private communication (April 1976).

46. E. M. Bohn et al., "Benchmark Experiments for Nuclear Data," Proc. Conf. Nuclear Cross Sections and Technology, Washington, D. C., March 3-7, 1975, p. 834.

47. Central $^{28}c/^{49}f$ ratio has obvious interest as a component of breeding ratio and at least for $^{238}U(n,\gamma)$ has very similar sensitivity profiles (see ref. 46).

APPENDIX A
DERIVATION OF THE EXPRESSION FOR k-SENSITIVITY

Consider the Boltzmann equation written in the form:

$$[A - \lambda B]\phi = 0 \tag{A-1}$$

and a perturbed system

$$[A' - \lambda' B']\phi' = 0 \tag{A-2}$$

The equation adjoint to (A-1) is

$$[A^* - \lambda B^*]\phi^* = 0 \tag{A-3}$$

Multiplying Eq. (A-3) by ϕ' and Eq. (A-2) by ϕ^*, subtracting and integrating over the volume of the reactor yields

$$\left\langle \phi^*(A' - \lambda' B')\phi \right\rangle - \left\langle \phi'(A^* - \lambda B^*)\phi^* \right\rangle = 0 \tag{A-4}$$

Defining:

$$\begin{aligned} A' &= A + dA \\ B' &= B + dB \\ \lambda' &= \lambda + d\lambda \end{aligned} \tag{A-5}$$

and using the property of adjointness for the operators A, A* and B, B* we find

$$\left\langle \phi^*(dA - \lambda\, dB - B\, d\lambda - d\lambda\, dB)\phi' \right\rangle = 0 \tag{A-6}$$

ignoring second order terms ($d\lambda\, dB$), and also thereby approximating ϕ' with ϕ, and solving for the reactivity perturbation

$$\frac{d\lambda}{\lambda} = \frac{\left\langle \phi^*(dA - \lambda\, dB)\phi \right\rangle}{\left\langle \phi^*\, \lambda\, B\phi \right\rangle} \tag{A-7}$$

Hence, the sensitivity of $\lambda(1/k)$ with respect to $\Sigma(\rho)$ becomes

$$\frac{d\lambda/\lambda}{d\Sigma(\underline{\rho})/\Sigma(\underline{\rho})} = \frac{\Sigma(\underline{\rho})}{\lambda} \frac{\left\langle \phi^* \left(\frac{dA}{d\Sigma(\underline{\rho})} - \lambda \frac{dB}{d\Sigma(\underline{\rho})} \right) \phi \right\rangle}{\left\langle \phi^* \, B \, \phi \right\rangle} \tag{A-8}$$

It should be noted here that since $\lambda \equiv 1/k$, $d\lambda/\lambda = - dk/k$ so that if one is interested in $(dk/k)/[d\Sigma(\underline{\rho})/\Sigma(\underline{\rho})]$, one would obtain:

$$\frac{dk/k}{d\Sigma(\rho)/\Sigma(\rho)} = - \frac{\Sigma(\rho)}{\lambda} \frac{\left\langle \phi^* \left(\frac{dA}{d\Sigma(\rho)} - \lambda \frac{dB}{d\Sigma(\rho)} \right) \phi \right\rangle}{\left\langle \phi^* \, B \, \phi \right\rangle} \tag{A-9}$$

or

$$\frac{dk/k}{d\Sigma(\underline{\rho})/\Sigma(\underline{\rho})} = - \frac{\Sigma(\underline{\rho})}{k} \frac{\left\langle \phi^* \left(\frac{dA}{d\Sigma(\underline{\rho})} - \frac{1}{k} \frac{dB}{d\Sigma(\underline{\rho})} \right) \phi \right\rangle}{\left\langle \phi^* \frac{1}{k^2} B \, \phi \right\rangle} \tag{A-10}$$

Appendix B

Nuclide Densities in the One-Dimensional Model for ZPR-6/7 and ZPR-6/6A

Assembly 7 Spherical Model Atom Densities (atoms/barn-cm)

Isotope	Core Radius = 88.16 cm	Blanket Thickness = 33.81 cm
^{239}Pu	0.00088672	-
^{240}Pu	0.00011944	-
^{241}Pu	0.0000133	-
^{235}U	0.0000126	0.0000856
^{238}U	0.00578036	0.0396179
Mo	0.0002357	0.0000038
Na	0.0092904	-
O	0.01390	0.000024
Fe	0.013431	0.004637
Cr	0.002842	0.001295
Ni	0.001291	0.0005635
Mn	0.000221	0.0000998

Assembly 6A Spherical Model Atom Densities (atom/barn-cm)

Isotope	Core	Blanket
^{235}U	0.001153	0.0000856
^{238}U	0.0058176	0.0395508
Na	0.0092904	-
O	0.01390	0.000023
Fe	0.013431	0.0044669
Ni	0.001291	0.0005407
Cr	0.002842	0.001247
Mn	0.000221	0.0000960

Acknowledgements

The authors take great pleasure in acknowledging the significant contributions made by J. E. White and R. Q. Wright in the preparation and testing all of the cross sections required for this study. In addition, the efforts of R. W. Roussin and J. B. Wright packaging the cross section data for distribution helped uncover several bugs. It was E. Tomlinson and T. J. Burns who had initial experience in testing and developing the generalized adjoint and uncertainty processing components of the system.

The authors wish to thank G. deSaussure, R. B. Perez, R. Gwin, L. W. Weston, and F. Difilippo for their interest in the development of the covariance files. Appreciation is also expressed to J. D. Drischler who obtained all the necessary plots and helped develop the entire uncertainty analysis system. Without the encouragement of F. C. Maienschein and continued financial support provided by P. B. Hemmig and J. E. Lewellen, this work would not have been possible.

Finally, special thanks are due to Virginia Glidewell who typed and organized this work through several drafts.

ORNL/TM-5563
Distribution Category UC-79d
(ENDF-236)

Internal Distribution

1. L. S. Abbott
2. R. G. Alsmiller, Jr.
3. D. E. Bartine
4. T. J. Burns
5. C. E. Clifford
6. G. deSaussure
7. F. C. Difillipo
8. J. D. Drischler
9. W. W. Engle, Jr.
10. G. F. Flanagan
11. W. E. Ford
12. H. Goldstein (consultant)
13. N. M. Greene
14. R. Gwin
15. W. O. Harms
16. J. D. Jenkins
17. J. L. Lucius
18. R. A. Lillie
19. F. C. Maienschein
20. J. H. Marable
21. F. R. Mynatt
22. E. M. Oblow
23. R. W. Peelle
24. F. G. Perey
25. R. B. Perez
26. L. M. Petrie
27. W. A. Rhoades
28. RSIC
29. D. Steiner
30. M. L. Tobias
31. D. B. Trauger
32. E. T. Tomlinson
33. D. R. Vondy
34-79. C. R. Weisbin
80. R. M. Westfall
81. L. W. Weston
82. J. E. White
83. G. E. Whitesides
84. J. B. Wright
85. R. Q. Wright
86. A. Zucker
87. P. Greebler (consultant)
88. W. W. Havens (consultant)
89. A. F. Henry (consultant)
90. R. E. Uhrig (consultant)
91-92. Central Research Library
93. ORNL Y-12 Technical Library
Document Reference Section
94. Laboratory Records Department
95. Laboratory Records ORNL RC
96. ORNL Patent Office

External Distribution

97. USERDA Oak Ridge Operations, Research and Technical Support Division, P.O. Box E, Oak Ridge, TN. 37830: Director
98. USERDA Oak Ridge Operations, Reactor Division, P.O. Box E, Oak Ridge, TN. 37830: Director
99-100. USERDA Division of Reactor Research and Development, Washington, D. C. 20545: Director
101-408. For distribution as shown in TID-4500 Distribution Category, UC-79d, Liquid Metal Fast Breeder Reactor Physics (60 copies - ENDF distribution)

☆ U.S. GOVERNMENT PRINTING OFFICE: 1976-748-189/54